

Non-radial oscillations in anisotropic dark energy stars

O. P. Jyothilakshmi,^{*} Lakshmi J. Naik,[†] and V. Sreekanth[‡]

Department of Physics, Amrita School of Physical Sciences, Amrita Vishwa Vidyapeetham, Coimbatore, India

(Dated: March 4, 2024)

We study the non-radial f -mode oscillations of both isotropic and anisotropic dark energy stars by using the modified Chaplygin prescription of dark energy to model the stellar matter. The anisotropic pressure in the system is modeled with Bowers-Liang prescription. By solving the stellar structure equations in presence of anisotropy, we study the global properties of the dark energy star and compare the mass-radius profiles with data from GW events and milli-second pulsars. We proceed to determine the prominent non-radial $l = 2$ f -mode frequencies of the anisotropic dark energy star by employing the Cowling approximation and analyse and quantify the spectra by varying the anisotropic parameter. We report that f -mode spectra of dark energy star have distinctly different behaviour compared to neutron star and quark star, and this may possibly help in its future identification. Further, the tidal deformability factors of the anisotropic dark energy stars have also been analyzed.

I. INTRODUCTION

Dark energy is the fluid component that governs the accelerated expansion of the universe [1–3]. It is found from various observations that dark energy fills up almost 70% of the universe [4]. The Λ CDM model (also known as the concordance model) [5] is one of the most accepted cosmological models describing dark energy. However, the Λ CDM model suffers from problems like the cosmological constant problem [6, 7], and the Hubble tension [8–10]. Therefore, many alternative models have been proposed in the last few decades. A detailed review on various dynamical models of dark energy such as cosmological constant, quintessence, K-essence, tachyon field, phantom field, dilatonic field, Chaplygin gas model, etc. are given in Ref. [11].

The fact that interior composition of a compact star is unknown to this date has motivated a lot of researchers to construct different models of compact stars. There are several stellar models that include dark energy such as false vacuum bubbles [12], non-singular black holes [13], gravastars [14], and dark energy stars [15]. Among these models, we are interested in the dark energy star, which was first proposed by Chapline [15]. The author gave an alternative explanation to astrophysically observed black holes suggesting that these compact objects may be dark energy stars. The author also proposed that matter is converted to dark energy when it falls through the event horizon.

Using the general relativistic prescriptions, the structure of compact stars can be obtained by describing the interior composition with an equation of state (EoS). Thus obtained global properties of compact objects are compared with the astrophysical observations to constrain the EoS. Recently detected gravitational waves (GWs) from binary neutron star mergers introduced a new way of restricting the dense matter EoS within neutron stars [16]. The constraints of EoS also include the maximum mass limit set by various observational data

from pulsars [17, 18]. GW asteroseismology is the study of the interior of compact objects using GW observations. The stellar oscillations can produce GWs, this has drawn a great interest recently in the field of GW asteroseismology. The analysis of stellar oscillations is used to understand the microscopic and macroscopic properties of compact objects [19–25]. The non-radial modes of stellar oscillations are an important class among these and the general relativistic treatment of the same can be found in Ref. [26, 27].

These stellar oscillations can be classified into various quasi-normal modes based on the force that restores the system back to equilibrium. Some examples include fundamental f -mode, pressure p -mode, gravity g -mode, rotational r -mode, and space-time w -mode [28]. Among these modes, f -modes are considered to be a promising candidate for GW emissions, which has frequencies in the sensitivity range of upcoming GW detectors [29].

Another important constraint imposed on EoS is by the tidal distortions caused from binary neutron star inspiral [30, 31]. The tidal deformability parameter Λ describes the gravitational wave signal emitted during a binary neutron star inspiral [30, 31]. It determines a star's quadrupole deformation caused by its companion star's tidal field.

This is in addition to the constraints previously provided by the electromagnetic studies of neutron stars, which include their masses, radii, spin, and gravitational redshift. The tidal properties of neutron stars can be measured from the GW signals [32].

In most of the astrophysical studies, the fluid matter within dense compact stars is assumed to be locally isotropic. However, the high density and strong gravity suggest that the interior of compact stars could be anisotropic, meaning the pressure in radial and tangential directions are different. Strong magnetic field, superfluid cores, phase transition, pion condensation etc. may give rise to pressure anisotropy. Ruderman in 1972 was the first to propose the idea of anisotropy in compact stars [33] and later, the relativistic stellar structure equations for anisotropic stars were obtained by Bowers and Liang [34].

Apart from this, various other anisotropy models are used in the study of compact stars [35–37]. See Ref. [38] for a recent review on anisotropic compact stars.

^{*} op_jyothilakshmi@cb.students.amrita.edu

[†] jn_lakshmi@cb.students.amrita.edu

[‡] v_sreekanth@cb.amrita.edu

The solar cycle 25 multi-spacecraft solar energetic particle event catalog of the SERPENTINE project

N. Dresing¹, A. Yli-Laurila¹, S. Valkila¹, J. Gieseler¹, D. E. Morosan¹, G. U. Farwa¹, Y. Kartavykh³, C. Palmroos¹, I. Jebaraj¹, S. Jensen³, P. Kühl³, B. Heber³, F. Espinosa⁴, R. Gómez-Herrero⁴, E. Kilpua², V.-V. Linho², P. Oleynik¹, L.A. Hayes⁹, A. Warmuth⁵, F. Schuller⁵, H. Collier^{7,8}, H. Xiao⁷, E. Asvestari², D. Trotta⁶, J.G. Mitchell¹⁰, C.M.S. Cohen¹¹, A.W. Labrador¹¹, M.E. Hill¹², and R. Vainio¹

¹ Department of Physics and Astronomy, University of Turku, Finland e-mail: nina.dresing@utu.fi

² Department of Physics, University of Helsinki, P.O. Box 64, FI-00014 Helsinki, Finland

³ Institute of Experimental and Applied Physics, Kiel University, Kiel, Germany

⁴ Universidad de Alcalá, Department of Physics, Space Research Group, Alcalá de Henares, Spain

⁵ Leibniz-Institut für Astrophysik Potsdam (AIP), An der Sternwarte 16, D-14482 Potsdam, Germany

⁶ The Blackett Laboratory, Department of Physics, Imperial College London, London, SW7 2AZ, UK

⁷ Fachhochschule Nordwestschweiz, Bahnhofstrasse 6, 5210 Windisch, Switzerland

⁸ ETH Zürich, Rämistrasse 101, 8092 Zürich Switzerland

⁹ European Space Agency, ESTEC, Keplerlaan 1 - 2201 AZ, Noordwijk, The Netherlands

¹⁰ NASA Goddard Space Flight Center, Greenbelt MD 20771, USA

¹¹ California Institute of Technology, Pasadena, CA 91125, USA

¹² Johns Hopkins University Applied Physics Laboratory, Laurel, MD 20723, USA

ABSTRACT

Context. The *Solar energetic particle analysis platform for the inner heliosphere* (SERPENTINE) project, funded through the H2020-SPACE-2020 call of the European Union's Horizon 2020 framework programme, employs measurements of the new inner heliospheric spacecraft fleet to address several outstanding questions of the origin of solar energetic particle (SEP) events. The data products of SERPENTINE include event catalogs, which are provided to the scientific community.

Aims. In this paper, we present SERPENTINE's new multi-spacecraft SEP event catalog for events observed in solar cycle 25. Observations from five different viewpoints are utilized, provided by Solar Orbiter, Parker Solar Probe, STEREO A, BepiColombo, and the near-Earth spacecraft Wind and SOHO. The catalog contains key SEP parameters for 25 – 40 MeV protons, ~ 1 MeV electrons, and ~ 100 keV electrons. Furthermore, basic parameters of the associated flare and type-II radio burst are listed, as well as the coordinates of the observer and solar source locations.

Methods. An event is included in the catalog if at least two spacecraft detect a significant proton event with energies of 25 – 40 MeV. SEP onset times are determined using the Poisson-CUSUM method. SEP peak times and intensities refer to the global intensity maximum. If different viewing directions are available, we use the one with the earliest onset for the onset determination and the one with the highest peak intensity for the peak identification. We furthermore aim at using a high time resolution to provide most accurate event times. Therefore, time averaging of the SEP intensity data is only applied if necessary to determine clean event onsets and peaks. Associated flares are identified using observations from near Earth and Solar Orbiter. Associated type II radio bursts are determined from ground-based observations in the metric frequency range and from spacecraft observations in the decametric range.

Results. The current version of the catalog contains 45 multi-spacecraft events observed in the period from Nov 2020 until May 2023, of which 13 were widespread events and four were classified as narrow-spread events. Using X-ray observations by GOES/XRS and Solar Orbiter/STIX, we were able to identify the associated flare in all but four events. Using ground-based and space-borne radio observations, we found an associated type-II radio burst for 40 events. In total, the catalog contains 142 single event observations, of which 20 (45) have been observed at radial distances below 0.6 AU (0.8 AU). It is anticipated to extend the catalog in the future.

Key words. solar energetic particles – flares – catalogs

1. Introduction

Solar energetic particle (SEP) events are large outbursts of energetic particle radiation from the Sun associated with solar eruptions, that is, solar flares and coronal mass ejections (CMEs). They can be classified based on their key observational properties, for example, in impulsive and gradual classes (e.g., Reames 1999). The classical picture relates impulsive events with flares and gradual events with fast and wide CMEs. While the broad lines of the origin of SEP events are mostly understood, many of the key aspects of the acceleration and transport of ions and

electrons in these events have remained elusive. The main obstacle preventing us from achieving a complete understanding has been the lack of observational coverage in the heliosphere: solar eruptions often fill a major part of the inner heliosphere with energetic particles, and using a scarce set of observing spacecraft does not allow one to conclusively separate the effects of particle transport from the properties of the source.

With the launch of the new space missions Solar Orbiter (Müller et al. 2020) and Parker Solar Probe (Parker; Fox et al. 2016), a unique era for multi-spacecraft observations of SEP events has begun. Combined with established space missions

A hands-on introduction to Physics-Informed Neural Networks for solving partial differential equations with benchmark tests taken from astrophysics and plasma physics

Hubert Baty*

Observatoire Astronomique, Université de Strasbourg, 67000 Strasbourg, France

March 4, 2024

Abstract

I provide an introduction to the application of deep learning and neural networks for solving partial differential equations (PDEs). The approach, known as physics-informed neural networks (PINNs), involves minimizing the residual of the equation evaluated at various points within the domain. Boundary conditions are incorporated either by introducing soft constraints with corresponding boundary data values in the minimization process or by strictly enforcing the solution with hard constraints. PINNs are tested on diverse PDEs extracted from two-dimensional physical/astrophysical problems. Specifically, we explore Grad-Shafranov-like equations that capture magnetohydrodynamic equilibria in magnetically dominated plasmas. Lane-Emden equations that model internal structure of stars in self-gravitating hydrostatic equilibrium are also considered. The flexibility of the method to handle various boundary conditions is illustrated through various examples, as well as its ease in solving parametric and inverse problems. The corresponding Python codes based on PyTorch/TensorFlow libraries are made available.

*Corresponding author: hubert.baty@unistra.fr

Gravitational waves in a cyclic Universe: resilience through cycles and vacuum state

Mariaveronica De Angelis,^{1,*} Adam Smith,^{1,†} William Giarè,^{1,‡} and Carsten van de Bruck^{1,§}

¹*School of Mathematics and Statistics, The University of Sheffield,
Hounsfield Road, S3 7RH Sheffield, United Kingdom*

We present a generalised calculation for the spectrum of primordial tensor perturbations in a cyclic Universe, making no assumptions about the vacuum state of the theory and accounting for the contribution of tensor modes produced in the dark energy phase of the previous cycle. We show that these modes have minimal impact on the spectrum observed in the current cycle, except for corrections on scales as large as the comoving Hubble radius today. These corrections are due to sub-horizon modes produced towards the end of the dark energy phase, persisting into the *ekpyrotic* phase of the next cycle as additional quanta. In relation to the vacuum state, we argue that non-Bunch-Davies quanta can easily overwhelm the energy density driving the dark energy phase, potentially compromising the model. Therefore, avoiding backreaction effects sets restrictive constraints on deviations away from the Bunch-Davies vacuum during this phase, limiting the overall freedom to consider alternative vacua in the cyclic Universe.

I. INTRODUCTION

The most compelling observational evidence supporting cosmological inflation [1–4] as the leading theory of the early Universe is currently provided by the Planck satellite measurement of the spectral index of scalar perturbations, $n_s = 0.9649 \pm 0.0042$ [5]. In the simplest single-field slow-roll inflationary models, the spectrum of scalar modes is expected to be almost but not exactly flat [6–9], with deviations from flatness are quantified in terms of how much n_s deviates from 1 [10–13]. As a result, the Planck data seem to be in excellent agreement with the theoretical predictions of inflationary models [5, 14], ruling out a Harrison-Zeldovich scale-invariant spectrum [15–17] (corresponding to $n_s = 1$) at a statistical level exceeding 8.5 standard deviations and lending weight to the inflationary paradigm.

That being said, with no aim to downplay the significance of this result or its interpretation, it is crucial to emphasise that, on its own, it does not provide conclusive evidence for cosmological inflation. Even hinging on a certain level of optimism and setting aside the uncertainty surrounding constraints on n_s from CMB experiments other than Planck¹ – or the potential implications arising from the well-known tensions [27–31] characterising the recent debate² – alternative theoretical mechanisms have been put forth, yielding an almost scale-invariant spectrum of primordial density fluctuations without invoking inflation.

An illustrative example of such mechanisms is the cyclic Universe [43–49] that, in contrast to the conventional cosmological framework, suggests a periodic history for the Cosmos. The model has been extensively studied and discussed in relation to a broad range of topics, including quantum gravity, modified gravity, gravitational waves and dark energy, see e.g., Refs. [50–83] or Refs. [84, 85] for reviews. In broad terms, each cycle comprises a phase recasting the standard Hot Big Bang theory (during which large-scale structures take shape), followed by a phase of slow, accelerated expansion mirroring the present-day observational evidence for a Dark Energy dominated dynamics. In the cyclic Universe, this latter stage also serves to dilute inhomogeneities and flatten the spatial geometry. Subsequently, a contraction phase ensues, generating nearly scale-invariant density perturbations. Finally, the cycle concludes with a big-crunch/big-bang transition, during which matter and radiation are generated, setting the stage for the next cycle.

Notice that both inflation and the cyclic Universe provide physical mechanisms to produce an almost scale-invariant spectrum of density perturbations [86–88]. In addition, they can both explain observational facts such as the homogeneity in the cosmic microwave background (CMB) radiation [89] and the fact that the present-day spatial geometry of the Universe appears to be flat, or at the very least nearly flat³. Therefore, at first glance, one might wonder how to distinguish between the two models. Focusing solely on scalar modes, this is a challenging knot to unravel [111, 112]. However, the two scenarios yield significantly distinct predictions for the stochastic background of gravitational waves [50]. Similar to scalar modes, inflation predicts a nearly scale-invariant (red-tilted) spectrum of tensor modes [12, 13, 113]. Conversely, in the cyclic Universe, the tensor spectrum is typically blue-tilted, and its amplitude is many orders of magnitude lower than that predicted by inflation, remaining well below any observable threshold achievable in the near future. Consequently, any measurement of primordial gravitational waves (e.g., through the effects left in the CMB B-mode polarisation at large angular scales) would offer conclusive evidence for inflation, discounting the cyclic model.

* mdeangelis1@sheffield.ac.uk

† asmith69@sheffield.ac.uk

‡ w.giare@sheffield.ac.uk

§ c.vandebruck@sheffield.ac.uk

¹ Over the years, constraints on the spectral index have been released by a multitude of Planck-independent CMB experiments such as WMAP [18, 19], the Atacama Cosmology Telescope (ACT) [20, 21], and the South Pole Telescope (SPT) [22, 23]. When considering these data at face value, Planck is currently the only experiment excluding $n_s = 1$ at a statistical significance much larger than 3σ . Conversely, ACT shows a preference for $n_s = 1$ [21, 24]. Different combinations of these data overall support the result $n_s \neq 1$, although sometimes they lead to discordant results in terms of the other inflationary parameters or the preferred inflationary models [25, 26].

² For studies suggesting potential implications of cosmological tensions for inflation, see, e.g., Refs. [32–42]

³ For recent discussions surrounding the spatial geometry of the Universe, see, e.g., [90–110]

Constraining the abundance of Galactic compact objects with continuous gravitational waves

GOPALKRISHNA PRABHU ^{1,*}, ADITYA KUMAR SHARMA ^{2,*}, R. PRASAD ² AND SHASVATH J. KAPADIA ¹

¹*Inter University Centre for Astronomy and Astrophysics, Post Bag 4, Ganeshkhind, Pune - 411007, India*

²*International Centre for Theoretical Sciences, Tata Institute of Fundamental Research, Bangalore 560089, India*

ABSTRACT

Galactic spinning compact objects (COs) with non-zero ellipticity are expected to be sources of continuous gravitational waves (CGWs). Certain classes of hypothetical COs, such as neutron stars with quark cores (hybrid stars), and quark stars, are thought to be capable of sustaining large ellipticities from theoretical considerations. Such exotic COs (eCOs) with large ellipticities should produce CGWs detectable by the current LIGO-Virgo-Kagra GW detector network. Since no detections for CGWs, from searches in LIGO-Virgo data, have so far been reported, we place constraints on the abundance of highly elliptical eCOs in our Galaxy. We formulate a Bayesian framework to place upper limits on the number count N_{tot} of highly deformed Galactic eCOs. We divide our constraints into two classes: an “agnostic” set of upper limits on N_{tot} evaluated on a CGW frequency and ellipticity grid that depend only on the choice of spatial distribution of COs; and a model-dependent set that additionally assumes prior information on the distribution of frequencies. We find that COs with ellipticities $\epsilon \gtrsim 10^{-5}$ have abundance upper limits at 90% confidence, of $N_{tot}^{90\%} \lesssim 100$, and those with $\epsilon \gtrsim 10^{-6}$ have $N_{tot}^{90\%} \lesssim 10^4$. We additionally place upper-limits on the ellipticity of Galactic COs informed by our choices of spatial distributions, given different abundances N_{tot} .

1. INTRODUCTION

The LIGO-Virgo-Kagra (LVK) network (Aasi et al. 2015; Acernese et al. 2015; Akutsu et al. 2021) of gravitational-wave (GW) detectors has completed three observing runs (O1, O2, O3) (Abbott et al. 2021a). These have produced ~ 100 detections, all of which correspond to compact binary coalescence (CBC) events. The majority of these are binary black hole mergers (BBHs), although binary neutron star (BNS) Abbott et al. (2017a, 2020) and neutron-star black hole (NSBH) events have also been observed (Abbott et al. 2021b).

The ongoing¹ O4 could triple the number of detections reported so far, thus firmly establishing the arrival of GW astronomy. Indeed, even the existing list of detections has provided a wealth of scientific riches. These include unique tests of general relativity (Abbott et al. 2021c), inference of population properties of BBHs that merge within Hubble time (Abbott et al. 2023a), distance-ladder-independent measurements of the Hubble constant (Abbott et al. 2023b), an understanding of the provenance of short-gamma-ray bursts and kilonovae (Abbott et al. 2017b), and probes of ultra-dense

matter via constraints on NS equations of state (Abbott et al. 2018).

Another class of GWs, produced by spinning NSs (or possibly other hypothetical compact objects), are also expected to be detected with improved detector sensitivity, although no such detection has so far been reported (Abbott et al. 2022a,b,c). Spinning NSs with axial asymmetry as quantified by the ellipticity parameter ϵ , will have a time-varying mass-quadrupole moment which in turn results in the production of GWs (see, e.g., Bonazzola & Gourgoulhon 1996a). However, unlike CBCs which are transient events with in-band durations of $O(\text{min})$ at most in the current LVK network, GWs from NSs will be persistent events. Such continuous (C) GWs are expected to maintain a near-constant frequency, although their amplitudes, even for Galactic sources, are four orders of magnitude (or more) smaller than typical transient CBC sources detectable by the LVK network (see, e.g. Riles 2023). However, their enormous in-band duration could mitigate their small amplitudes by accumulating signal-to-noise ratio (SNR) across several cycles (see, e.g. Jaranowski et al. 1998a).

The detectability of CGWs from Galactic COs crucially depends on the spin-frequencies of the COs, their ellipticities, and their distances from the Earth (see, e.g. Piccinni 2022, and references therein). Current upper

* Equal contribution from both authors.

¹ at the time of writing

Collective excitations and low-energy ionization signatures of relativistic particles in silicon detectors

Rouven Essig,^a Ryan Plestid,^b Aman Singal^{a,c}

^a*C. N. Yang Institute for Theoretical Physics, Stony Brook University, Stony Brook, NY 11794, USA*

^b*Walter Burke Institute for Theoretical Physics, California Institute of Technology, Pasadena, CA 91125*

^c*Institute for Advanced Computational Sciences, Stony Brook University, Stony Brook, NY 11794, USA*

E-mail: rouven.essig@stonybrook.edu, rplestid@caltech.edu,
aman.singal@stonybrook.edu

ABSTRACT: Solid-state detectors with a low energy threshold have several applications, including in direct-detection searches of non-relativistic halo dark-matter particles with sub-GeV masses. Moreover, when searching for relativistic or quasi-relativistic beyond-the-Standard-Model particles (i.e., $v/c \gtrsim 0.01$) that have an enhanced cross section for small energy transfers, a comparatively small detector with a low energy threshold may have better sensitivity than a larger detector with a higher energy threshold. In this paper, we provide accurate calculations of the low-energy ionization spectrum from high-velocity particles scattering in a dielectric material. We focus on silicon, although our results can be easily applied to other materials. We consider the full material response, in particular also the excitation of bulk plasmons. We generalize the energy-loss function to relativistic kinematics, and benchmark existing tools used for halo dark-matter scattering against publicly available electron energy-loss spectroscopy data. Compared to calculations of energy loss that are commonly used in the literature, such as the Photo-Absorption-Ionization model or the free-electron model, the inclusion of collective effects shifts the recoil ionization spectrum towards higher energies, typically peaking around 4–6 electron-hole pairs. We apply our results to the three benchmark examples: millicharged particles produced in a beam, neutrinos with a magnetic dipole moment produced in a reactor, and dark-matter particles that are upscattered by cosmic rays or in the Sun. Our results show that the proper inclusion of collective effects typically enhances a detector’s sensitivity to these particles, since detector backgrounds, such as dark counts, peak at lower energies.

Sudden breakdown of effective field theory near cool Kerr-Newman black holes

Gary T. Horowitz,¹ Maciej Kolanowski,¹ Grant N. Remmen,² Jorge E. Santos³

¹*Department of Physics, University of California, Santa Barbara, CA 93106, U.S.A.*

²*Center for Cosmology and Particle Physics, Department of Physics, New York University, New York, NY 10003, U.S.A.*

³*DAMTP, Centre for Mathematical Sciences, University of Cambridge, Wilberforce Road, Cambridge CB3 0WA, UK*

horowitz@ucsb.edu, mkolanowski@ucsb.edu, grant.remmen@nyu.edu,
jss55@cam.ac.uk

ABSTRACT: It was recently shown that (near-)extremal Kerr black holes are sensitive probes of small higher-derivative corrections to general relativity. In particular, these corrections produce diverging tidal forces on the horizon in the extremal limit. We show that adding a black hole charge makes this effect qualitatively stronger. Higher-derivative corrections to the Kerr-Newman solution produce tidal forces that scale inversely in the black hole temperature. We find that, unlike the Kerr case, for realistic values of the black hole charge large tidal forces can arise before quantum corrections due to the Schwarzian mode become important, so that the near-horizon behavior of the black hole is dictated by higher-derivative terms in the effective theory.

An improved calendar ring hole-count for the Antikythera mechanism

Graham Woan *

Joseph Bayley †

School of Physics and Astronomy, University of Glasgow, Glasgow G12 8QQ, United Kingdom

29 February 2024

Abstract

We present a new analysis of the positions of holes beneath the calendar ring of the Antikythera mechanism, as measured by Budiselic et al. (2020). We significantly refine their estimate for the number of holes that were present in the full ring. Our 68%-credible estimate for this number, taking account of all the data, is $355.24^{+1.39}_{-1.36}$. If holes adjacent to fractures are removed from the analysis, our estimate becomes $354.08^{+1.47}_{-1.41}$. A ring of 360 holes is strongly disfavoured, and one of 365 holes is not plausible, given our model assumptions.

1 Introduction

The Antikythera mechanism is a multi-component device recovered from a shipwreck close to the Greek island of Antikythera in 1901. It is believed to be the remains of a complex mechanical calculator of ancient origin, and has undergone considerable investigation and analysis to determine its true form and function [3].

In a recent paper [1], Budiselic et al. presented new, high resolution, X-ray data on one of the components of the mechanism, the so-called front dial calendar ring, found in Fragment C. Only a part of the full ring survives, and it is fractured into several sections. Budiselic et al. made careful measurements of the positions of closely spaced holes beneath the ring. These holes are thought to have been used to rotationally align the calendar ring, and their number is crucial for the interpretation of the ring's function. The authors generously made their measurements of the hole positions available [5], and this paper is based entirely on these data.

In this paper, we infer the number of holes that were present in the complete ring, N , given these measurements and some reasonable assumptions. Budiselic et al. presented an analysis that resulted in an estimator for N with a 99% confidence interval of 346.8 to 367.2. However, using the same data, a clearer and more stringent statement can be made about N using a Bayesian analysis and an improved model for the positional errors in hole placement. Bayesian methods have several distinct advantages over frequentist methods for addressing problems such as this: first, one can make simple probabilistic statements about the value of N itself, something that frequentist methods are not able to do, by definition. As a result, there is no need to choose a statistic of the data against which to test a null hypothesis. It is also straightforward to include

*ORCID iD 0000-0003-0381-0394

†ORCID iD 0000-0003-2306-4106

Optical modeling of systematic uncertainties in detector polarization angles for the Atacama Cosmology Telescope

COLIN C. MURPHY¹, STEVE K. CHOI^{2,1,3*}, RAHUL DATTA⁴, MARK J. DEVLIN⁵, MATTHEW HASSELFIELD⁶, BRIAN J. KOOPMAN⁷, JEFF MCMAHON⁴, SIGURD NAESS⁸, MICHAEL D. NIEMACK^{1,3}, LYMAN A. PAGE⁹, SUZANNE T. STAGGS⁹, ROBERT THORNTON¹⁰ AND EDWARD J. WOLLACK¹¹

¹*Cornell University, Department of Physics*

²*University of California, Riverside, Department of Physics and Astronomy*

³*Cornell University, Department of Astronomy*

⁴*The University of Chicago, Department of Astronomy and Astrophysics*

⁵*University of Pennsylvania, Department of Physics and Astronomy*

⁶*Flatiron Institute, Center for Computational Astrophysics*

⁷*Yale University, Department of Physics*

⁸*University of Oslo, Institute for theoretical astrophysics*

⁹*Princeton University, Department of Physics*

¹⁰*West Chester University, Department of Physics*

¹¹*NASA/Goddard Space Flight Center*

*steve.choi@ucr.edu

Abstract: We present an estimate of the Atacama Cosmology Telescope (ACT) detector polarization angle systematic uncertainty from optics perturbation analysis using polarization-sensitive ray tracing in CODE V optical design software. Uncertainties in polarization angle calibration in CMB measurements can limit constraints on cosmic birefringence and other cosmological measurements. Our framework estimates the angle calibration systematic uncertainties from possible displacements in lens positions and orientations, and anti-reflection coating (ARC) thicknesses and refractive indices. With millimeter displacements in lens positions and percent-level perturbations in ARC thicknesses and indices from design, we find the total systematic uncertainty for three ACT detector arrays operating between 90–220 GHz to be at the tenth of degree scale. Reduced lens position and orientation uncertainties from physical measurements could lead to a reduction in the systematic uncertainty estimated with the framework presented here. This optical modeling can inform polarization angle systematic uncertainties for current and future microwave polarimeters, such as the CCAT Observatory, Simons Observatory, and CMB-S4.

1. Introduction

1.1. Cosmic birefringence

Detection of cosmic birefringence, or the rotation of linearly polarized light as it propagates over cosmological distances through empty space, would be evidence for charge, parity, and time reversal symmetry (CPT) violating physics [1, 2]. Proposed pseudoscalar fields produced by axion-like dark matter candidate particles that couple to electromagnetism would modify the dispersion relation for electromagnetic waves in vacuum [3]. This modified dispersion relation would differ for left and right circularly-polarized light, inducing a rotation in the linear polarization angle of photons that grows linearly with propagation distance. The cross-correlation between cosmic microwave background (CMB) polarization in E and B modes is sensitive to cosmic birefringence or other parity-violating physics [4]. In a universe with no parity-violating

Orbital analysis of stars in the nuclear stellar disc of the Milky Way

N. Nieuwmunster^{1,2}, M. Schultheis¹, M. Sormani³, F. Fragkoudi⁴, F. Nogueras-Lara⁵, R. Schödel⁶, and P. McMillan^{2,7}

¹ Université Côte d'Azur, Observatoire de la Côte d'Azur, Laboratoire Lagrange, CNRS, Blvd de l'Observatoire, 06304 Nice, France
e-mail: niels.nieuwmunster@oca.eu

² Division of Astrophysics, Department of Physics, Lund University, Box 43, SE-22100 Lund, Sweden

³ Department of Physics, University of Surrey, Guildford GU2 7XH, UK

⁴ Institute for Computational Cosmology, Department of Physics, Durham University, South Road, Durham DH1 3LE, UK

⁵ Max-Planck Institute for Astronomy, Königstuhl 17, 69117 Heidelberg, Germany

⁶ Instituto de Astrofísica de Andalucía (CSIC), Glorieta de la Astronomía s/n, 18008 Granada, Spain

⁷ School of Physics & Astronomy, University of Leicester, University Road, Leicester, LE1 7RH, UK

Received December 18, 2023; accepted February 21, 2024

ABSTRACT

Context. While orbital analysis studies were so far mainly focused on the Galactic halo, it is possible now to do these studies in the heavily obscured region close to the Galactic Centre.

Aims. We aim to do a detailed orbital analysis of stars located in the nuclear stellar disc (NSD) of the Milky Way allowing us to trace the dynamical history of this structure.

Methods. We integrated orbits of the observed stars in a non-axisymmetric potential. We used a Fourier transform to estimate the orbital frequencies. We compared two orbital classifications, one made by eye and the other with an algorithm, in order to identify the main orbital families. We also compared the Lyapunov and the frequency drift techniques to estimate the chaoticity of the orbits.

Results. We identified several orbital families as chaotic, z -tube, x -tube, banana, fish, saucer, pretzel, 5:4, and 5:6 orbits. As expected for stars located in a NSD, the large majority of orbits are identified as z -tubes (or as a sub-family of z -tubes). Since the latter are parented by x_2 orbits, this result supports the contribution of the bar (in which x_2 orbits are dominant in the inner region) in the formation of the NSD. Moreover, most of the chaotic orbits are found to be contaminants from the bar or bulge which would confirm the predicted contamination from the most recent NSD models.

Conclusions. Based on a detailed orbital analysis, we were able to classify orbits into various families, most of which are parented by x_2 -type orbits, which are dominant in the inner part of the bar.

1. Introduction

The nuclear stellar disc (NSD) is a dense stellar structure in the centre of the Milky Way and surrounds the massive nuclear star cluster (NSC) with its central massive black hole (Launhardt et al. 2002). The NSD is a flattened disc with a radius of ~ 200 pc and a scale height of ~ 50 pc (Launhardt et al. 2002; Nishiyama et al. 2013, Gallego-Cano et al. 2020). Increasing evidence is reported that the NSD is a distinct structure from the NSC and the nuclear bulge: Nogueras-Lara et al. (2020) determined the SFH in the NSD using the GALACTICNUCLEUS data (Nogueras-Lara et al. 2018) and analysing the luminosity function together with stellar evolutionary models. They found that $\sim 80\%$ of the stars formed more than 8 Gyr ago, followed by a quenching phase and then by a recent star formation activity, about 1 Gyr ago, in which about 5% of the NSD mass was formed. While most of studies agree that the NSD has a relatively early formation time, the detailed SFH is still under discussion (see e.g. Nogueras-Lara et al. 2023, Sanders et al. 2023), and much more work is clearly needed.

By using a large sample of KMOS observations in the NSD (Fritz et al. 2021), Schultheis et al. (2021) found a difference in the chemistry, that is, in the metallicity distribution function, between the NSC, NSD, and the nuclear bulge that reinforces a different formation scenario of the NSD. Furthermore, they found some evidence that metal-rich stars may have formed in the central molecular zone, while metal-poor stars show more similarities to the surrounding Galactic bulge.

Kinematic studies relying on radial velocity measurements or proper motion studies show evidence that the NSD is rotating (see e.g. Lindqvist et al. 1992, Schönrich et al. 2015, Fritz et al. 2021, Shahzamanian et al. 2022). Linking the rotation to the chemistry, Schultheis et al. (2021) found that metal-rich stars rotate faster than metal-poor stars, with some hints of counter-rotation for the most metal-poor stars.

Extragalactic studies showed that many barred galaxies host nuclear discs or rings (Gadotti et al. 2019, 2020). So far, the most likely formation scenario of a nuclear disc, called inside-out formation, is linked to the galactic bar (Bittner et al. 2020). According to this scenario, a nuclear disc is a built up from a series of gaseous rings (i.e. nuclear rings) that grow in radius over time. The growth is caused by the gas that is moved towards the galactic centre by the bar.

Based on the 3D velocities, Sormani et al. (2022) constructed axisymmetric self-consistent equilibrium dynamical models of the NSD providing the full 6D distribution function (position and velocity) of the NSD. These models provide the best description of the rotation curve in the innermost few hundred parsecs of the Milky Way, and they are implemented in the AGAMA (Vasiliev 2019) software package.

A powerful method for obtaining a complete picture of the properties of the individual orbits is the so-called frequency analysis (Laskar 1993, Valluri & Merritt 1998, Vasiliev 2013) where the three fundamental frequencies of the orbit oscillation can be extracted accurately. This frequency analysis can be used to distinguish between regular and chaotic orbits and to classify the

Investigating Ionization in the Intergalactic Medium

BRAD KOPLITZ ¹, ANJALI RAMESH ¹ AND SANCHAYEETA BORTHAKUR ¹

¹*School of Earth & Space Exploration, Arizona State University, 781 Terrace Mall, Tempe, AZ 85287, USA*

ABSTRACT

The Intergalactic Medium (IGM) contains >50% of the baryonic mass of the Universe, yet the mechanisms responsible for keeping the IGM ionized has not been fully explained. Hence, we investigate ion abundances from the largest blind QSO absorption catalog for clouds that show C IV, N V, and O VI simultaneously. The wavelength range of present UV spectrographs, however, make it possible to probe C IV and O VI over a small range of redshift ($z \approx 0.12 - 0.15$). As a result, we only have five IGM absorbing clouds, yet these provide a powerful and representative tool to probe the IGM ionization state. We found one cloud to be in collisional ionization equilibrium while three of five showed signs of being produced by non-equilibrium processes, specifically conductive interfaces and turbulent mixing layers. None of the models we explore here were able to reproduce the ionization state of the remaining system. Energetic processes, such as galactic feedback from star formation and AGN winds, would be excellent candidates that can cause such widespread ionization.

Keywords: Intergalactic medium (813); Quasar absorption line spectroscopy (1317); Collisional processes (2286); Photoionization (2060)

1. INTRODUCTION

Most of the baryonic matter in the universe is not contained in stars and galaxies, but is between galaxies in a dilute, multi-phase, ionized gas called the Intergalactic Medium (IGM; Meiksin 2009; McQuinn 2016). This reservoir is thought to regulate the growth of galaxies by facilitating accretion (e.g., Kereš et al. 2005; Dekel & Birnboim 2006; Dekel et al. 2009; Hafen et al. 2022; Decataldo et al. 2023) and harboring a large fraction of what gets ejected through outflows (e.g., Martin 1999; Martin et al. 2010; Steidel et al. 2010; Peeples et al. 2014; Oppenheimer et al. 2016). Many studies of this diffuse gas have been done at intermediate redshifts ($z \approx 2 - 5$) to allow for the simultaneous detection of multiple Lyman transitions of hydrogen as well as metals such as C IV or O VI (e.g., Bergeron et al. 1994; Jannuzi et al. 1998; Lopez et al. 1999; Richter et al. 2004; Simcoe et al. 2004; Adelberger et al. 2005; Chen et al. 2005; Danforth & Shull 2008; Turner et al. 2014; Morrison et al. 2021; Borthakur 2022).

Metals, in particular, are an import tracer of this diffuse gas as 70% of Ly α forest absorbers are found to have accompanying metal lines (Simcoe et al. 2004) and can be present even when the Lyman series is weak (Danforth et al. 2016). The IGM at $z \approx 2 - 3$ is also known to be enriched with carbon and oxygen (e.g., Davé et al. 1998; Aracil et al. 2004; Pieri et al. 2006) and is thought to have retained it and other metals to the present day (e.g., Richter et al. 2004; Aguirre et al. 2008; Danforth & Shull 2008; Tripp et al. 2008; Muzahid et al. 2012; Danforth et al. 2016). Additionally, metal absorption lines are often unsaturated, allowing for more components within a single cloud to be detected (e.g., Chen & Mulchaey 2009; Danforth et al. 2016; Pachat et al. 2017; Sankar et al. 2020; Ahoranta et al. 2021). This makes metals a key window into the ionization processes that govern the IGM.

Furthermore, analyzing metals has revealed the multiphase nature of the IGM (e.g., Heckman et al. 2002; Savage et al. 2005; Narayanan et al. 2009; Shull et al. 2012; Ahoranta et al. 2021; Haislmaier et al. 2021), with a cool $T \approx 10^{4.5}$ K phase and a warm-hot phase, known as the warm ionized IGM or WHIM, at $T \approx 10^5 - 10^6$ K. The presence of the WHIM could indicate that collisions are likely a dominate ionization process in the IGM since many of these processes produces radiatively cooling gas

On the properties and implications of collapse-driven MHD turbulence

Enrique Vázquez-Semadeni,^{1*} Yue Hu,² Siyao Xu,³ Rubén Guerrero-Gamboa¹ and Alex Lazarian²

¹*Instituto de Radioastronomía y Astrofísica, Universidad Nacional Autónoma de México, Apdo. Postal 3-72, Morelia, Michoacán, 58090, México*

²*Department of Astronomy, University of Wisconsin-Madison, Madison, WI 53706, USA*

³*Department of Physics, University of Florida, 2001 Museum Rd., Gainesville, FL 32611, USA*

4 March 2024

ABSTRACT

We investigate the driving of MHD turbulence by gravitational contraction using simulations of an idealized, initially spherical, isothermal, globally magnetically supercritical molecular cloud core in the presence of initial transonic and trans-Alfvénic turbulence. To this end, we perform a Helmholtz decomposition of the velocity field, and investigate the evolution of its solenoidal and compressible parts, as well as of the velocity component along the gravitational acceleration vector, which can be considered as the infall component of the velocity field. We find that: 1) In spite of being supercritical, the core first contracts to a sheet perpendicular to the mean magnetic field, and the sheet itself collapses. 2) The solenoidal component of the turbulence remains at roughly its initial level throughout the of the simulation, while the compressible component increases continuously. This implies that turbulence does *not* dissipate towards the center of the core. 3) The distribution of simulation cells in the B - ρ plane occupies a wide triangular region at low densities, bounded below by the expected trend for fast MHD waves ($B \propto \rho$, applicable for high local Alfvénic Mach number M_A) and above by the trend expected for slow waves ($B \sim \text{constant}$, applicable for low local M_A). At high densities, the distribution follows a single trend $B \propto \rho^{\gamma_{\text{eff}}}$, with $1/2 < \gamma_{\text{eff}} < 2/3$, as expected for gravitational compression. 4) The mass-to-magnetic flux ratio λ increases with the radius r out to which it is measured in the core, due to the different scalings of the mass and magnetic flux with r . At a fixed radius, λ increases with time due to the accretion of material along field lines. 5) The solenoidal energy fraction is much smaller than the total turbulent component, indicating that the collapse drives the turbulence mainly compressibly, even in directions orthogonal to that of the collapse.

Key words: MHD – Gravitation – Turbulence – ISM: clouds – stars: formation

1 INTRODUCTION

In recent years, the driving of turbulence by gravitational collapse at various scales has received considerable attention, in particular in relation to whether enough gravitational energy is available in the collapsing material for driving the turbulence in the central accreting objects, from the scale of accreting galactic disks to molecular clouds to protostellar disks (Klessen & Hennebelle 2010); whether it can act as a possible reservoir for the gravitational energy released during the collapse, so that this energy could be stored in the turbulence and possibly delay the collapse (e.g., Robertson & Goldreich 2012; Murray & Chang 2015; Murray et al. 2017; Li 2018; Xu & Lazarian 2020a), and what is its equivalent thermodynamic behavior (e.g., Vázquez-Semadeni et al. 1998; Guerrero-Gamboa & Vázquez-Semadeni 2020).

However, one issue that has not been studied in depth is whether the random motions driven by collapse really qualify as turbulence, exhibiting standard turbulence properties. Indeed, the nature of the driving in the collapse-driven case is significantly different from that in other, more standard cases. For example, the energy-injection scale shrinks over time rather than being constant, at least during the prestellar stage of the collapse. In the particular case of the collapse of molecular cloud cores (objects of typical densities $n \sim 10^4 \text{ cm}^{-3}$

and sizes $\sim 0.1 \text{ pc}$), this can be understood because the prestellar stage of collapse in spherical geometry is characterized by a flat-density central core with a radius of the order of the Jeans length, at which the largest infall speeds also occur (e.g., Whitworth & Summers 1985; Keto & Caselli 2010; Naranjo-Romero et al. 2015). Since the central density increases over time, the Jeans length for the central density decreases over time. Thus, the energy-injection scale decreases over time, if it is of the order of the Jeans length, where the infall speed peaks.

In addition, if the energy-injection rate is of the order of the release rate of gravitational energy at the Jeans length, then it is also expected to vary over time, as it is given approximately by (Guerrero-Gamboa & Vázquez-Semadeni 2020)

$$\dot{E}_g \approx - \left(\frac{2|E_g|^3}{M_{L_J} L_J^2} \right)^{1/2}, \quad (1)$$

where L_J is the Jeans length at the central density, M_{L_J} is the mass contained within a radius $R = L_J$, and $E_g \approx GM^2(L_J)/L_J$ is the gravitational energy of this mass distribution. Therefore, since L_J decreases over time, both E_g and \dot{E}_g increase (in absolute value) over time (since M_J is expected to be constant). In summary, both the energy-injection scale and the energy-injection rate vary over time during the collapse, thus calling for an examination of whether the turbulence driven by gravitational contraction maintains the properties of turbulence driven at a fixed rate and scale. Indeed, Guerrero-

* E-mail: e.vazquez@irya.unam.mx

Numerical challenges for energy conservation in N -body simulations of collapsing self-interacting dark matter haloes

Moritz S. Fischer^{1,2}, Klaus Dolag^{1,3}, Hai-Bo Yu⁴

¹ Universitäts-Sternwarte, Fakultät für Physik, Ludwig-Maximilians-Universität München, Scheinerstr. 1, D-81679 München, Germany

e-mail: mfischer@usm.lmu.de

² Excellence Cluster ORIGINS, Boltzmannstrasse 2, D-85748 Garching, Germany

³ Max-Planck-Institut für Astrophysik, Karl-Schwarzschild-Str. 1, D-85748 Garching, Germany

⁴ Department of Physics and Astronomy, University of California, Riverside, California 92521, USA

Received XX Month, 20XX / Accepted XX Month, 20XX

ABSTRACT

Context. Dark matter (DM) haloes can be subject to gravothermal collapse if DM is not collisionless but has strong self-interactions. When the scattering is capable of efficiently transferring heat from the centre to the outskirts, the central region of the halo collapses and can reach densities much higher than those for collisionless DM. This phenomenon is potentially observable in studies of strong lensing. Current theoretical efforts are motivated by observations of surprisingly dense substructures. However, a comparison with observations requires accurate predictions. One method to obtain such predictions is to use N -body simulations. The collapsed haloes are extreme systems that pose severe challenges to state-of-the-art codes used in the field of self-interacting dark matter (SIDM).

Aims. In this work, we investigate the root of such problems with a focus on energy non-conservation. Moreover, we discuss strategies to avoid them.

Methods. We run N -body simulations with and without DM self-interactions of an isolated DM-only halo and change numerical parameters relevant to the accuracy of the simulation.

Results. We find that not only the numerical scheme for the DM self-interactions can lead to energy non-conservation but also the modelling of gravitational interaction and the time integration are problematic. The issues we found are: (a) particles changing their time step in a non-time-reversible manner; (b) the asymmetry in the tree-based gravitational force evaluation; (c) SIDM velocity kicks break the symplectic nature and time symmetry.

Conclusions. In principle, tuning the parameters of the simulation to achieve a high accuracy allows for conserving energy not only at early stages of the evolution but also at late ones. However, the cost of the simulations becomes prohibitively large. Some of the problems making the simulations of the gravothermal collapse phase inaccurate, can be overcome by choosing appropriate numerical schemes. However, others remain challenging. Our findings motivate further work on addressing the challenges in simulating strong dark matter self-interactions.

Key words. methods: numerical — dark matter

1. Introduction

Self-interacting dark matter (SIDM) is an alternative scenario to the collisionless cold dark matter (CDM) of the standard cosmological model, and it was originally proposed by Spergel & Steinhardt (2000) to address problems on small scales, i.e. galactic scales (for a review of small-scale problems see Bullock & Boylan-Kolchin 2017). Various signatures of dark matter (DM) scatterings are explored, e.g. the formation of density cores (e.g. Mastromarino et al. 2023), rounder halo shapes (e.g. Gonzalez et al. 2024) or DM–galaxy offsets in mergers of galaxy clusters (e.g. Sabarish et al. 2023). These features allow for constraining the particle physics properties of DM (e.g. Gopika & Desai 2023; Zhang et al. 2024; Wittman et al. 2023). For a review of SIDM, we refer the reader to Tulin & Yu (2018) and Adhikari et al. (2022).

Observations of surprisingly dense substructures (e.g. Vegetti et al. 2010; Meneghetti et al. 2020; Minor et al. 2021; Granata et al. 2022) motivate SIDM studies with relatively large cross-sections at low velocities. Potentially such models can explain objects denser than expected from CDM (e.g. Yang & Yu

2021; Nadler et al. 2023; Yang et al. 2023; Zeng et al. 2023). An SIDM halo can collapse due to an effective heat outflow arising from the self-interactions. When a system bound by self-gravity loses energy it becomes more compact and its velocity dispersion in the centre increases, i.e. it becomes hotter. This enhances the energy outflow even more. The gravothermal evolution of a self-gravitating system is well known from globular clusters (e.g. Lynden-Bell & Eggleton 1980). However, making accurate predictions by modelling the late stages of the collapse of SIDM haloes is challenging as we discuss in this paper.

N -body simulations provide a crucial way of making SIDM predictions and probing the available parameter space for SIDM models. Burkert (2000) developed the first SIDM simulation of that kind, which employs a Monte Carlo scheme. Further implementations of this scheme were followed (e.g. Kochanek & White 2000; Davé et al. 2001; Colin et al. 2002). The simulation techniques for SIDM have evolved since then. But all modern SIDM codes rely on a Monte Carlo scheme with the notable exception of Huo et al. (2020). Vogelsberger et al. (2012) and Rocha et al. (2013) largely improved the estimate of the scattering probability by using the actual phase space distribution.

MIGHTEE-H I: H I galaxy properties in the large scale structure environment at $z \sim 0.37$ from a stacking experiment

Francesco Sinigaglia,^{1,2,3,4*} Giulia Rodighiero,^{1,2} Ed Elson,⁵ Alessandro Bianchetti,^{1,2} Mattia Vaccari,^{6,7,8} Natasha Maddox,^{9,10} Anastasia A. Ponomareva,¹¹ Bradley S. Frank,^{6,7,12,13} Matt J. Jarvis,^{11,5} Barbara Catinella,^{14,15} Luca Cortese,^{14,15} Sambit Roychowdhury,¹⁶ Maarten Baes,¹⁷ Jordan D. Collier,^{7,18,19} Olivier Ilbert,²¹ Ali A. Khostovan,²² Sushma Kurapati,¹² Hengxing Pan,¹¹ Isabella Prandoni,⁸ Sambatriniaina H. A. Rajohnson,¹² Mara Salvato,²³ Srikrishna Sekhar,^{24,7} Gauri Sharma⁵

¹Department of Physics and Astronomy, Università degli Studi di Padova, Vicolo dell'Osservatorio 3, I-35122, Padova, Italy

²INAF - Osservatorio Astronomico di Padova, Vicolo dell'Osservatorio 5, I-35122, Padova, Italy

³Instituto de Astrofísica de Canarias, Calle Via Láctea s/n, E-38205, La Laguna, Tenerife, Spain

⁴Departamento de Astrofísica, Universidad de La Laguna, E-38206, La Laguna, Tenerife, Spain

⁵Department of Physics and Astronomy, University of the Western Cape, Robert Sobukwe Rd, 7535 Bellville, Cape Town, South Africa

⁶Inter-university Institute for Data Intensive Astronomy, Department of Physics and Astronomy, University of the Western Cape, 7535 Bellville, Cape Town, South Africa

⁷Inter-university Institute for Data Intensive Astronomy, Department of Astronomy, University of Cape Town, 7701 Rondebosch, Cape Town, South Africa

⁸INAF - Istituto di Radioastronomia, via Gobetti 101, 40129 Bologna, Italy

⁹School of Physics, H.H. Wills Physics Laboratory, Tyndall Avenue, University of Bristol, Bristol, BS8 1TL, UK

¹⁰Faculty of Physics, Ludwig-Maximilians-Universität, Scheinerstr. 1, 81679 Munich, Germany

¹¹Oxford Astrophysics, Denys Wilkinson Building, University of Oxford, Keble Rd, Oxford, OX1 3RH, UK

¹²Department of Astronomy, University of Cape Town, Private Bag X3, Rondebosch 7701, South Africa

¹³South African Radio Astronomy Observatory, 2 Fir Street, Black River Park, Observatory, 7925, South Africa

¹⁴International Centre for Radio Astronomy Research (ICRAR), University of Western Australia, 35 Stirling Highway, Crawley, WA 6009, Australia

¹⁵ARC Centre of Excellence for All-Sky Astrophysics in 3 Dimensions (ASTRO 3D), Australia

¹⁶University Observatory, Faculty of Physics, Ludwig-Maximilians-Universität, Scheinerstr. 1, 81679 München, Germany

¹⁷Sterrenkundig Observatorium, Universiteit Gent, Krijgslaan 281 S9, 9000 Gent, Belgium

¹⁸School of Science, Western Sydney University, Locked Bag 1797, Penrith, NSW 2751, Australia

¹⁹CSIRO, Space and Astronomy, PO Box 1130, Bentley, WA, 6102, Australia

²⁰Centre for Radio Astronomy Techniques and Technologies, Department of Physics and Electronics, Rhodes University, PO Box 94, Makhanda 6140, South Africa

²¹Aix Marseille Univ, CNRS, CNES, LAM, Marseille, France

²²Laboratory for Multiwavelength Astrophysics, School of Physics and Astronomy, Rochester Institute of Technology, 84 Lomb Memorial Drive, Rochester, NY 14623, USA

²³Max Planck Institute for Extraterrestrial Physics, Giessebachstrasse 1, D-857498, Garching, Germany

²⁴National Radio Astronomy Observatory, 1003 Lopezville Road, Socorro, NM 87801, USA

Accepted XXX. Received YYY; in original form ZZZ

arXiv:2403.00734v1 [astro-ph.GA] 1 Mar 2024

© 2023 The Authors

2 *F. Sinigaglia et al.*

ABSTRACT

We present the first measurement of HI mass of star-forming galaxies in different large scale structure environments from a blind survey at $z \sim 0.37$. In particular, we carry out a spectral line stacking analysis considering 2875 spectra of colour-selected star-forming galaxies undetected in HI at $0.23 < z < 0.49$ in the COSMOS field, extracted from the MIGHTEE-HI Early Science datacubes, acquired with the MeerKAT radio telescope. We stack galaxies belonging to different subsamples depending on three different definitions of large scale structure environment: local galaxy overdensity, position inside the host dark matter halo (central, satellite, or isolated), and cosmic web type (field, filament, or knot). We first stack the full star-forming galaxy sample and find a robust HI detection yielding an average galaxy HI mass of $M_{\text{HI}} = (8.12 \pm 0.75) \times 10^9 M_{\odot}$ at $\sim 11.8\sigma$. Next, we investigate the different subsamples finding a negligible difference in M_{HI} as a function of the galaxy overdensity. We report an HI excess compared to the full sample in satellite galaxies ($M_{\text{HI}} = (11.31 \pm 1.22) \times 10^9$, at $\sim 10.2\sigma$) and in filaments ($M_{\text{HI}} = (11.62 \pm 0.90) \times 10^9$). Conversely, we report non-detections for the central and knot galaxies subsamples, which appear to be HI-deficient. We find the same qualitative results also when stacking in units of HI fraction (f_{HI}). We conclude that the HI amount in star-forming galaxies at the studied redshifts correlates with the large scale structure environment.

Key words: galaxies: formation – evolution – emission lines, cosmology: large scale structure of Universe

1 INTRODUCTION

The evolution of galaxies, including mass assembly, star formation and morphological transformations of galaxies, is known to be strongly connected to the availability of fresh molecular Hydrogen (H_2) supporting the star formation process. Star-forming H_2 clumps arise via gravitational instability and collapse out of large diffuse HI clouds, whose existence represents therefore the necessary condition to trigger the formation of new stars. While part of the galactic HI can be produced by either recombination of ionized Hydrogen (HII) or other reprocessing mechanisms of the internal gas, hydrogen accretion on galaxies from the circumgalactic and intergalactic media plays a fundamental role to ensure the availability of HI reservoirs.

In this context, the environment surrounding a galaxy and its physical conditions may assume a primary importance in regulating gas accretion and removal, galaxy interactions, and other relevant evolutionary phenomena. In fact, galaxy surveys have measured the position of millions of galaxies and demonstrated that at cosmological scales smaller than a few hundred Mpc, matter is no longer uniformly distributed, but forms a filamentary pattern called *cosmic web* (e.g. Bond et al. 1996), which is constituted by filaments interconnecting massive knots and surrounding large voids. In the standard inflationary Λ CDM scenario, the cosmic web naturally emerges from gravitational instability and growth of cosmic structures (e.g. Zel'dovich 1970; Bond et al. 1996), happening as a result of the presence of small inhomogeneities in the primordial matter field. While driven by dark matter, the formation of the cosmic web also involves baryons. As a result, gas exhibits different properties (temperature, rotation and dispersion velocities, ionization state, among others) depending on the environment it lives in (e.g. Martizzi et al. 2019; Galárraga-Espinosa et al. 2020; Sinigaglia et al. 2021, and references therein), and therefore it may impact the evolution of the galaxies it feeds in a different way. The large scale structure has been shown to correlate with several galaxy properties, for instance star formation history and quenching

(e.g. Darvish et al. 2014; Vulcani et al. 2019; Kraljic et al. 2020; Malavasi et al. 2022, and references therein), colour (e.g. Chen et al. 2017; Pandey & Sarkar 2020), stellar mass and its assembly (e.g. Alpaslan et al. 2016; Chen et al. 2017; Malavasi et al. 2017; Kraljic et al. 2020), angular momentum magnitude and alignment (e.g. Libeskind et al. 2012; Tempel & Libeskind 2013; Krolewski et al. 2019; Barsanti et al. 2022), and the stellar mass - gas metallicity relation (Donnan et al. 2022), among others.

In this picture, the role of HI has been investigated only in the nearby universe at $z < 0.1$ (e.g. Kleiner et al. 2017; Crone Odekon et al. 2018; Tudorache et al. 2022; Cortese et al. 2021), while it has remained unexplored at higher redshift due to the difficulty in detecting the 21-cm emission line and the general lack of deep complete spectroscopic surveys covering volumes large enough to reconstruct the cosmological large-scale environment.

Statistical approaches such as spectral line stacking (Zwaan et al. 2001) can be adopted to exploit the property of Gaussianity of the noise and to extract a global mean HI signal out of the investigated population, at the expense of the information about the HI content of the individual galaxies constituting the sample. The spectral line stacking technique has been widely used in the last decades to probe the HI content in galaxies at different redshift, and in particular to unveil correlations such as the presence and abundance of HI in galaxy clusters (Zwaan 2000; Chengalur et al. 2001; Lah et al. 2009; Healy et al. 2021), HI galaxy scaling relations (Fabello et al. 2011a; Geréb et al. 2015; Brown et al. 2017; Sinigaglia et al. 2022c; Bera et al. 2022; Chowdhury et al. 2022c; Bera et al. 2023; Pan et al. 2023), the HI mass function (Pan et al. 2020; Bera et al. 2022), the M_{HI} content of AGN host galaxies (Fabello et al. 2011a; Geréb et al. 2013, 2015), the baryonic Tully-Fisher relation (Meyer et al. 2016), the HI cosmic density evolution with redshift (Lah et al. 2007; Delhaize et al. 2013; Kanekar et al. 2016; Rhee et al. 2018; Bera et al. 2019; Chowdhury et al. 2020; Chen et al. 2021; Chowdhury et al. 2021, 2022a,b,c), the HI content of galaxy groups and the $M_{\text{HI}}-M_{\text{halo}}$ relation (Guo et al. 2020; Chauhan et al. 2021; Roychowdhury et al. 2022; Dev et al. 2023), among others. Spectral line stacking has been successfully applied to other

* Email: francesco.sinigaglia@phd.unipd.it

Lessons learned from NASA’s DART impact about disrupting rubble-pile asteroids

S. D. Raducan¹, M. Jutzi¹, C. C. Merrill², P. Michel^{3,4}, Y. Zhang⁵, M. Hirabayashi⁶, and A. Mainzer⁷

¹Space Research and Planetary Sciences, Physikalisches Institut, University of Bern, Bern, Switzerland

²Sibley School of Mechanical and Aerospace Engineering, Cornell University, Ithaca, NY, USA

³Université Côte d’Azur, Observatoire de la Côte d’Azur, CNRS, Laboratoire Lagrange, Nice, France

⁴The University of Tokyo, Department of Systems Innovation, School of Engineering, Tokyo, Japan

⁵Department of Climate and Space Sciences and Engineering, University of Michigan, Ann Arbor, MI 48109, USA

⁶Georgia Institute of Technology, Atlanta, GA, USA

⁷University of Arizona, Lunar and Planetary Laboratory, Tucson, AZ, USA

Abstract

We present a series of numerical simulations using a shock physics smoothed particle hydrodynamics (SPH) code, investigating energetic impacts on small celestial bodies characterised by diverse internal structures, ranging from weak and homogeneous compositions to rubble-pile structures with varying boulder volume packing. Our findings reveal that the internal structure of these rubble-pile bodies significantly influences the impact outcomes. Specifically, we observe that the same impact energy can either catastrophically disrupt a target with a low boulder packing ($\lesssim 30$ vol%), or result in the ejection of only a small fraction of material from a target with the same mass but high boulder packing ($\gtrsim 40$ vol%). This finding highlights the pivotal role played by the rubble-pile structure, effectively acting as a bulk shear strength, which governs the size and behaviour of the resulting impact. Consequently, understanding and characterising the internal structure of asteroids will be of paramount importance for any future efforts to deflect or disrupt an asteroid on a collision course with Earth.

1 Introduction

In a significant milestone for human history, NASA’s DART (Double Asteroid Redirection Test) spacecraft impacted the asteroid Dimorphos, the secondary of the Didymos asteroid binary system, on September 26th, 2022 (UTC) (Chabot et al., 2023; Daly et al., 2023; Rivkin et al., 2021). The impact resulted in an orbital change of approximately 33 minutes of Dimorphos around its primary, Didymos (Thomas et al., 2023). This groundbreaking achievement demonstrated the capability to redirect the trajectory of a potentially hazardous asteroid, paving the way for future efforts to protect our planet from potential threats. The DART spacecraft with a mass of 580 kg collided with Dimorphos at 6.15 km/s, hitting the target within 25 m of the centre of figure of the asteroid and at an incidence angle of only $16.7 \pm 7.4^\circ$ from the average surface normal. This angle was calculated based on a 1.5-meter radius around the impact point, using data from the global digital terrain model (DTM) of the impact site (Daly et al., 2023).

Transiting exoplanets with the Mid-InfraRed Instrument on board the James Webb Space Telescope: From simulations to observations

A. Dyrek¹, E. Ducrot^{1*}, P-O. Lagage¹, P. Tremblin², S. Kendrew³, J. Bouwman⁴, and R. Bouffet¹

¹ Université Paris Cité, Université Paris-Saclay, CEA, CNRS, AIM, F-91191, Gif-sur-Yvette, France

² Université Paris-Saclay, UVSQ, CNRS, CEA, Maison de la Simulation, 91191, Gif-sur-Yvette, France

³ European Space Agency, Space Telescope Science Institute, 3700 San Martin Dr., Baltimore, MD 21218, USA

⁴ Max Planck Institute for Astronomy (MPIA), Königstuhl 17, D-69117 Heidelberg, Germany

March 4, 2024

ABSTRACT

Context. The James Webb Space Telescope (JWST) has now started its exploration of exoplanetary worlds. In particular, the Mid-InfraRed Instrument (MIRI) with its Low-Resolution Spectrometer (LRS) carries out transit, eclipse, and phase-curve spectroscopy of exoplanetary atmospheres with an unprecedented precision in a so far almost uncharted wavelength range.

Aims. The precision and significance in the detection of molecules in exoplanetary atmospheres relies on a thorough understanding of the instrument itself and on accurate data reduction methods. This paper aims to provide a clear description of the instrumental systematics that affect observations of transiting exoplanets through the use of simulations.

Methods. We carried out realistic simulations of transiting-exoplanet observations with the MIRI LRS instrument that included the model of the exoplanet system, the optical path of the telescope, the MIRI detector performances, and instrumental systematics and drifts that could alter the atmospheric features we are meant to detect in the data. After we introduce our pipeline, we show its performance on the transit of L168-9b, a super-Earth-sized exoplanet observed during the commissioning of the MIRI instrument.

Results. This paper provides a better understanding of the data themselves and of the best practices in terms of reduction and analysis through comparisons between simulations and real data. We show that simulations validate the current data-analysis methods. Simulations also highlight instrumental effects that impact the accuracy of our current spectral extraction techniques. These simulations are proven to be essential in the preparation of JWST observation programs and help us to assess the detectability of various atmospheric and surface scenarios.

Key words. Space vehicles: Instruments – Methods: Data analysis – Techniques: Spectroscopic – Planets and satellites: Atmospheres – Infrared: Planetary systems – Planets and satellites: Terrestrial planets

1. Introduction

The long-awaited James Webb Space Telescope (JWST) was launched on 25 December 2021. Equipped with its four instruments NIRISS¹, NIRCам², NIRSpec³, and MIRI⁴ it has now started to provide its first observations in the infrared. Each instrument has different modes for photometry or spectroscopy and covers various regions of the spectra, from 0.6 to 28 μm . In particular, the instrument that covers the longer wavelengths is MIRI.

The demands for observations with MIRI are high, and a significant part of the observations is dedicated to exoplanet observations, either directly or indirectly. When considering all Cycle 1 programs proposed for Early Release Science (ERS), Guaranteed Time Observation (GTO) and General Observations (GO), 115 distinct transiting exoplanets are being observed with the JWST. Twenty-one of these 115 planets have been observed with the MIRI instrument, 9 of them with the Low Resolution Spec-

trometer (LRS) (Kendrew et al. 2015). These programs with MIRI LRS are mainly focused on small planets as this instrument is best-suited to observing the thermal emission of temperate rocky or sub-Neptune planets. The scientific impact of these observations is very high as the characterisation of rocky temperate exoplanetary atmospheres has just started (Greene et al. 2023; Zieba et al. 2023). In this context, the knowledge of the instrumental effects of MIRI LRS and its expected performance is key.

Although the quality of the first LRS data for transiting exoplanets is exquisite (Bouwman et al. 2022), some instrumental effects remain poorly understood. In this regard, being able to create realistic simulated data that account for the specificity of the MIRI LRS data brings remarkable prospects in understanding these effects, in strengthening our data reduction methods, and in providing accurate spectra for characterising the physical and chemical composition of atmospheres. More than this, simulations are able to depict the accuracy of complex retrieval methods. The physical parameters that we expect to retrieve from the analysis of our simulations must be consistent with those that were injected. In addition, these simulations are very valuable for the community for confidently preparing upcoming obser-

* Paris Region Fellow, Marie Skłodowska-Curie Action

¹Near-InfraRed Imager and Slitless Spectrograph

²Near-InfraRed Camera

³Near-InfraRed Spectrograph

⁴Mid-InfraRed Instrument

Physical properties of asteroid Dimorphos as derived from the DART impact

S.D. Raducan^{*1}, M. Jutzi¹, A.F. Cheng², Y. Zhang³, O. Barnouin², G. S. Collins⁴, R. T. Daly², T. M. Davison⁴, C.M. Ernst², T. L. Farnham³, F. Ferrari⁵, M. Hirabayashi^{6,7}, K. M. Kumamoto⁸, P. Michel^{9,10}, N. Murdoch¹¹, R. Nakano^{6,7}, M. Pajola¹², A. Rossi¹³, H. F. Agrusa^{9,3}, B. W. Barbee¹⁴, M. Bruck Syal⁸, N. L. Chabot², E. Dotto¹⁵, E. G. Fahnestock¹⁶, P. H. Hasselmann¹⁵, I. Herreros¹⁷, S. Ivanovski¹⁸, J.-Y. Li¹⁹, A. Lucchetti¹², R. Luther²⁰, J. Ormö¹⁷, M. Owen⁸, P. Pravec²¹, A. S. Rivkin², C. Q. Robin¹¹, P. Sánchez²², F. Tusberti¹², K. Wünnemann²⁰, A. Zinzi²³, E. Mazzotta Epifani¹⁵, C. Manzoni²⁴, and B. H. May²⁴

¹Space Research and Planetary Sciences, Physics Institute, University of Bern, Switzerland

²Johns Hopkins University Applied Physics Laboratory, Laurel, MD, USA

³Department of Aerospace Engineering, University of Maryland, College Park, MD, USA

⁴Department of Earth Science and Engineering, Imperial College London, UK

⁵Department of Aerospace Science and Technology, Politecnico di Milano, Italy

⁶Guggenheim School of Aerospace Engineering, Georgia Institute of Technology, Atlanta, GA, USA

⁷Department of Aerospace Engineering, Auburn University, Auburn, AL, USA

⁸Lawrence Livermore National Laboratory, Livermore, CA, USA

⁹Université Côte dAzur, Observatoire de la Côte dAzur, CNRS, Laboratoire Lagrange, Nice, France

¹⁰University of Tokyo, Department of Systems Innovation, School of Engineering, Tokyo, Japan

¹¹Institut Supérieur de l'Aéronautique et de l'Espace (ISAE-SUPAERO), Université de Toulouse, Toulouse, France

¹²INAF-OAPD Astronomical Observatory of Padova, Italy

¹³IFAC-CNR, Sesto Fiorentino (FI), Italy

¹⁴NASA/Goddard Space Flight Center, Greenbelt, MD, USA

¹⁵INAF-Osservatorio Astronomico di Roma, Italy

¹⁶Jet Propulsion Laboratory, California Institute of Technology, Pasadena, CA, USA

¹⁷Centro de Astrobiología (CAB), CSIC-INTA, Carretera de Ajalvir km4, 28850 Torrejón de Ardoz, Spain

¹⁸INAF-Osservatorio Astronomico di Trieste, Trieste, Italy

¹⁹Planetary Science Institute, Tucson, AZ, USA

²⁰Museum für Naturkunde, Leibniz Institute for Evolution and Biodiversity Science, Berlin, Germany

²¹Astronomical Institute of the Czech Academy of Sciences, Czech Republic

²²Colorado Center for Astrodynamics Research, University of Colorado Boulder, Boulder, CO, USA

²³Agenzia Spaziale Italiana; ASI Space Science Data Center, Italy

²⁴London Stereoscopic Company, London, UK

1

On September 26, 2022, NASA's Double Asteroid Redirection Test (DART) mission successfully impacted Dimorphos, the natural satellite of the binary near-Earth asteroid (65803) Didymos. Numerical simulations of the impact provide a means to explore target surface material properties and structures, consistent with the observed momentum deflection efficiency, ejecta cone geometry, and ejected mass. Our simulation, which best matches observations, indicates that Dimorphos is weak, with a cohesive strength of less than a few pascals (Pa), similar to asteroids (162173) Ryugu and (101955) Bennu. We find that a bulk density of Dimorphos, ρ_B , lower than $\approx 2400 \text{ kg/m}^3$, and a low volume fraction of boulders ($\lesssim 40 \text{ vol}\%$) on the surface and in the shallow subsurface, are consistent with measured data from the DART experiment. These findings suggest Dimorphos is a rubble pile that might have formed through rotational mass shedding and re-accumulation from Didymos. Our simulations indicate that the DART impact caused global deformation and resurfacing of Dimorphos. ESA's upcoming Hera mission may find a re-shaped asteroid, rather than a well-defined crater.

Introduction

DART was a planetary defense mission to demonstrate the feasibility of using a kinetic impactor to change the trajectory of an asteroid [1]. The impact was successful and highly effective, resulting in a reduction in Dimorphos' orbital period around Didymos, which was initially 11 hours and 55 minutes, by 33 ± 1 minutes [2]. The LICIACube Unit Key Explorer (LUKE) instrument onboard the cubesat [3] captured images of the system between 29 and 320 seconds after impact, revealing filamentary streams of ejecta and other complex patterns that expanded for several kilometres from the impact site [4]. Moreover, the dramatic brightening of the Didymos system by solar illumination of released impact ejecta was observed from ground- and space-based telescopes [2, 5, 6] for many weeks after the impact.

The obtained 33-minute reduction in the binary orbital period [2] implies a momentum transfer to Dimorphos that exceeded the incident momentum of the DART spacecraft by a factor β , ranging from 2.2 to 4.9, depending on the mass of Dimorphos [7] – which is not currently known but will be measured by the ESA Hera spacecraft in early 2027 [8]. The β parameter is defined as the ratio of the target momentum increment after the impact to the impactor momentum, in the direction of the net ejecta momentum, and is related to the additional thrust from the production of impact ejecta [7, 9]. β strongly depends on impact conditions (i.e., impact velocity and impact angle [1]) and target material properties, such as strength, porosity, bulk density and target surface structure [10–12].

The spacecraft information, location and impact angle for the DART impact are well understood [1]. However, the mass and surface properties of Dimorphos are still ambiguous. It was not possible to directly measure the mass and bulk density of Dimorphos with DART or LICIACube. Instead, these parameters were estimated from the total mass of the binary system, derived from Dimorphos' orbit [13], and updated volume estimates of Didymos and Dimorphos provided by DART [1]. The estimated bulk density of Dimorphos ranges from $\rho_B = 1500$ to 3300 kg/m^3 [1, 7].

The surface material properties and sub-surface structure of Dimorphos were also not directly measured. However, these target parameters are vital for understanding the impact process and transforming the kinetic impactor method from a full-scale experiment by DART into a well-understood and reliable mitigation technique for planetary defence. Moreover, knowledge of the material properties of Dimorphos relates to the origin and evolution of the Didymos-Dimorphos system, as well as the overall characteristics of rubble-pile asteroids and binary asteroid systems.

In this work, we simulate the DART impact numerically and compare the results with observations to infer the properties of Dimorphos. We performed numerical simulations of the DART impact using the shock physics code *Bern SPH* [14, 15] over a range of assumed sets of material properties and interior structures for Dimorphos. We represented the DART spacecraft as a low-density spherical projectile of equivalent mass (see Projectile section in Methods), and the impact velocity and angle were also kept fixed. We simulated the asteroid's response to the DART impact for up to one hour after the time of impact, using the numerical approach developed in [16, 17] to model late-stage, low-speed deformation (see Modelling approach for the late stage evolution in Methods). *Bern SPH*'s fast-integration scheme was

*sabina.raducan@unibe.ch

New probe of non-Gaussianities with primordial black hole induced gravitational waves

Theodoros Papanikolaou,^{1,2,3,*} Xin-Chen He,^{4,5,6,†} Xiao-Han Ma,^{4,5,6,7,‡}
 Yi-Fu Cai,^{4,5,6,§} Emmanuel N. Saridakis,^{3,4,5,8,¶} and Misao Sasaki^{7,9,10,**}

¹*Scuola Superiore Meridionale, Largo San Marcellino 10, 80138 Napoli, Italy*

²*Istituto Nazionale di Fisica Nucleare (INFN), Sezione di Napoli, Via Cinthia 21, 80126 Napoli, Italy*

³*National Observatory of Athens, Lofos Nymfon, 11852 Athens, Greece*

⁴*Department of Astronomy, School of Physical Sciences,
 University of Science and Technology of China, Hefei 230026, China*

⁵*CAS Key Laboratory for Researches in Galaxies and Cosmology, School of Astronomy and Space Science,
 University of Science and Technology of China, Hefei, Anhui 230026, China*

⁶*Deep Space Exploration Laboratory, Hefei 230088, China*

⁷*Kavli Institute for the Physics and Mathematics of the Universe (WPI),*

UTIAS The University of Tokyo, Kashiwa, Chiba 277-8583, Japan

⁸*Departamento de Matemáticas, Universidad Católica del Norte,
 Avda. Angamos 0610, Casilla 1280 Antofagasta, Chile*

⁹*Center for Gravitational Physics, Yukawa Institute for Theoretical Physics, Kyoto University, Kyoto 606-8502, Japan*

¹⁰*Leung Center for Cosmology and Particle Astrophysics, National Taiwan University, Taipei 10617*

We propose a new probe of primordial non-Gaussianities (NGs) through the observation of gravitational waves (GWs) induced by ultra-light ($M_{\text{PBH}} < 10^9 \text{g}$) primordial black holes (PBHs). Interestingly enough, the existence of primordial NG can leave imprints on the clustering properties of PBHs and the spectral shape of induced GW signals. Focusing on a scale-dependent local-type NG, we identify a distinct double-peaked GW energy spectrum that, contingent upon M_{PBH} and the abundance of PBHs at the time of formation, denoted as $\Omega_{\text{PBH},f}$, may fall into the frequency bands of upcoming GW observatories, including LISA, ET, SKA, and BBO. Thus, such a signal can serve as a novel portal for probing primordial NGs. Intriguingly, combining BBN bounds on the GW amplitude, we find for the first time the joint limit on the product of the effective non-linearity parameter for the primordial tri-spectrum, denoted by $\bar{\tau}_{\text{NL}}$, and the primordial curvature perturbation power spectrum $\mathcal{P}_{\mathcal{R}}(k)$, which reads as $\bar{\tau}_{\text{NL}} \mathcal{P}_{\mathcal{R}}(k) < 4 \times 10^{-20} \Omega_{\text{PBH},f}^{-17/9} \left(\frac{M_{\text{PBH}}}{10^4 \text{g}} \right)^{-17/9}$.

Introduction – Primordial non-Gaussianity (NG), as a fundamental statistical characteristic of primordial perturbations, arises from potential nonlinear processes during inflation [1–4]. The investigation of primordial NG yields crucial insights into the early Universe, elucidating inflationary dynamics and field contents across a wide range of energy scales, complementing the search for primordial gravitational waves (GWs) [5–8]. As indicators of NG, high-order correlations of primordial perturbations have been well studied theoretically [9–11]. However, despite the cosmic microwave background (CMB) measurements constraining primordial bispectra (e.g. $f_{\text{NL}}^{\text{local}} = -0.9 \pm 5.1$ [12]), the observational limits on other higher-order correlations (namely trispectra) remain loose.

Facing the limitations in observing high-order correlations, primordial black holes (PBHs) [13–15], originating from large amplitude curvature perturbations during inflation (see [16, 17] for recent reviews), may provide a loophole in measuring primordial NGs on small scales. Currently, most efforts are made to constrain the PBH abundances across a broad range of mass scales [18]. Meanwhile, the distribution of PBHs has recently drawn much attention because Gaussian primordial fluctuations

cannot lead to clustering beyond a Poisson distribution [19–22]. This implies that a possible detection of nontrivial spatial distributions of PBHs can strongly hint the existence of primordial NGs [23–31].

Notably, ultra-light PBHs with $M_{\text{PBH}} < 10^9 \text{g}$, which evaporate before Big Bang Nucleosynthesis (BBN) and hence escape from the current direct observational constraints on their abundance, can be produced in the early Universe [32–37] and give rise to an early matter-dominated (eMD) phase before BBN [32, 33, 38, 39], yielding a very rich phenomenology [40–44]. In particular, a PBH-matter dominated universe can be modeled as a gravitationally interacting gas on large scales, possessing its own density perturbations [40, 41]. As the PBH evaporation triggers a nearly sudden transition from the eMD era to the late radiation-dominated (IRD) era [45, 46], these perturbations can evolve into large, rapidly oscillating inhomogeneities, resulting in observable induced GWs [40, 41, 47]. If there were primordial NGs, these GWs would be influenced and thus retain their information appropriately.

As a demonstration, in this Letter we consider a general scale-dependent local-type trispectrum that can amplify the two-point correlation function of PBHs on large

Resolved ALMA observations of the water content of the inner astronomical units of HL Tau

Stefano Facchini^{1*}, Leonardo Testi², Elizabeth Humphreys^{3,4,5},
Mathieu Vander Donckt⁶, Andrea Isella⁷, Ramon Wrzosek⁷,
Alain Baudry⁸, Malcom D. Gray⁹, Anita M. S. Richards¹⁰,
Wouter Vlemmings¹¹

^{1*}Dipartimento di Fisica, Università degli Studi di Milano, via Celoria
16, Milano, Italy.

²Dipartimento di Fisica e Astronomia “Augusto Righi”, Università di
Bologna, Viale Berti Pichat 6/2, Bologna, Italy.

³ European Southern Observatory, Karl-Schwarzschild-Strasse 2,
Garching bei München, D-85748, Germany.

⁴ Joint ALMA Observatory, Alonso de Cordova 3107, Santiago, Chile.

⁵ European Southern Observatory (ESO) Vitacura, Alonso de Cordova
3107, Santiago, Chile.

⁶ Space sciences, Technologies & Astrophysics Research (STAR)
Institute, University of Liège, Liège, Belgium.

⁷Department of Physics and Astronomy, Rice University, 6100 Main
Street, MS-108, Houston, 77005, TX, USA.

⁸Laboratoire d’Astrophysique de Bordeaux, Univ. de Bordeaux, CNRS,
B18N, allée Geoffroy Saint-Hilaire, Pessac, 33615, France.

⁹ National Astronomical Research Institute of Thailand, 260 Moo 4, T.
Donkaew, A. Maerim, Chiangmai, 50180, Thailand.

¹⁰JBCA, University of Manchester, M13 9PL, UK.

¹¹Department of Space, Earth and Environment, Chalmers University of
Technology, Göteborg, SE-412 96, Sweden.

*Corresponding author(s). E-mail(s): stefano.facchini@unimi.it;

1

Abstract

The water molecule is a key ingredient in the formation of planetary systems, with the water snowline being a favorable location for the growth of massive planetary cores. Here we present ALMA data of the ringed protoplanetary disk orbiting the young star HL Tauri that show centrally peaked, bright emission from water vapour in three distinct transitions of the main water isotopologue. The spatially and spectrally resolved water content probes gas in a thermal range down to the water sublimation temperature. Our analysis implies a stringent lower limit of 3.7 Earth oceans of water vapour available within the inner 17 astronomical units. We show that our observations probe the water content in the atmosphere of the disk, due to the high dust column density and absorption, and indicate the main water isotopologue as the best tracer to spatially resolve water vapour in protoplanetary disks.

The water molecule is undoubtedly one of the most important molecular species in the whole universe. Being an extremely efficient solvent, water had a key role in the emergence of life as we know it on our planet. For this reason, the chemical characterization of exoplanetary atmospheres is often focused on detecting this particular molecular species [1–3]. Formed by the common H and O atoms, water plays a fundamental role in the physics of the formation of planetary systems, due to its very high abundance in both gaseous and icy forms [4, 5]. Theoretical models predict that at the location of the phase transition from gaseous to solid form, dust grains can accumulate and grow very efficiently, promoting the fast formation of planetary cores. Across this particular radial location, called ‘snowline’, grains can drastically change their drift and fragmentation velocity, composition, and opacity. In synergy with vapour radial diffusion [6], these physical discontinuities can lead to the accumulation and growth of dust grains into planetesimals [7, 8]. The position of the snowline also defines the chemistry of the available planet building blocks. Since the H₂O molecule is the major elemental oxygen carrier in the disk, its desorption and freezing affect the elemental C/O ratio in both the gas and solid phases [9–11].

Because of its large binding energy, the H₂O transition from ice to gas happens a few astronomical units (au) from the young star where the midplane temperatures are

2

Atmospheric entry and fragmentation of small asteroid 2024 BX1: Bolide trajectory, orbit, dynamics, light curve, and spectrum

P. Spurný¹, J. Borovička¹, L. Shrubný¹, M. Hankey², and R. Neubert³

¹ Astronomical Institute of the Czech Academy of Sciences, Fričova 298, 25165 Ondřejov, Czech Republic
e-mail: pavel.spurny@asu.cas.cz

² American Meteor Society LTD, 54 Westview Crescent, Geneseo, New York 14454, USA

³ Thüringer Landessternwarte Tautenburg, Sternwarte 5, D-07778 Tautenburg, Germany

Received 26 February 2024, Accepted xxx 2024

ABSTRACT

Asteroid 2024 BX1 was the eighth asteroid discovered shortly before colliding with the Earth. The associated bolide was recorded by dedicated instruments of the European Fireball Network and the AllSky7 network on January 21, 2024 at 0:32:38–44 UT. Here we report a comprehensive analysis of this instrumentally observed meteorite fall, which occurred as predicted west of Berlin, Germany. The atmospheric trajectory was quite steep with an average slope to the Earth’s surface 75°6. The entry speed was 15.20 km s⁻¹. The heliocentric orbit calculated from the bolide data agrees very well with the asteroid data. However, the bolide was fainter than expected for a reportedly meter-sized asteroid. The absolute magnitude reached -14.4 and the entry mass was estimated to 140 kg. The recorded bolide spectrum was low in iron from what an enstatite-rich meteorite was expected. Indeed, the recovered meteorites, called Ribbeck, were classified as aubrites. The high albedo of enstatite (E-type) asteroids can explain the size discrepancy. The asteroid was likely smaller than 0.5 meter and should be rather called a meteoroid. During the atmospheric entry, the meteoroid severely fragmented into much smaller pieces already at a height of 55 km under the aerodynamic pressure of 0.12 MPa. The primary fragments were then breaking-up again, most frequently at heights 39–29 km (0.9–2.2 MPa). Numerous small meteorites and up to four stones larger than 100g were expected to land. Within a few days of publishing the strewnfield dozens of meteorites were found in the area we predicted.

Key words. Meteorites, meteors, meteoroids – Minor planets, asteroids: individual: 2024 BX1

1. Introduction

On January 20, 2024 at 21:48 UT, Krisztián Sárneczky at the Hungarian Piszkestető Observatory discovered a small asteroid 2024 BX1 (M. P. C. Staff 2024), which was on a collision course with Earth, as quickly confirmed by subsequent observations at more than ten other European observatories. As determined by imminent impact monitoring services such as JPL’s Scout, ESA’s Meerkat and MPC’s internal warning system, the collision should have occurred around 0:33 UT in the area of Berlin, Germany (M. P. C. Staff 2024). This prediction was subsequently confirmed by the observation of a very bright bolide, which, from locations where it was clear and within range of the bolide, was seen by a large number of mostly casual observers, but was also recorded by instruments, both by casual witnesses and by systems specifically designed for the purpose of bolide observations.

Here we give a detailed analysis of this bolide using our standard methods as it was recorded by the various instruments of the European Fireball Network and partly by the cameras of the AllSky7 system. We will first describe what instrumental records we used and from where, then how we determined the atmospheric trajectory and heliocentric orbit of the body, its velocity and deceleration in the atmosphere, its luminosity and fragmentation, where its debris hit the Earth’s surface, and also what its composition and physical properties were from the analysis of the spectra we took. Finally, we summarize the main results and compare them to both the pre-collisional analyses and to what

meteorites were found. Since the meteorites have already been officially named Ribbeck (Meteoritical Bulletin 2024), we call the observed bolide the same hereafter.

2. Instruments and data

In this case, the bolide fortunately passed within range of the core of the European Fireball Network (EN), especially the Czech part of the EN, whose centre is located at the Ondřejov Observatory. Details regarding the current distribution of stations of this longest running fireball network in the world and the modern instruments it uses for bolide observations can be found in Spurný et al. (2017) or Borovička et al. (2022). This part of the EN currently consists of 21 stations located in the Czechia (15), Slovakia (4), and partly also Germany (1) and Austria (1). As to the observation of this event we were also lucky in the weather because it was clear over almost all stations. In order to accurately determine the bolide’s trajectory in the atmosphere and its original orbit in the solar system (in this case it was only a confirmation of the already known orbit from pre-atmospheric observations), we used a total of 17 optical records (10 digital all-sky images and 7 video records) of which 15 were from the EN and 2 video records were from the German part of the AllSky7 network (Hankey et al. 2020). The image of the bolide taken by the video camera from the EN station Frýdlant is shown in Fig. 1. In addition, we used 3 radiometric and 3 spectral records exclusively from the EN network to determine asteroid properties. In Fig. 2, as an example of an important record,

The First Spatially-resolved Detection of ¹³CN in a Protoplanetary Disk and Evidence for Complex Carbon Isotope Fractionation

TOMOHIRO C. YOSHIDA ^{1,2} HIDEKO NOMURA ^{1,2} KENJI FURUYA ¹ RICHARD TEAGUE ³ CHARLES J. LAW ^{4,*}
TAKASHI TSUKAGOSHI ⁵ SEOKHO LEE ⁶ CHRISTIAN RAB ^{7,8} KARIN I. ÖBERG ⁹ AND RYAN A. LOOMIS ¹⁰

¹National Astronomical Observatory of Japan, 2-21-1 Osawa, Mitaka, Tokyo 181-8588, Japan

²Department of Astronomical Science, The Graduate University for Advanced Studies, SOKENDAI, 2-21-1 Osawa, Mitaka, Tokyo 181-8588, Japan

³Department of Earth, Atmospheric, and Planetary Sciences, Massachusetts Institute of Technology, Cambridge, MA 02139, USA

⁴Department of Astronomy, University of Virginia, Charlottesville, VA 22904, USA

⁵Faculty of Engineering, Ashikaga University, Ohmae-cho 268-1, Ashikaga, Tochigi, 326-8558, Japan

⁶Korea Astronomy and Space Science Institute (KASI), 776 Daedeokdae-ro, Yuseong-gu, Daejeon 34055, Republic of Korea

⁷University Observatory, Faculty of Physics, Ludwig-Maximilians-Universität München, Scheinerstr. 1, 81679 Munich, Germany

⁸Max-Planck-Institut für extraterrestrische Physik, Giessenbachstrasse 1, 85748 Garching, Germany

⁹Center for Astrophysics | Harvard & Smithsonian, 60 Garden St., Cambridge, MA 02138, USA

¹⁰National Radio Astronomy Observatory, 520 Edgemont Rd., Charlottesville, VA 22903, USA

Submitted to ApJ

ABSTRACT

Recent measurements of carbon isotope ratios in both protoplanetary disks and exoplanet atmospheres have suggested a possible transfer of significant carbon isotope fractionation from disks to planets. For a clearer understanding of the isotopic link between disks and planets, it is important to measure the carbon isotope ratios in various species. In this paper, we present a detection of the ¹³CN $N = 2 - 1$ hyperfine lines in the TW Hya disk with the Atacama Large Millimeter/submillimeter Array. This is the first spatially-resolved detection of ¹³CN in disks, which enables us to measure the spatially resolved ¹²CN/¹³CN ratio for the first time. We conducted non-local thermal equilibrium modeling of the ¹³CN lines in conjunction with previously observed ¹²CN lines to derive the kinetic temperature, H₂ volume density, and column densities of ¹²CN and ¹³CN. The H₂ volume density is found to range between $(4 - 10) \times 10^7 \text{ cm}^{-3}$, suggesting that CN molecules mainly reside in the disk upper layer. The ¹²CN/¹³CN ratio is measured to be 70^{+9}_{-6} at $30 < r < 80$ au from the central star, which is similar to the ¹²C/¹³C ratio in the interstellar medium. However, this value differs from the previously reported values found for other carbon-bearing molecules (CO and HCN) in the TW Hya disk. This could be self-consistently explained by different emission layer heights for different molecules combined with preferential sequestration of ¹²C into the solid phase towards the disk midplane. This study reveals the complexity of the carbon isotope fractionation operating in disks.

Keywords: Protoplanetary disks (1300); Astrochemistry (75)

1. INTRODUCTION

The physical and chemical structure of protoplanetary disks are now routinely well-studied using the unique capabilities of the Atacama Large Millime-

ter/submillimeter Array (ALMA). It is now clear that the rings and gaps are ubiquitous in the mm dust (e.g., the DSHARP project, Andrews et al. 2018; Huang et al. 2018a) and molecular gas distributions (e.g., the MAPS project, Öberg et al. 2021; Law et al. 2021a) of large planet-forming disks. At least some of these substructures are thought to be related to ongoing planet formation in these disks. The next question that we

tomohiroyoshida.astro@gmail.com

* NASA Hubble Fellowship Program Sagan Fellow

The GAPS Programme at TNG

LV: A He I survey of close-in giant planets hosted by M-K dwarf stars with GIANO-B[★]

G. Guilluy¹, M. C. D'Arpa^{2,3}, A. S. Bonomo¹, R. Spinelli², F. Biassoni^{4,5}, L. Fossati⁶, A. Maggio², P. Giacobbe¹, A. F. Lanza⁷, A. Sozzetti¹, F. Borsa⁵, M. Rainer⁵, G. Micela², L. Affer², G. Andreuzzi^{8,9}, A. Bignamini¹⁰, W. Boschin^{8,11,12}, I. Carleo^{11,12}, M. Ceconi⁸, S. Desidera¹³, V. Fardella^{2,3}, A. Ghedina⁸, G. Mantovan^{13,14}, L. Mancini^{1,15,16}, V. Nascimbeni¹³, C. Knapic¹⁰, M. Pedani⁸, A. Petralia², L. Pino¹⁷, G. Scandariato⁷, D. Sicilia⁷, M. Stangret¹³, and T. Zingales^{13,14}

(Affiliations can be found after the references)

Received date ; Accepted date

ABSTRACT

Context. Atmospheric escape plays a fundamental role in shaping the properties of exoplanets. The metastable near-infrared (nIR) helium triplet at 1083.3 nm (He I) is a powerful proxy of extended and evaporating atmospheres.

Aims. We used the GIARPS (GIANO-B + HARPS-N) observing mode of the Telescopio Nazionale Galileo to search for He I absorption in the upper atmospheres of five close-in giant planets hosted by the K and M dwarf stars of our sample, namely WASP-69 b, WASP-107 b, HAT-P-11 b, GJ 436 b, and GJ 3470 b.

Methods. We focused our analysis on the nIR He I triplet, performing high-resolution transmission spectroscopy by comparing the in-transit and out-of-transit observations. In instances where nightly variability in the He I absorption signal was identified, we investigated the potential influence of stellar magnetic activity on the planetary absorption signal by searching for variations in the H α transmission spectrum.

Results. We spectrally resolve the He I triplet and confirm the published detections for WASP-69 b ($3.91 \pm 0.22\%$, 17.6σ), WASP-107 b ($8.17^{+0.80}_{-0.76}\%$, 10.5σ), HAT-P-11 b ($1.36 \pm 0.17\%$, 8.0σ), and GJ 3470 b ($1.75^{+0.39}_{-0.36}\%$, 4.7σ). We do not find evidence of extra absorption for GJ 436 b. We observe night-to-night variations in the He I absorption signal for WASP-69 b, associated with variability in H α , which likely indicates the influence of pseudo-signals related to stellar activity. Additionally, we find that the He I signal of GJ 3470 b originates from a single transit observation, thereby corroborating the discrepancies found in the existing literature. An inspection of the H α line reveals an absorption signal during the same transit event.

Conclusions. By combining our findings with previous analyses of GIANO-B He I measurements of planets orbiting K dwarfs, we explore potential trends with planetary and stellar parameters that are thought to affect the absorption of metastable He I. Our analysis is unable to identify clear patterns, thus emphasising the necessity for additional measurements and the exploration of potential additional parameters that may be important in controlling He I absorption in planetary upper atmospheres.

Key words. planets and satellites: atmospheres – techniques: spectroscopic - methods: observational - infrared: planetary systems

1. Introduction

The atmospheres of exoplanets orbiting close to their host stars can be significantly influenced by stellar irradiation which can cause the upper atmospheric layers to expand and, in some cases, even evaporate (e.g., [Bourrier & des Etangs 2018](#)). Atmospheric loss due to photo-evaporation could have featured the close-in exoplanets demographic carving both the Neptunian Desert, i.e. the dearth of planets with sizes between terrestrial and jovian close to the host stars ([Lecavelier Des Etangs 2007](#); [Davis & Wheatley 2009](#); [Szabó & Kiss 2011](#); [Beaugé & Nesvorný 2013](#)) and the radius gap, which separates the dense super-Earths from the larger and puffer mini-Neptunes ([Fulton et al. 2017](#); [Fulton & Petigura 2018](#)). The pioneering investigations on atmospheric escape took place two decades ago (e.g., [Vidal-Madjar](#)

[et al. 2003, 2004](#)). These studies focused on the Ly- α transition of Hydrogen, which is the dominant element in hot gas giants' atmospheres. The atomic hydrogen resulting from thermal dissociation of H₂, absorbs the stellar X-ray and extreme ultraviolet (EUV; together XUV) radiation in the thermosphere significantly increasing the local temperature, which finally can lead to atmospheric expansion and escape. Yet, Ly- α observations are both contaminated by interstellar medium absorption (ISM) and geocoronal emission, which pose challenges to the interpretations of the observations.

[Seager & Sasselov \(2000\)](#) and [Oklopčić & Hirata \(2018\)](#) identified the He I 2³S triplet at 1083.3 nm (referred to as He I) as a robust diagnostic for studying atmospheric expansion and possibly mass loss. This tracer resides in a region of the near-infrared (nIR) spectrum unaffected by both ISM and geocoronal emissions. Since the groundbreaking discovery of an extended atmosphere surrounding the super-Neptune WASP-107 b ([Spake et al. 2018](#)), the field has made tremendous strides, with nearly 40 planets to date being searched for the presence of He I ([Dos Santos 2023](#)). However, despite this quite large sample, the un-

[★] Based on observations made with the Italian Telescopio Nazionale Galileo (TNG) operated on the island of La Palma by the Fundacion Galileo Galilei of the INAF at the Spanish Observatorio Roque de los Muchachos of the IAC in the frame of the program Global Architecture of the Planetary Systems (GAPS).

X-Shaped Radio Galaxies: Probing Jet Evolution, Ambient Medium Dynamics, and Their Intricate Interconnection

Gourab Giri^{1,2,*}, Christian Fendt³, Kshitij Thorat¹, Gianluigi Bodo⁴, Paola Rossi⁴

¹*Department of Physics, University of Pretoria, Private Bag X20, Hatfield 0028, South Africa*

²*South African Radio Astronomy Observatory, 2 Fir St, Black River Park, Observatory 7925, South Africa*

³*Max Planck Institute for Astronomy, Königstuhl 17, D-69117 Heidelberg, Germany*

⁴*INAF/Osservatorio Astrofisico di Torino, Strada Osservatorio 20, 10025 Pino Torinese, Italy*

Correspondence*:

Gourab Giri; Christian Fendt

gourab.giri@up.ac.za; fendt@mpia.de

ABSTRACT

This review explores the field of X-shaped radio galaxies (XRGs), a distinctive subset of winged radio sources that are identified by two pairs of jetted lobes which aligned by a significant angle, resulting in an inversion-symmetric structure. These lobes, encompassing active (primary) and passive (secondary) phases, exhibit a diverse range of properties across the multiple frequency bands, posing challenges in discerning their formation mechanism. The proposed mechanisms can broadly be categorized into those related either to a triaxial ambient medium, into which the jet propagates, or to a complex, central AGN mechanism, where the jet is generated. The observed characteristics of XRGs as discovered in the most substantial sample to date, challenge the idea that there is universal process at work that produces the individual sources of XRGs. Instead, the observational and numerical results rather imply the absence of an universal model and infer that distinct mechanisms may be at play for the specific sources. By scrutinizing salient and confounding properties, this review intends to propose the potential direction for future research to constrain and constrict individual models applicable to XRGs.

Keywords: galaxies: active, (galaxies:) quasars: supermassive black holes, galaxies: jets, ISM: jets and outflows, radio continuum: galaxies, X-rays: galaxies: clusters, galaxies: clusters: intracluster medium, (magnetohydrodynamics) MHD

1 INTRODUCTION

The examination of emission spectrum observed from a galaxy allows for the categorization of galaxies into two primary types: normal and active galaxies. The emission from the core of a normal galaxy primarily arises from stars characterized by a black-body spectrum and is comparable to the emission from the rest of the galaxy. However, in active galaxies, the emission from the central region (Active Galactic Nuclei; AGN) is much higher, $\sim 100 - 1000$ times greater than the emission from other regions of the galaxy, and produces

Broadband spectral and temporal study of Ton 599 during the brightest January 2023 flare

Aaqib Manzoor^{1*}, Zahir Shah^{2†}, Sunder Sahayanathan^{3,4}, Naseer Iqbal¹ & Athar A. Dar^{1,2}

¹Department of Physics, University of Kashmir, Srinagar 190006, India.

²Department of Physics, Central University of Kashmir, Ganderbal 191201, India.

³Astrophysical Sciences Division, Bhabha Atomic Research Center, Mumbai 400085, India.

⁴Homi Bhabha National Institute, Mumbai 400094, India.

Accepted XXX. Received YYY; in original form ZZZ

ABSTRACT

In this work, we provide a detailed analysis of the broadband temporal and spectral properties of the blazar Ton 599 by using the observations from *Fermi*-LAT and *Swift*-XRT/UVOT telescopes, during its brightest γ -ray flaring. The one-day bin γ -ray light curve exhibits multiple substructures with asymmetric and symmetric profiles. Notably, the γ -ray light curve shows a maximum flux of $3.63 \times 10^{-6} \text{ ph cm}^{-2} \text{ s}^{-1}$ on MJD 59954.50, which is the highest flux ever observed from this source. The correlation between the γ -ray flux and γ -ray spectral indices suggests a moderate harder when the brighter trend. Taking γ -ray light curve as the reference, a strong correlation is observed with X-ray, optical, and UV energies. Additionally, the γ -rays and optical/UV emissions exhibit higher variability compared to X-rays. To understand the parameter variation during the active state of the source, we conducted a statistical broadband spectral modelling of the source in 10 flux intervals of equal duration. A one-zone leptonic model involving synchrotron, synchrotron-self-Compton, and external-Compton processes successfully reproduces the broadband SED in each of these flux intervals. We observed that the flux variation during the active state is mainly associated with the variation in the magnetic field and the particle spectral indices.

Key words: radiation mechanisms: non-thermal – galaxies: active – individual: Ton 599 – gamma-rays: galaxies.

1 INTRODUCTION

Blazars are radio-loud Active Galactic Nuclei (AGN) with a powerful relativistic jet inclined close to the observer’s line of sight. These are powered by a supermassive black hole (SMBH) located at their centre (Urry & Padovani 1995). The small angle of inclination of the relativistic jet induces Doppler boosting in blazar emission, leading to distinctive observational features in all the energy bands (Böttcher et al. 2013; Ulrich et al. 1997). The temporal variability of blazars extends from years (Raiteri et al. 2013) to minutes (Aharonian et al. 2007; Albert et al. 2007). Blazars are categorized into two main classes: Flat Spectrum Radio Quasars (FSRQs) and BL Lacertae (BL Lacs) objects, FSRQs are characterised by prominent emission line features, whereas BL Lacs typically display either weak or no emission line features (Urry & Padovani 1995).

Blazars display a distinctive broadband spectral energy distribution (SED) marked by two prominent broad peaks. The first peak is typically observed in the Optical/UV/X-ray energy spectrum, while the subsequent peak is observed in the γ -ray energy range (Fossati et al. 1998; Mao et al. 2016). The lower energy peak results from the synchrotron cooling of electrons within the blazar jet, while investigations into the precise mechanisms governing the high energy emission are still ongoing. The high energy peak in the SED is generally associated with the inverse-Compton (IC) scattering

(Abdo et al. 2010b). The seed photons for IC scattering can be the synchrotron photons from the jet, and IC scattering of synchrotron photons is described as synchrotron-self-Compton process (SSC: Jones et al. 1974; Ghisellini et al. 1985; Costamante & Ghisellini 2002)). They can also originate from outside the jet, and IC scattering of these photons is described as an external-Compton process (EC: Dermer et al. 1992; Sikora et al. 1994; Błażejowski et al. 2000; Shah et al. 2017a)). The outside photon sources primarily include the broad line region (BLR: Ghisellini & Madau 1996), dusty torus (Błażejowski et al. 2000; Ghisellini & Tavecchio 2008) and accretion disk (Dermer & Schlickeiser 1993; Boettcher et al. 1997). In some cases, the high energy component of blazar SED is explained with a hadronic model through proton synchrotron process and/or by pion decay processes (Mannheim & Biermann 1992; Mannheim 1993; Mücke & Protheroe 2001; Mücke et al. 2003). Generally, the preference for the leptonic model over the hadronic model typically stems from the considerable jet power demanded by the latter. (Böttcher et al. 2013; Petropoulou & Dermer 2016). The peak synchrotron frequency (ν_{syn}^p) for blazars in the $\nu - \nu f_\nu$ plot is an important observational feature that distinguishes FSRQs from BL Lacs (Fossati et al. 1998). For FSRQs ν_{syn}^p ranges between $10^{12.5}$ and $10^{14.5}$ Hz, while in BL Lacs its value is between 10^{13} and 10^{17} Hz (Abdo et al. 2010b). BL Lacs are categorised into three groups depending on the position of ν_{syn}^p within the SED: low-energy peaked BL Lacs (LBL) if ν_{syn}^p is below 10^{14} Hz, intermediate-energy peaked BL Lacs (IBL) if ν_{syn}^p falls between 10^{14} Hz and 10^{15} Hz, and high-

* E-mail: aqibmanzoor1111@gmail.com

† E-mail: shahzahir4@gmail.com

The EDIBLES Survey

VIII. Band profile alignment of diffuse interstellar bands

A. Ebenbichler¹, J. V. Smoker^{2,3}, R. Lallement⁴, A. Farhang⁵, N. L. J. Cox⁶, C. Joblin⁷, J. Th. van Loon⁸,
H. Linnartz^{9,*}, N. Przybilla¹, P. Ehrenfreund⁹, J. Cami^{10,11,12}, and M. Cordiner^{13,14}

¹ Universität Innsbruck, Institut für Astro- und Teilchenphysik, Technikerstr. 25/8, 6020 Innsbruck, Austria
e-mail: Alexander.Ebenbichler@uibk.ac.at

² European Southern Observatory, Alonso de Cordova 3107, Vitacura, Santiago, Chile

³ UK Astronomy Technology Centre, Royal Observatory, Blackford Hill, Edinburgh EH9 3HJ, UK

⁴ GEPI, Observatoire de Paris, PSL Research University, CNRS, Université Paris-Diderot, Sorbonne Paris Cité, Place Jules Janssen, 92195 Meudon, France

⁵ School of Astronomy, Institute for Research in Fundamental Sciences, 19395-5531 Tehran, Iran

⁶ Centre d'Etudes et de Recherche de Grasse, ACRI-ST, Av. Nicolas Copernic, Grasse 06130, France

⁷ Institut de Recherche en Astrophysique et Planétologie (IRAP), Université Toulouse III - Paul Sabatier, CNRS, CNES, 9 Av. du Colonel Roche, 31028 Toulouse Cedex 04, France

⁸ Lennard-Jones Laboratories, Keele University, ST5 5BG, UK

⁹ Laboratory for Astrophysics, Leiden Observatory, Leiden University, P.O. Box 9513, 2300 RA Leiden, The Netherlands

¹⁰ Department of Physics and Astronomy, The University of Western Ontario, London, ON N6A 3K7, Canada

¹¹ Institute for Earth and Space Exploration, The University of Western Ontario, London, ON N6A 3K7, Canada

¹² SETI Institute, 189 Bernardo Ave, Suite 100, Mountain View, CA 94043, USA

¹³ Astrochemistry Laboratory, NASA Goddard Space Flight Center, Code 691, 8800 Greenbelt Road, Greenbelt, MD 20771, USA

¹⁴ Department of Physics, The Catholic University of America, Washington, DC 20064, US

Received 7 December 2024; accepted 16 February 2024

ABSTRACT

Context. There have been many attempts to identify families of diffuse interstellar bands (DIBs) with perfectly correlating band strengths. Although major efforts have been made to classify broadly based DIB families and important insights have been gained, no family has been identified with sufficient accuracy or statistical significance to prove that a series of selected DIBs originates from the same carrier. This can be attributed in part to the exclusive use of equivalent widths to establish DIB families.

Aims. In a change of strategy, we search for DIBs that are highly correlated in both band strength *and* profile shape. This approach increases the chance of correlating DIBs being members of one family and originating from the same carrier molecule. We also search for correlations between DIB profile families and atomic interstellar lines, with the goal of further chemically constraining possible DIB carriers.

Methods. We adapted the well-known method of time-series alignment to perform a spectral alignment; that is, DIB alignment. In a second step, we analysed the alignment results using a clustering analysis. This method required a statistically significant data set of DIB sight lines. The ESO Diffuse Interstellar Bands Large Exploration Survey (EDIBLES) data were perfectly suited for this application.

Results. We report eight DIB families with correlating strengths and profiles, as well as four previously unreported DIBs in the visual range, found using DIB alignment. All profile family members show Pearson correlation coefficients in band strength higher than 0.9. In particular, we report the 6614 – 6521 Å DIB pair, in which both DIBs show the same triple-peak substructure and an unprecedented band strength Pearson correlation coefficient of 0.9935. The presented approach opens up new perspectives that can guide the laboratory search for DIB carriers.

Key words. dust, extinction – ISM: lines and bands – ISM: molecules – Line: profiles – Methods: data analysis

1. Introduction

At the time of writing, diffuse interstellar bands (DIBs) have been known for a little more than 100 years, since their first detection by Heger (1922). They originate from material, most probably large molecules in the gas phase, populating the interstellar medium (ISM) and show a good but not perfect correlation with interstellar extinction (Herbig 1995). Diffuse interstellar bands have been observed mostly in the visual wave-

length range (e.g. Hobbs et al. 2008, 2009), while more recently discovered DIBs were identified in the near-infrared (Geballe et al. 2011; Cox et al. 2014; Ebenbichler et al. 2022; Hamano et al. 2022). Close to 600 DIBs are known at this time (Fan et al. 2019), but only four have an unambiguously identified carrier molecule, the Buckminster fullerene cation C_{60}^+ (Foing & Ehrenfreund 1994; Campbell et al. 2015; Spieler et al. 2017; Cordiner et al. 2019). Over the last three decades, several DIB surveys have been reported (Herbig & Leka 1991; Jenniskens & Desert 1994; Tuairisg et al. 2000; Hobbs et al. 2009; Cox et al. 2014), systematically extending the number of DIBs and updat-

* This paper is dedicated to the memory of Harold Linnartz, who passed away far too early on December 31, 2023.

Encounter circumstances of asteroid 99942 Apophis with the catalogue of known asteroids

PAUL WIEGERT^{1,2} AND BEN HYATT³

¹*Department of Physics and Astronomy
The University of Western Ontario
London Ontario Canada*

²*Institute for Earth and Space Exploration
The University of Western Ontario
London Ontario Canada*

³*Department of Physics and Astronomy
University of Waterloo
Waterloo Ontario Canada*

ABSTRACT

Asteroid 99942 Apophis will pass near the Earth in April 2029. Expected to miss our planet by a safe margin, that could change if Apophis' path was perturbed by a collision with another asteroid in the interim. Though the statistical chance of such a collision is minuscule, the high risk associated with Apophis motivates us to examine even this very unlikely scenario. In this work, we identify encounters between known asteroids and Apophis up to April 2029. Here we show that Apophis will encounter the 1300 m diameter asteroid 4544 Xanthus in December 2026. Their Minimum Orbit Intersection Distance (MOID) is less than 10,000 km, with Xanthus passing that closest point just four hours after Apophis. Though a direct collision is ruled out, the encounter is close enough that material accompanying Xanthus (if any) could strike Apophis. We also identify other asteroid encounters that deserve monitoring.

1. INTRODUCTION

Asteroid 99942 Apophis is one of the most studied near-Earth asteroids, stemming in large part from its close passages to the Earth. Initially thought to pose an impact danger, careful observations of its trajectory and properties have shown the risk of a collision with our planet during any of its upcoming close approaches in 2029 and 2036 is nil¹. However, these assessments e.g. [Farnocchia et al. \(2013\)](#); [Vokrouhlický et al. \(2015\)](#) among many others, have assumed that the motion of the asteroid will continue uninterrupted by any impulsive perturbations such as might arise from Apophis' collision with another asteroid.

The *a priori* probability of an asteroid colliding with Apophis during the period of a few years between now and that asteroid's close approach to Earth in 2029 is extremely low. Nevertheless, asteroid collisions are believed to occur. Asteroid families are thought to originate from a disruptive collision between asteroids ([Michel et al. 2001](#)). Also, the probable collision of smaller asteroids with larger ones has been observed at least twice in the recent past: P/2010 A2 is thought to have been struck in 2009 by an object a few meters in size ([Snodgrass et al. 2010](#); [Jewitt et al. 2010](#)), and asteroid 596 Scheila in 2011 by a 35 meter-sized body ([Ishiguro et al. 2011](#); [Jewitt et al. 2011](#)).

Even if a particular asteroid might not directly collide with Apophis, material accompanying that asteroid (whether gravitationally bound or not) could also pose some risk. Binary and multiple asteroids are seen among all asteroid populations, including the near-Earth asteroids ([Margot et al. 2015](#)). Solar system bodies may also shed material from their surface through processes driven by water ice sublimation. A comet is the classic example, and usually has a meteoroid stream composed of material shed from its surface travelling along its orbit. So-called 'active asteroids' may also release material through a wide array of mechanisms: impact disruption, rotational destabilization ([Hsieh 2017](#)), thermal fracturing ([Knight et al. 2016](#)), radiation pressure sweeping and electrostatic levitation ([Jewitt et al. 2015](#)). Active asteroids may release substantial amounts of mass. For example, active asteroid 3200 Phaethon shows

¹ <https://www.jpl.nasa.gov/news/nasa-analysis-earth-is-safe-from-asteroid-apophis-for-100-plus-years>

Water vapour masers in long-period variable stars

III. Mira variables U Her and RR Aql[★]

A. Winnberg¹, J. Brand², and D. Engels³

¹ Onsala Rymdobservatorium, Observatorievägen, S-43992 Onsala, Sweden

² INAF - Istituto di Radioastronomia & Italian ALMA Regional Centre, Via P. Gobetti 101, I-40129 Bologna, Italy

³ Hamburger Sternwarte, Universität Hamburg, Gojenbergsweg 112, D-21029 Hamburg, Germany

Received date; accepted date: 12/2/24

ABSTRACT

Context. Water maser emission is often found in the circumstellar envelopes of evolved stars, i.e. asymptotic-giant-branch stars and red supergiants with oxygen-rich chemistry. The H₂O emission shows strong variability in evolved stars of all these types.

Aims. We wish to understand the reasons for the strong variability of water masers emitted at 22 GHz. In this paper we study U Her and RR Aql as representatives of Mira variable stars.

Methods. We monitored U Her and RR Aql in the 22-GHz maser line of water vapour with single-dish telescopes. The monitoring period covered about two decades between 1990 and 2011, with a gap between 1997 and 2000 in the case of RR Aql. Observations were taken also in 1987 and 2015 before and after the period of contiguous monitoring. In addition, maps were obtained in the period 1990–1992 of U Her with the Very Large Array.

Results. We find that the strongest emission in U Her is located in a shell with boundaries 11 – 25 AU. The gas crossing time is 8.5 years. We derive lifetimes for individual maser clouds of ≤ 4 years, based on the absence of detectable line-of-sight velocity drifts of the maser emission. The shell is not evenly filled, and its structure is maintained on timescales much longer than those of individual maser clouds. Both stars show brightness variability on several timescales. The prevalent variation is periodic, following the optical variability of the stars with a lag of 2–3 months. Superposed are irregular fluctuations, of a few months' duration, of increased or decreased excitation at particular locations, and long-term systematic variations on timescales of a decade or more.

Conclusions. The properties of the maser emission are governed by those of the stellar wind while traversing the H₂O maser shell. Inhomogeneities in the wind affecting the excitation conditions and prevalent beaming directions likely cause the variations seen on timescales longer than the stellar pulsation period. We propose the existence of long-living regions in the shells, which maintain favourable excitation conditions on timescales of the wind crossing times through the shells or orbital periods of (sub-)stellar companions. The H₂O maser properties in these two Mira variables are remarkably similar to those in the semiregular variables studied in our previous papers, regarding shell location, outflow velocities, and lifetimes. The only difference is the regular brightness variations of the Mira variables caused by the periodic pulsation of the stars.

Key words. Water masers – Stars: AGB and post-AGB, U Her, RR Aql – circumstellar matter

1. Introduction

Maser emission of SiO, H₂O and OH is frequently found in the circumstellar shells or envelopes (CSEs) of oxygen-rich stars on the asymptotic giant branch (AGB) and in several red supergiants (RSGs). Within the CSEs, where conditions are favourable for the excitation of one or another of these masers depends on local density, temperature and dynamics and thus in practice on distance to the stellar surface. In the case of Mira variables the H₂O masers are typically found at radii of 5 to 50 AU (Bowers et al. 1993; Bowers & Johnston 1994; Colomer et al. 2000; Bains et al. 2003; Imai et al. 2003; Xu et al. 2022).

Early observing programs to monitor water masers found strong variability in their spectra (Schwartz et al. 1974; Berulis et al. 1983; Habing 1996, and references therein) particularly noticeable in the integrated maser emission (Berulis et al. 1998).

Send offprint requests to: J. Brand or D. Engels,
e-mail: brand@ira.inaf.it, dengels@hs.uni-hamburg.de

[★] The maser spectra and the VLA data cubes are available via anonymous ftp to cdsarc.u-strasbg.fr (130.79.128.5) or via <http://cdsarc.u-strasbg.fr/cgi-bin/qcat?J/A+A/>

Depending on the type of star observed and the duration of the monitoring, several types of variability can be recognised. The first and often most evident is a variation in delayed sync with the light variations of the central star (same period but with an offset in phase); superposed on this regular variation there often is an erratic variability, occurring on shorter timescales, including bursts of individual maser lines lasting weeks to months. If the monitoring takes place over long periods of time, variability in overall brightness of the maser emission may be detected, lasting many years (Brand et al. 2020) and may have repetitive patterns ('superperiods'; Rudnitskii & Pashchenko 2005).

Maps made from interferometric observations taken many months apart show that also the distribution of the maser emission sites in the CSEs changes considerably (Johnston et al. 1985). The masers are thought to reside in clouds of size 2–5 AU (Bains et al. 2003; Richards et al. 2011) embedded in the stellar wind, which in the case of Semiregular and Mira variables are identifiable for at most a few years (Bains et al. 2003; Winnberg et al. 2008). The crossing times through the H₂O maser shells, located within ~50 stellar radii, have timescales of decades, so that the disappearance of the emission of particular maser features after few years would

Cloud properties across spatial scales in simulations of the interstellar medium

Tine Colman^{1*}, Noé Brucy^{2,**}, Philipp Girichidis^{2,***}, Simon C. O. Glover², Milena Benedettini³, Juan D. Soler³, Robin G. Tress⁴, Alessio Traficante³, Patrick Hennebelle¹, Ralf S. Klessen^{2,5}, Sergio Molinari³, and Marc-Antoine Miville-Deschênes⁶

¹ AIM, CEA, CNRS, Université Paris-Saclay, Université Paris Diderot, Sorbonne Paris Cité, 91191 Gif-sur-Yvette, France

² Universität Heidelberg, Zentrum für Astronomie, Institut für Theoretische Astrophysik, Albert-Ueberle-Str. 2, 69120 Heidelberg, Germany

³ INAF – Istituto di Astrofisica e Planetologia Spaziali, via Fosso del Cavaliere 100, 00133 Roma, Italy

⁴ Institute of Physics, Laboratory for Galaxy Evolution and Spectral Modelling, EPFL, Observatoire de Sauvigny, Chemin Pegais 51, 1290 Versoix, Switzerland

⁵ Universität Heidelberg, Interdisziplinäres Zentrum für Wissenschaftliches Rechnen, Im Neuenheimer Feld 205, 69120 Heidelberg, Germany

⁶ Laboratoire de Physique de l'École Normale Supérieure, ENS, Université PSL, CNRS, Sorbonne Université, Université de Paris, F-75005 Paris, France

Received December 17, 2023; accepted xxxx xx, xxxx

ABSTRACT

Context. Molecular clouds (MC) are structures of dense gas in the interstellar medium (ISM), that extend from ten to a few hundred parsecs and form the main gas reservoir available for star formation. Hydrodynamical simulations of varying complexity are a promising way to investigate MC evolution and their properties. However, each simulation typically has a limited range in resolution and different cloud extraction algorithms are used, which complicates the comparison between simulations.

Aims. In this work, we aim to extract clouds from different simulations covering a wide range of spatial scales. We compare their properties, such as size, shape, mass, internal velocity dispersion and virial state.

Methods. We apply the HOP cloud detection algorithm on (M)HD numerical simulations of stratified ISM boxes and isolated galactic disk simulations that were produced using FLASH, RAMSES and AREPO.

Results. We find that the extracted clouds are complex in shape ranging from round objects to complex filamentary networks in all setups. Despite the wide range of scales, resolution, and sub-grid physics, we observe surprisingly robust trends in the investigated metrics. The mass spectrum matches in the overlap between simulations without rescaling and with a high-mass power-law index of -1 for logarithmic bins of mass, in accordance with theoretical predictions. The internal velocity dispersion scales with the size of the cloud as $\sigma \propto R^{0.75}$ for large clouds ($R \gtrsim 3$ pc). For small clouds we find larger σ compared to the power-law scaling, as seen in observations, which is due to supernova-driven turbulence. Almost all clouds are gravitationally unbound with the virial parameter scaling as $\alpha_{\text{vir}} \propto M^{-0.4}$, which is slightly flatter compared to observed scaling, but in agreement given the large scatter. We note that the cloud distribution towards the low-mass end is only complete if aggressive refinement is used that also refines more dilute gas rather than only collapsing regions.

Key words. molecular clouds – interstellar medium – code comparison

1. Introduction

Historically, (molecular) clouds have been considered important building blocks in the interstellar medium (ISM). The warm and diffuse gas condenses to form cloud-like structures with masses of $\sim 10^4 - 10^6 M_{\odot}$, typical sizes of $\sim 10 - 100$ pc, mean densities of $n_{\text{H}_2} \sim 100 \text{ cm}^{-3}$, and temperatures of $T \sim 10$ K (e.g. Solomon et al. 1987; Scoville et al. 1987; Dame et al. 1987, 2001, or Klessen & Glover 2016 for a review). Most of the mass in these conditions is in the form of molecular hydrogen, hence the term molecular clouds (MCs). However, most of the dynamical properties and the connection to hydrodynamical evolution does not require the gas being molecular. One particularly impor-

tant aspect connected to clouds is that they harbour the coldest (~ 10 K) regions of the ISM including the collapsing cores that eventually form stars.

For a long time, clouds were considered to be stable and long-lived structures that are gravitationally bound and supported against collapse by e.g. magnetic fields (e.g. Mouschovias & Spitzer 1976; Shu et al. 1987; Mouschovias & Ciolek 1999). This paradigm has changed. In particular, the idea that clouds are magnetically supported has given way to a picture in which they are formed by a combination of gravity and turbulence (e.g. Ballesteros-Paredes et al. 1999; Ballesteros-Paredes & Mac Low 2002; Mac Low & Klessen 2004; Krumholz & McKee 2005; Ballesteros-Paredes 2006; Hennebelle & Chabrier 2008; Ballesteros-Paredes et al. 2011; Vázquez-Semadeni et al. 2017, 2019), with the magnetic field playing an important but not dominant role (e.g. Crutcher 2012; Girichidis 2021; Whitworth et al.

* e-mail: tine.colman@cea.fr

** e-mail: noe.brucy@uni-heidelberg.de

*** e-mail: philipp@girichidis.com

Quijote-PNG: Optimizing the summary statistics to measure Primordial non-Gaussianity

GABRIEL JUNG,^{1,*} ANDREA RAVENNI,^{2,3,4,*} MICHELE LIGUORI,^{2,3,5} MARCO BALDI,^{6,7,8} WILLIAM R. COULTON,^{9,10}
FRANCISCO VILLAESCUSA-NAVARRO,^{11,12} AND BENJAMIN D. WANDELT^{13,11}

¹*Université Paris-Saclay, CNRS, Institut d’Astrophysique Spatiale, 91405, Orsay, France*

²*Dipartimento di Fisica e Astronomia “G. Galilei”, Università degli Studi di Padova, via Marzolo 8, I-35131, Padova, Italy*

³*INFN, Sezione di Padova, via Marzolo 8, I-35131, Padova, Italy*

⁴*ICC, University of Barcelona, IEEC-UB, Martí i Franquès, 1, E-08028 Barcelona, Spain*

⁵*Dipartimento di Fisica, Università degli Studi di Trento, Via Sommarive 14, I-38123 Povo (TN), Italy*

⁶*Dipartimento di Fisica e Astronomia, Alma Mater Studiorum - University of Bologna, Via Piero Gobetti 93/2, 40129 Bologna BO, Italy*

⁷*INAF - Osservatorio Astronomico di Bologna, Via Piero Gobetti 93/3, 40129 Bologna BO, Italy*

⁸*INFN - Istituto Nazionale di Fisica Nucleare, Sezione di Bologna, Viale Berti Pichat 6/2, 40127 Bologna BO, Italy*

⁹*Kavli Institute for Cosmology Cambridge, Madingley Road, Cambridge CB3 0HA, UK*

¹⁰*DAMTP, Centre for Mathematical Sciences, University of Cambridge, Wilberforce Road, Cambridge CB3 0WA, UK*

¹¹*Center for Computational Astrophysics, Flatiron Institute, 162 5th Avenue, New York, NY 10010, USA*

¹²*Department of Astrophysical Sciences, Princeton University, 4 Ivy Lane, Princeton, NJ 08544 USA*

¹³*Sorbonne Université, CNRS, UMR 7095, Institut d’Astrophysique de Paris, 98 bis bd Arago, 75014 Paris, France*

ABSTRACT

We apply a suite of different estimators to the QUIJOTE-PNG halo catalogues to find the best approach to constrain Primordial non-Gaussianity (PNG) at non-linear cosmological scales, up to $k_{\max} = 0.5 h \text{Mpc}^{-1}$. The set of summary statistics considered in our analysis includes the power spectrum, bispectrum, halo mass function, marked power spectrum, and marked modal bispectrum. Marked statistics are used here for the first time in the context of PNG study. We perform a Fisher analysis to estimate their cosmological information content, showing substantial improvements when marked observables are added to the analysis. Starting from these summaries, we train deep neural networks (NN) to perform likelihood-free inference of cosmological and PNG parameters. We assess the performance of different subsets of summary statistics; in the case of $f_{\text{NL}}^{\text{equil}}$, we find that a combination of the power spectrum and a suitable marked power spectrum outperforms the combination of power spectrum and bispectrum, the baseline statistics usually employed in PNG analysis. A minimal pipeline to analyse the statistics we identified can be implemented either with our ML algorithm or via more traditional estimators, if these are deemed more reliable.

1. INTRODUCTION

Primordial non-Gaussianity (PNG) provides a potentially powerful tool to discriminate between different Early Universe scenarios and its investigation plays therefore an important role in observational cosmology.

However, extracting PNG information is a task made significantly difficult by the smallness of the expected signal, which at low redshifts is several orders of magnitude below that generated by non-linear gravitational evolution of cosmological perturbations. For this reason, most observational studies of primordial non-Gaussian parameters have so far focused on linear cosmological probes, such as the Cosmic Microwave Background (CMB) (Planck Collaboration 2020), or the galaxy

power spectrum and bispectrum on large scales (Cabass et al. 2022a,b; D’Amico et al. 2022; Cagliari et al. 2023; Ivanov et al. 2024).

While challenging, as we have just stressed, a Large Scale Structure (LSS) analysis at non-linear scales could potentially be very rewarding: most of the PNG constraining power comes in fact from the cosmological perturbation bispectrum and a simple mode counting argument suggests that large improvements could be achieved in this regime, provided we are able to at least partially clean the total non-Gaussianity signal from late-time non-linear contributions. In this work—which is connected to a series of previous studies in the QUIJOTE-PNG series (Coulton et al. 2023a; Jung et al. 2023a,b)—we investigate this possibility by performing a thorough analysis of the dark matter halo field in N-

* Equal contributions.

Inferring solar differential rotation and viscosity via passive imaging with inertial waves

 Tram T. N. Nguyen^{1,*}, Thorsten Hohage^{1,2}, Damien Fournier¹, Laurent Gizon^{1,3}
¹Max-Planck Institute for Solar System research, Göttingen, Germany

²Institute for Numerical and Applied Mathematics, University of Göttingen, Germany

³Institute for Astrophysics, University of Göttingen, Germany

*Email: nguyen@mps.mpg.de

Abstract

The recent discovery of inertial waves on the surface of the Sun offers new possibilities to learn about the solar interior. These waves are long-lived with a period on the order of the Sun rotation period (~ 27 days) and are sensitive to parameters deep inside the Sun. They are excited by turbulent convection, leading to a passive imaging problem. In this work, we present the forward and inverse problem of reconstructing viscosity and differential rotation on the Sun from cross-covariance observations of these inertial waves.

Keywords: inverse problems, passive imaging, inertial waves, partial differential equations.

1 Introduction

Helioseismology aims at recovering parameters in the solar interior from surface observations using mostly acoustic *modes* (eigenfunctions). These modes have maximum sensitivity close to the surface and inferring deep inside the Sun is an extremely difficult task. The recent discovery of many inertial modes [2] opens up new opportunities for helioseismology. A linearized analysis of purely toroidal (i.e. divergence-free) modes on the surface of the Sun can already explain several observed features, such as the eigenfrequencies and eigenfunctions of Rossby modes and of high-latitude modes [1]. We use this forward model with an additional source to take into account the stochastic excitation of the waves, and solve an inverse problem to recover the solar differential rotation and the viscosity.

As this source is stochastic, we approach this from a *passive imaging* perspective; that is, we replace the source by its auto-correlation, which is an accessible entity known as the *source strength*, leading to a higher-dimensional problem and exacerbated nonlinearity, for which special strategies are required.

2 Solar inertial waves

We consider the dynamic of a moving particle in an incompressible fluid. Its velocity $\mathbf{v} = \mathbf{v}(\mathbf{r}, t)$ is described by the Navier-Stokes equation

$$\rho \left(\frac{\partial \mathbf{v}}{\partial t} + \mathbf{v} \cdot \nabla \mathbf{v} \right) = -\nabla p + \nabla \cdot (\rho \gamma \boldsymbol{\tau}) + \mathbf{f} - 2\boldsymbol{\Omega}_{\text{ref}} \times \mathbf{v}.$$

The restoring forces on the right hand side include acoustic pressure p , viscous stress $\boldsymbol{\tau} := \nabla \mathbf{v} + (\nabla \mathbf{v})^T$ and external source \mathbf{f} (e.g. random source); ρ denotes density. The Coriolis force ($2\boldsymbol{\Omega}_{\text{ref}} \times \mathbf{v}$) results from observing the Sun in a rotating reference frame, often chosen as the Carrington frame with the angular velocity $\Omega_{\text{ref}} = 14.7^{\circ}/\text{days}$.

We decompose \mathbf{v} into a background flow \mathbf{u}_0 and a perturbation (wave field) \mathbf{u} in spherical coordinates

$$\mathbf{v} = \mathbf{u}_0 + \mathbf{u}, \quad \mathbf{u}_0 := (\Omega(r, \theta) - \Omega_{\text{ref}})[0; 0; r \sin \theta],$$

and suppose that the fluid is strongly stratified [3]. Considering the horizontal motion and expressing it via the stream function Ψ yields

$$\rho \mathbf{u} = \nabla \times \boldsymbol{\Psi}, \quad \boldsymbol{\Psi} := [\Psi(t, \theta, \phi); 0; 0].$$

In the frequency-latitude wave number domain, i.e. for each (ω, m) , the inertial oscillation satisfies the scalar equation on $I := (0, \pi)$

$$-\gamma \Delta_m^2 \Psi - i\omega \Delta_m \Psi + im\beta \Delta_m \Psi - im\alpha \Psi = f$$

with $\gamma \in \mathbb{R}$, $\beta(\theta) := \Omega(\theta) - \Omega_{\text{ref}}$ $\theta \in I$

$$\alpha(\theta) := \frac{1}{r^2 \sin \theta} \frac{d}{d\theta} \left(\frac{1}{\sin \theta} \frac{d}{d\theta} (\Omega(\theta) \sin^2 \theta) \right),$$

$$\Delta_m \Psi := \frac{1}{r^2 \sin \theta} \frac{d}{d\theta} \left(\sin \theta \frac{d}{d\theta} \Psi \right) - \frac{m^2}{r^2 \sin^2 \theta} \Psi, \quad (1)$$

where Δ_m is the Laplace-Beltrami operator on the sphere. Supposing that the flow is continuous at the poles, we endow at the boundaries

$$\Psi(0) = \Psi(\pi) = 0, \quad \Psi'(0) = \Psi'(\pi) = 0. \quad (2)$$

WAVES 2024, Berlin, Germany

2

The system (1)-(2) is the underlying model for the inverse problem of recovering viscosity γ and differential rotation β . Equation (1) reduces to that studied in [3] if $\gamma = 0$ and in [1] if $f = 0$.

3 Correlation-based passive imaging

On the Sun, the source of excitation f is passive, i.e. ambient noise near the surface of the convection zone. Consequently, the oscillation Ψ is a realization of a random wave. If f is spatially uncorrelated with $\mathbb{E}[f] = 0$, then its cross-correlation between two locations is

$$\text{Cov}[f, f](\theta, \theta') = \mathbb{E}[f(\theta) \overline{f(\theta')}] =: \Pi_f(\theta) \delta(\theta - \theta'),$$

where $\overline{(\cdot)}$ denotes the complex conjugate, δ is the Dirac function, and Π_f represents the source strength. In this spirit, averaging J correlated wave fields acquired separately yields

$$\text{Cov}[\Psi, \Psi] \approx \text{Cov}(\Psi)(\theta, \theta') := \frac{1}{J} \sum_{j=1}^J \Psi_j(\theta) \overline{\Psi_j(\theta')},$$

referred to as the *empirical reprocessed data*. It is important to note that the source term f is typically not available, with only the source strength Π_f assumed known.

We formulate the passive imaging problem for solar viscosity and differential rotation as

$$\text{Find } (\gamma, \beta) \in \mathbb{R} \times X : \quad \text{Cov}(\Psi) = y^{\text{obs}} \\ \text{s.t. } \Psi \text{ solves (1)-(2)}$$

given Π_f and noisy observed data y^{obs} .

4 Inversion numerical results

We implemented an accelerated Nesterov Landweber algorithm to simultaneously reconstruct the scalar viscosity γ and latitude-dependent rotation β from a single frequency-latitude wave number.

Figure 1 shows the reconstruction results (top) and the corresponding covariance images (bottom). We initiate the algorithm with $\beta_{\text{init}} = 0$, i.e. no prior knowledge, and γ_{init} very far from the ground truth. Despite this, the reconstruction approximates the ground truth extremely well. The algorithm required 200 iterations over 2 seconds on an i7-1255U CPU (4.70 GHz).

Outlook. Going forward, we will perform imaging with solar-like parameters and real data acquired from the Helioseismic and Magnetic Imager on board the Solar Dynamics Observatory.

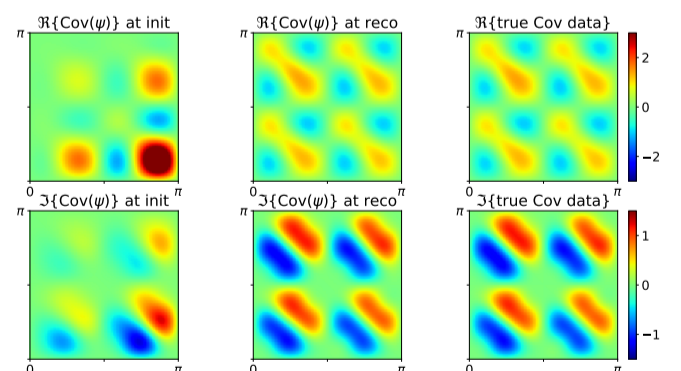
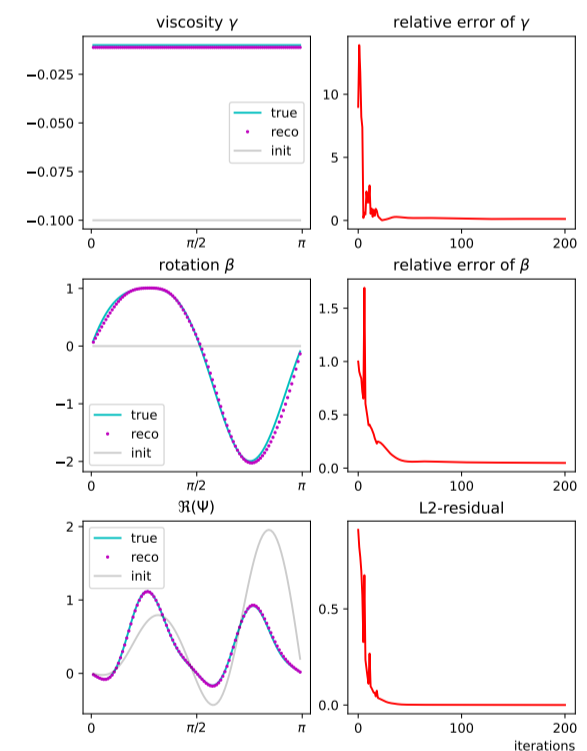


Figure 1: Simultaneous reconstruction of viscosity/rotation (top) and resulting covariance images (bottom).

References

- [1] D. Fournier, L. Gizon, and L. Hyest, Viscous inertial modes on a differentially rotating sphere: Comparison with solar observations, *Astronomy & Astrophysics* **664** (2022), 16 pp.
- [2] L. Gizon et al., Solar inertial modes: Observations, identification, and diagnostic promise, *Astronomy & Astrophysics* **652** (2017), 22 pp.
- [3] M. Watson, Shear instability of differential rotation in stars, *Astronomy & Astrophysics* **16(1)** (1981), pp. 285–298.

Observational Evidence for Hot Wind Impact on pc-scale in Low-luminosity Active Galactic Nucleus

FANGZHENG SHI ¹, FENG YUAN ², ZHIYUAN LI ³, ZHAO SU ³ AND SUOQING JI ¹

¹*Shanghai Astronomical Observatory, Chinese Academy of Sciences, Shanghai, People's Republic of China*

²*Center for Astronomy and Astrophysics and Department of Physics, Fudan University, Shanghai 200438, People's Republic of China*

³*School of Astronomy and Space Science, Nanjing University, Nanjing, People's Republic of China*

ABSTRACT

Supermassive black holes in galaxies spend majority of their lifetime in the low-luminosity regime, powered by hot accretion flow. Strong winds launched from the hot accretion flow have the potential to play an important role in active galactic nuclei (AGN) feedback. Direct observational evidence for these hot winds with temperature around 10 keV, has been obtained through the detection of highly ionized iron emission lines with Doppler shifts in two prototypical low-luminosity AGNs, namely M81* and NGC 7213. In this work, we further identify blueshifted H-like O/Ne emission lines in the soft X-ray spectra of these two sources. These lines are interpreted to be associated with additional outflowing components possessing velocity around several 10^3 km/s and lower temperature ($\sim 0.2-0.4$ keV). Blue-shifted velocity and the X-ray intensity of these additional outflowing components are hard to be explained by previously detected hot wind freely propagating to larger radii. Through detailed numerical simulations, we find the newly detected blue-shifted emission lines would come from circumnuclear gas shock-heated by the hot wind instead. Hot wind can provide larger ram pressure force on the clumpy circumnuclear gas than the gravitational force from central black hole, effectively impeding the black hole accretion of gas. Our results provide strong evidences for the energy and momentum feedback by the hot AGN wind.

1. INTRODUCTION

Actively accreting supermassive black holes (SMBHs) located at the center of galaxies can considerably influence the evolution of their host galaxies through radiation or different kinds of outflows (e.g., Kormendy & Ho 2013). Accretion and corresponding feedback can be classified into hot and cold modes, depending on whether the mass accretion rate of the SMBHs is below or above $\sim 2\%$ of \dot{M}_{Edd} (Yuan & Narayan 2014). The majority of local galaxies host low-luminosity active galactic nuclei (LLAGNs), resulting in hot (kinetic) mode accretion and feedback within these galaxies.

Numerical simulations of hot accretion flows have predicted the existence of energetic outflows in the form of uncollimated hot winds with a large opening angle

(Yuan et al. 2012a,b; Narayan et al. 2012; Yuan et al. 2015; Yang et al. 2021). Furthermore, simulations have shown that, unless the black hole spin is extremely high, the kinetic energy and momentum carried by the hot wind will be comparable, if not larger than that carried by jet (Yuan et al. 2015; Yang et al. 2021). This result, combined with the fact that the opening angle of wind is much larger than that of jet, suggests that hot winds serve as an essential component of kinetic mode feedback, in addition to the widely considered relativistic jets. The importance of the hot winds and radiation in the hot feedback mode has been investigated by numerical simulations of AGN feedback in an isolated elliptical galaxy (Yoon et al. 2019). Adopting *MACER* model (Yuan et al. 2018), where radiation and wind of AGN have been carefully incorporated based on the state-of-the-art physics of black hole accretion in both the hot (radio) and cold (quasar) modes, they found AGN activity and black hole mass would become significantly higher if hot mode feedback is turned off. And the suppression effect of hot mode feedback is dominated by wind rather than radiation.

fzshi@shao.ac.cn

fyuan@fudan.edu.cn

zyli@nju.edu.cn

AUTONOMOUS ROBOTIC ARM MANIPULATION FOR PLANETARY MISSIONS USING CAUSAL MACHINE LEARNING

Cian McDonnell¹, Miguel Arana-Catania², and Saurabh Upadhyay²

¹*MSc Astronautics and Space Engineering, Cranfield University, United Kingdom, cian@mcdonnell.eu*

²*School of Aerospace, Transport and Manufacturing, Cranfield University, United Kingdom, miguel.aranacatania@cranfield.ac.uk, saurabh.upadhyay@cranfield.ac.uk*

ABSTRACT

Autonomous robotic arm manipulators have the potential to make planetary exploration and in-situ resource utilization missions more time efficient and productive, as the manipulator can handle the objects itself and perform goal-specific actions. We train a manipulator to autonomously study objects of which it has no prior knowledge, such as planetary rocks. This is achieved using causal machine learning in a simulated planetary environment. Here, the manipulator interacts with objects, and classifies them based on differing causal factors. These are parameters, such as mass or friction coefficient, that causally determine the outcomes of its interactions. Through reinforcement learning, the manipulator learns to interact in ways that reveal the underlying causal factors. We show that this method works even without any prior knowledge of the objects, or any previously-collected training data. We carry out the training in planetary exploration conditions, with realistic manipulator models.

Key words: Planetary manipulators; reinforcement learning; interaction-based learning; planetary exploration; causal analysis.

1. INTRODUCTION

Autonomous manipulation has significant potential in planetary missions, as it can increase the amount of time spent exploring the environment and doing science activities. We review current methods for autonomous manipulation of objects, both on Earth and in planetary exploration environments. We see that approaches to manipulation of unknown objects usually must leverage a large amount of training data to work.

Reinforcement learning is commonly used to teach a robot manipulator certain skills, such as pick and place operations on objects, to solve specific tasks. In [1] the manipulator chooses its policy from a set of actions, and over time learns to use more of those actions that gave the











best results in the past. These are scored based on how close the object gets to a target position. Here we follow a different causal approach [2] using reinforcement learning to find which actions give the most information about the “causal factors”, the main parameters that determine the dynamics of the objects, so that this knowledge can be used to carry out any general task. The manipulator learns which actions produce the most distinguishable interactions for each factor. For example, it may learn about an object’s frictional properties by pushing it along the ground, and studying the distance travelled, which is directly affected by the friction.

There are relatively few papers on autonomous manipulators in planetary environments. Typically, two types of objects are considered in the existing literature: known objects where the robot has prior knowledge (e.g. size, shape, mass of a known scientific device), and objects which are completely unknown to the robot, e.g. planetary rocks. In [3], the authors present a design for a light-weight rover that can pick up and assemble known objects. The objects are detected based on machine-learning classification by colour. The same rover is used in [4] to demonstrate the placement, testing and collection of payload instruments, in a simulated lunar environment on Earth.

More sophisticated techniques are required to learn to manipulate unknown objects. In [5], the authors train a robot to grasp objects on the Moon, using 3D octree representations of the environment. A convolutional neural network is used in conjunction with actor-critic reinforcement learning to allow the robot to detect objects, choose the most efficient pose, and pick the objects up. The policy, learned in simulation, is then passed to a real-world rover in a lunar analogue centre.

Finally, it is also helpful to look at work on the problem of manipulation in terrestrial environments. While this is not carried out with planetary exploration in mind, many techniques can be transferred, especially when the work involves manipulation of unknown objects. In [6], several real-world robots are used to attempt to grasp unknown objects, using a single colour camera as input. The grasp attempts are then passed to a self-supervised reinforce-

A ‘MeerKAT-meets-LOFAR’ study of the complex multi-component (mini-)halo in the extreme sloshing cluster Abell 2142

C. J. Riseley ^{1,2}, A. Bonafede ^{1,2}, L. Bruno ^{1,2}, A. Botteon ², M. Rossetti ³, N. Biava ^{4,2},
E. Bonnassieux ^{5,6,2}, F. Loi ⁷, T. Vernstrom ^{8,9}, M. Balboni ^{4,10}

¹ Dipartimento di Fisica e Astronomia, Università degli Studi di Bologna, via P. Gobetti 93/2, 40129 Bologna, Italy
e-mail: christopher.riseley@unibo.it

² INAF – Istituto di Radioastronomia, via P. Gobetti 101, 40129 Bologna, Italy

³ INAF – IASF Milano, Via A. Corti 12, 20133 Milano, Italy

⁴ Thüringer Landessternwarte, Sternwarte 5, 07778 Tautenburg, Germany

⁵ Julius-Maximilians-Universität Würzburg, Fakultät für Physik und Astronomie, Institut für Theoretische Physik und Astrophysik, Lehrstuhl für Astronomie, Emil-Fischer-Str. 31, D-97074 Würzburg, Germany

⁶ Observatoire de Paris, 5 place Jules Janssen, 92195 Meudon, France

⁷ INAF – Osservatorio Astronomico di Cagliari, via della Scienza 3, Selargius, Italy

⁸ ICRAR, The University of Western Australia, 35 Stirling Hw, 6009 Crawley, Australia

⁹ CSIRO Space & Astronomy, PO Box 1130, Bentley, WA 6102, Australia

¹⁰ DiSAT, Università degli Studi dell’Insubria, via Valleggio 11, I-22100 Como, Italy

Received 23rd February 2024; accepted 29th February 2024; in original form 13th December 2023

ABSTRACT

Context. Clusters of galaxies are known to be turbulent environments, whether they are merging systems where turbulence is injected via the conversion of gravitational potential energy into the intracluster medium (ICM), or whether they are relaxed systems in which small-scale core sloshing is occurring within the potential well. In many such systems, diffuse radio sources associated with the ICM are found: radio haloes and mini-haloes.

Aims. Abell 2142 is a rich cluster undergoing an extreme episode of core sloshing, which has given rise to four cold fronts and a complex multi-component radio halo. Recent work revealed that there are three primary components to the halo, which spans a distance of up to around 2.4 Mpc. The underlying physics of particle acceleration on these scales is poorly-explored, and requires high-quality multi-frequency data with which to perform precision spectral investigation. We aim to perform such an investigation.

Methods. We use new deep MeerKAT L-band (1283 MHz) observations in conjunction with LOFAR HBA (143 MHz) data as well as X-ray data from *XMM-Newton* and *Chandra* to study the spectrum of the halo and the connection between the thermal and non-thermal components of the ICM.

Results. We confirm the presence of the third halo component, detecting it for the first time at 1283 MHz and confirming its ultra-steep spectrum nature, as we recover an integrated spectrum of $\alpha_{\text{H3, total}} = -1.68 \pm 0.10$. All halo components follow power-law spectra with increasingly steep spectra moving toward the cluster outskirts. We profile the halo along three directions, finding evidence of asymmetry and spectral steepening along an axis perpendicular to the main axis of the cluster. Our thermal/non-thermal investigation shows sub-linear correlations that are steeper at 1283 MHz than 143 MHz, and we find evidence of different thermal/non-thermal connections in different components of the halo. In particular, we find both a moderate anti-correlation (H1, the core) and positive correlation (H2, the ridge) between radio spectral index and X-ray temperature.

Conclusions. Our results are broadly consistent with an interpretation of turbulent (re-)acceleration following an historic minor cluster merger scenario in which we must invoke some inhomogeneities. However, the anti-correlation between radio spectral index and X-ray temperature in the cluster core is challenging to explain; the presence of three cold fronts and a generally lower temperature may provide the foundations of an explanation, but detailed bespoke modelling is required to study this further.

Key words. galaxies: clusters: individual: Abell 2142 – galaxies: clusters: intracluster medium

1. Introduction

In the hierarchical model of structure formation, galaxy clusters form from over-dense seeds at high redshift, growing over cosmic time into the largest gravitationally-bound structures in the Universe. Clusters are dominated by dark matter, which makes up some $\sim 80\%$ of the mass budget, whereas galaxies comprise only around five per cent of the mass. The remaining $\sim 15\%$ of the mass budget is comprised of the intra-cluster medium (ICM), a hot and rarefied plasma ($T \sim 10^7 - 10^8$ K, $n_e \sim 10^{-3}$ cm $^{-3}$) which emits at X-ray wavelengths via the Bremsstrahlung mech-

anism and scatters Cosmic Microwave Background (CMB) photons via the Sunyaev-Zel’dovich (SZ) effect.

While the dividing line between galaxy groups and clusters is somewhat arbitrary, clusters typically have a mass $M_{500} \geq 10^{14} M_{\odot}$ (where M_{500} is the mass contained within a radius of r_{500} , and r_{500} is the radius at which the mean cluster overdensity is $500\times$ the critical density of matter in the Universe at the cluster redshift; e.g. [Planck Collaboration et al. 2016](#)) with the most massive clusters having upwards of $10^{15} M_{\odot}$. Located at the nodes and intersections of the Cosmic Web, clusters grow through a variety of processes from continuous accretion of mat-

Deep Optical Emission-Line Images of Nine Known and Three New Galactic Supernova Remnants

ROBERT A. FESEN,¹ MARCEL DRECHSLER,² XAVIER STROTTNER,³ BRAY FALLS,⁴ YANN SAINTY,⁵ NICOLAS MARTINO,⁶
RICHARD GALLI,⁷ MATHEW LUDGATE,⁸ MARKUS BLAUENSTEINER,⁹ WOLFGANG REICH,¹⁰ SEAN WALKER,¹¹
DENNIS DI CICCO,¹¹ DAVID MITTELMAN,¹¹ CURTIS MORGAN,⁴ AZIZ ETTAHAR KAEOUACH,¹² JUSTIN RUPERT,¹³ AND
ZOUHAIR BENKHALDOUN¹⁴

¹6127 Wilder Lab, Department of Physics and Astronomy, Dartmouth College, Hanover, NH, 03755, USA

²Équipe StDr, Bärenstein, Feldstraße 17, 09471 Bärenstein, Germany

³Équipe StDr, Montfraise, 01370 Saint Etienne Du Bois, France

⁴Sierra Remote Observatories, Auberry, CA, 93602, USA

⁵YSTY Astronomy, 54000 Nancy, Lorraine, France

⁶Various Amateur Observatory Sites, Lorraine, France

⁷Oukaimeden Observatory, Oukaimeden, Morocco

⁸Ross Creek Observatory, Dunedin 9010, New Zealand

⁹Fachgruppe Astrofotografie, PO Box 1169, D-64629, Heppenheim, Germany

¹⁰Max-Planck-Institut für Radioastronomie, Auf dem Hügel 69, 53121 Bonn, Germany

¹¹MDW Sky Survey, New Mexico Skies Observatory, Mayhill, NM 88339, USA

¹²High Atlas Observatory, Oukaimeden Observatory, Oukaimeden, Morocco

¹³MDM Observatory, Kitt Peak National Observatory, 950 N. Cherry Ave., Tucson, AZ 85719, USA

¹⁴Oukaimeden Observatory, High Energy Physics and Astrophysics Lab, Faculty of Sciences Semlalia, Cadi Ayyad University, Marrakech, Morocco

ABSTRACT

Deep optical emission-line images are presented for nine known plus three new Galactic supernova remnants (SNRs), all but one having at least one angular dimension greater than one degree. Wide-field images taken in H α and [O III] λ 5007 reveal many new and surprising remnant structures including large remnant shock extensions and ‘blowout’ features not seen in published optical or radio data. These images represent over 12,000 individual images totaling more than 1000 hours of exposure time taken over the last two years mainly using small aperture telescopes which detected fainter nebular line emissions than published emission-line images. During the course of this imaging program, we discovered three new SNRs, namely G107.5-5.1 (the Nereides Nebula), G209.9-8.2, and G210.5+1.3, two of which have diameters $> 1.5^\circ$. Besides offering greater structural detail on the nine already known SNRs, a key finding of this study is the importance of [O III] emission-line imaging for mapping the complete shock emissions of Galactic SNRs.

Keywords: Interstellar medium; supernova remnants; emission nebulae; filamentary nebulae

1. INTRODUCTION

1.1. Background and History

At present there are just over 300 confirmed Galactic supernova remnants (SNRs) cataloged (Ferrand & Safi-Harb 2012; Green 2019). Most are less than a degree in angular size, located within five degrees of the Galactic plane, more than 1 kpc distant, and have typical estimated ages between 10^4 and 10^5 yr (Green 2004; Shan et al. 2018; Ranasinghe & Leahy 2022). The vast majority are discovered through radio observations due to their characteristic synchrotron nonthermal emission associated with shocked gas leading to a power law flux density, S , with $S \propto \nu^{-\alpha}$ where α is the emission spectral index with typical values between 0.3 and 0.7 (Reynolds 2011; Dubner & Giacani 2015).

Only a fraction of Galactic SNRs exhibit optical emissions. van den Bergh et al. (1973) was the first to publish an atlas of optical images for 23 of the 24 Galactic SNRs known at that time to exhibit optical emission. Subsequently, focused searchers for optical SNRs used a variety of telescopes and wide-field Schmidt cameras to search for optical SNR emissions (van den Bergh 1978; Zealey et al. 1979). Coincidence of optical emission with that of a remnant’s nonthermal radio emission using the first and second Palomar Observatory Sky Survey (POSS I, POSS II) images and their digitized versions (DSS1, DSS2), plus Schmidt images of the southern hemisphere led to several new optical SNR detections.

The first comprehensive optical survey of the Galactic plane to uncover new optical SNRs was the photographic

Discovery of Asymmetric Spike-like Structures of 10 au Disk around the Very Low-luminosity Protostar Embedded in the Taurus Dense Core MC 27/L1521F with ALMA

KAZUKI TOKUDA,^{1,2} NAOTO HARADA,¹ MITSUKI OMURA,¹ TOMOAKI MATSUMOTO,³ TOSHIKAZU ONISHI,⁴ KAZUYA SAIGO,⁵ AYUMU SHOSHI,¹ SHINGO NOZAKI,¹ KENGO TACHIHARA,⁶ NAOFUMI FUKAYA,⁶ YASUO FUKUI,⁶ SHU-ICHIRO INUTSUKA,⁶ AND MASASHIRO N. MACHIDA¹

¹*Department of Earth and Planetary Sciences, Faculty of Science, Kyushu University, Nishi-ku, Fukuoka 819-0395, Japan*

²*National Astronomical Observatory of Japan, National Institutes of Natural Sciences, 2-21-1 Osawa, Mitaka, Tokyo 181-8588, Japan*

³*Faculty of Sustainability Studies, Hosei University, Fujimi, Chiyoda-ku, Tokyo 102-8160, Japan*

⁴*Department of Physics, Graduate School of Science, Osaka Metropolitan University, 1-1 Gakuen-cho, Naka-ku, Sakai, Osaka 599-8531, Japan*

⁵*Graduate School of Science and Engineering, Kagoshima University, 1-21-40 Korimoto Kagoshima-city Kagoshima, 890-0065, Japan*

⁶*Department of Physics, Nagoya University, Furo-cho, Chikusa-ku, Nagoya 464-8601, Japan*

ABSTRACT

Recent ALMA observations have revealed an increasing number of compact protostellar disks with radii of less than a few tens of au, and the young Class 0/I objects have an intrinsic size diversity. To deepen our understanding of the origin of such tiny disks, we performed the highest resolution configuration observations with ALMA at a beam size of $\sim 0''.03$ (4 au) on the very low luminosity Class 0 protostar embedded in the Taurus dense core MC 27/L1521F. The 1.3 mm continuum measurement successfully resolved a tiny, faint (~ 1 mJy) disk with a major axis length of ~ 10 au, one of the smallest examples in the ALMA protostellar studies. In addition, we detected spike-like components in the northeastern direction at the disk edge. Gravitational instability or other fragmentation mechanisms cannot explain the structures, given the central stellar mass of $\sim 0.2 M_{\odot}$ and the disk mass of $\gtrsim 10^{-4} M_{\odot}$. Instead, we propose that these small spike structures were formed by a recent dynamic magnetic flux transport event due to interchange instability that would be favorable to occur if the parental core has a strong magnetic field. The presence of complex arc-like structures on a larger (~ 2000 au) scale in the same direction as the spike structures suggests that the event was not single. Such episodic, dynamical events may play an important role in maintaining the compact nature of the protostellar disk in the complex gas envelope during the main accretion phase.

Keywords: Star formation (1569); Protostars (1302); Molecular clouds (1072); Interstellar medium (847); Circumstellar envelopes (237); Magnetic fields (994)

1. INTRODUCTION

Understanding the star formation process is a fundamental topic in astronomy and astrophysics. The collapse of molecular clouds leading to protostar formation (e.g., Shu et al. 1987; Andre et al. 2000) and the subsequent interaction between stellar objects and surrounding envelopes are crucial to deciphering the mechanism to determine stellar mass (e.g., Arce & Sargent 2006; Machida & Hosokawa 2013). The product of the star formation process also provides initial conditions for planet formation, i.e., protoplanetary disks. Multiple physical processes, such as turbulence (e.g., Padoan & Nordlund 2002; Offner et al. 2008), magnetic fields (e.g., Crutcher 2012), and self-gravity, are intricately coupled throughout the dynamical collapse and mass accretion phases (e.g., Matsumoto & Hanawa 2011). To observationally elucidate such processes, recent millimeter and sub-millimeter facilities, including interferometers offering high spatial and density dynamic range observations, have been playing effective roles.

Advances in ALMA observations of later stages of star formation, particularly the potential planet-forming phase, have been remarkable over the past decade. The ubiquity of substructures such as rings and gaps within protoplanetary disks is increasingly evident in larger disks, typically those exceeding ~ 50 au in size, as highlighted by numerous high angular resolution observations (e.g., Andrews et al. 2018). However, it is becoming clear that not all protoplanetary

Magnetic flux in the Sun emerges unaffected by supergranular-scale surface flows

PRASAD MANI,¹ CHRIS S. HANSON,² SIDDHARTH DHANPAL,¹ SHRAVAN HANASOGE,^{1,2} SRIJAN BHARATI DAS,³ AND
MATTHIAS REMPEL⁴

¹*Department of Astronomy and Astrophysics, Tata Institute of Fundamental Research, Mumbai, India*

²*Center for Astrophysics and Space Science, NYUAD Institute, New York University Abu Dhabi, Abu Dhabi, UAE*

³*Department of Geosciences, Princeton University, Princeton, NJ, USA*

⁴*High Altitude Observatory, National Center for Atmospheric Research, Boulder, CO 80307, USA*

ABSTRACT

Magnetic flux emergence from the convection zone into the photosphere and beyond is a critical component of the behaviour of large-scale solar magnetism. Flux rarely emerges amid field-free areas at the surface, but when it does, the interaction between magnetism and plasma flows can be reliably explored. Prior ensemble studies identified weak flows forming near emergence locations, but the low signal-to-noise required averaging over the entire dataset, erasing information about variation across the sample. Here, we apply deep learning to achieve improved signal-to-noise, enabling a case-by-case study. We find that these associated flows are dissimilar across instances of emergence and also occur frequently in the quiet convective background. Our analysis suggests diminished influence of supergranular-scale convective flows and magnetic buoyancy on flux rise. Consistent with numerical evidence, we speculate that small-scale surface turbulence and / or deep-convective processes play an outsize role in driving flux emergence.

1. INTRODUCTION

Active regions (ARs) are spatially and temporally extensive magnetic phenomena, extending from the solar interior to the corona, with a lifetime marked by formation, emergence, and eventual decay (van Driel-Gesztelyi & Green 2015) through dispersion of magnetic elements (Strous et al. 1996; Schunker et al. 2019, 2020) into the background turbulent convective field. Most ARs play host to sunspots (Rempel & Schlichenmaier 2011; Rempel 2012) - magnetic features characterized by evolving umbrae, penumbrae, and fine-structures, with high field strengths (few \sim kG, Siu-Tapia et al. 2019). The dynamics of tangled magnetic field lines in morphologically complex active regions and sunspots underpin high-energy eruptive events such as flares (Toriumi & Wang 2019) and coronal mass ejections (Webb & Howard 2012). A detailed inquiry into large-scale solar magnetism, vis-a-vis ARs, has indirect implications for understanding space-weather (Temmer 2021).

ARs are hypothesized to be the surface manifestations of thin magnetic flux tubes (Cheung & Isobe 2014) generated in the interior (Charbonneau 2020), which then rise up (Birch et al. 2016) to the surface and above through a collection of processes termed *emergence*. The precise location of the dynamo is contested, with suggestions ranging from the base of the convection zone (Spiegel & Weiss 1980) to the near-surface layers (Brandenburg 2005). A comprehensive understanding of solar magnetism warrants that ARs be studied over the full domain - from birth to decay. Their associated flows have drawn attention (Gizon et al. 2001; Komm et al. 2008; Hindman et al. 2009) since magnetic fields and solar convection are thought to be intertwined (Stein 2012). A medley of findings, courtesy of individual emerging-active-region (EAR) studies (Kosovichev 2009; Zharkov & Thompson 2008; Komm et al. 2008; Hartlep et al. 2011), fail to form a coherent picture of flux-emergence physics. This has motivated ensemble studies of isolated ARs, which report near-surface flows forming around an averaged EAR several hours prior to emergence. Chiefly, precursor-like horizontal convergent flows (inflows) in the vicinity of EARs (Martin-Belda & Cameron 2017; Löptien et al. 2017; Birch et al. 2019; Braun 2019; Gottschling et al. 2021) are commonly found to be correlated with emerging

Neural Simulation-Based Inference of the Neutron Star Equation of State directly from Telescope Spectra

Len Brandes,^{1,*} Chirag Modi,^{2,3} Aishik Ghosh,^{4,5} Delaney Farrell,⁶ Lee Lindblom,⁷
Lukas Heinrich,¹ Andrew W. Steiner,^{8,9} Fridolin Weber,^{6,7} and Daniel Whiteson⁴

¹*Technical University of Munich, TUM School of Natural Sciences, Physics Department, 85747 Garching, Germany*

²*Center for Computational Astrophysics, Flatiron Institute, New York, NY, 11226, USA*

³*Center for Computational Mathematics, Flatiron Institute, New York, NY, 11226, USA*

⁴*Department of Physics and Astronomy, University of California, Irvine, CA 92697, USA*

⁵*Physics Division, Lawrence Berkeley National Laboratory, Berkeley, CA 94720, USA*

⁶*Department of Physics, San Diego State University, San Diego, CA 92115, United States*

⁷*Department of Physics, University of California at San Diego, La Jolla, CA 92093, United States*

⁸*Department of Physics and Astronomy, University of Tennessee, Knoxville, Tennessee 37996, USA*

⁹*Physics Division, Oak Ridge National Laboratory, Oak Ridge, Tennessee 37831, USA*

Neutron stars provide a unique opportunity to study strongly interacting matter under extreme density conditions. The intricacies of matter inside neutron stars and their equation of state are not directly visible, but determine bulk properties, such as mass and radius, which affect the star's thermal X-ray emissions. However, the telescope spectra of these emissions are also affected by the stellar distance, hydrogen column, and effective surface temperature, which are not always well-constrained. Uncertainties on these nuisance parameters must be accounted for when making a robust estimation of the equation of state. In this study, we develop a novel methodology that, for the first time, can infer the full posterior distribution of both the equation of state and nuisance parameters directly from telescope observations. This method relies on the use of neural likelihood estimation, in which normalizing flows use samples of simulated telescope data to learn the likelihood of the neutron star spectra as a function of these parameters, coupled with Hamiltonian Monte Carlo methods to efficiently sample from the corresponding posterior distribution. Our approach surpasses the accuracy of previous methods, improves the interpretability of the results by providing access to the full posterior distribution, and naturally scales to a growing number of neutron star observations expected in the coming years.

CONTENTS

I. Introduction	2
II. Simulated neutron stars	3
A. Equation of state	3
B. Modeling X-ray spectra with XSPEC	3
C. Nuisance parameters	3
III. Previous work	4
IV. Bayesian inference with neural likelihood estimation	5
A. Neural likelihood estimation	5
B. Posterior sampling with Hamiltonian Monte Carlo	5
C. Scaling to multiple observations	6
V. Results	6
A. Example posterior distribution	6
B. Increasing the number of observations	8
C. Average performance on test set	9
VI. Discussion & outlook	10
VII. Conclusion	12

* len.brandes@tum.de

Unveiling two expanding stellar groups formed through violent relaxation in The Lagoon Nebula Cluster.

Andrea Bonilla-Barroso¹, Javier Ballesteros-Paredes¹, Jesús Hernández²,
Luis Aguilar², and Manuel Zamora-Avilés³ *

¹*Instituto de Radioastronomía y Astrofísica, UNAM, campus Morelia. PO Box 3-72. 58090. Morelia, Michoacán, México*

²*Universidad Nacional Autónoma de México, Instituto de Astronomía, AP 106, Ensenada 22800, BC, México*

³*Instituto Nacional de Astrofísica, Óptica y Electrónica, Luis E. Erro 1, 72840 Tonantzintla, Puebla, México*

Accepted 2024 February 27. Received 2024 February 27; in original form 2023 January 03

ABSTRACT

The current kinematic state of young stellar clusters can give clues on their actual dynamical state and origin. In this contribution, we use Gaia DR3 data of the Lagoon Nebula Cluster (LNC) to show that the cluster is composed of two expanding groups, likely formed from different molecular cloud clumps. We find no evidence of massive stars having larger velocity dispersion than low-mass stars or being spatially segregated across the LNC, as a whole, or within the Primary group. However, the Secondary group, with 1/5th of the stars, exhibits intriguing features. On the one hand, it shows a bipolar nature, with an aspect ratio of $\sim 3:1$. In addition, the massive stars in this group exhibit larger velocity dispersion than the low-mass stars, although they are not concentrated towards the center of the group. This suggests that this group may have undergone dynamical relaxation, first, and some explosive event afterward. However, further observations and numerical work have to be performed to confirm this hypothesis. The results of this work suggest that, although stellar clusters may form by the global and hierarchical collapse of their parent clump, still some dynamical relaxation may take place.

Key words: turbulence – stars: formation – ISM: clouds – ISM: kinematics and dynamics – galaxies: star formation.

1 INTRODUCTION

The detailed way stars are born is one of the most fundamental unsolved problems in astronomy, and so it is how stellar clusters form. To understand the physical processes that allow the formation of stellar clusters, one has to use numerical simulations and theoretical studies and compare the outcomes with the observational properties that such dynamical and chaotic systems exhibit.

Recently, contrasting results were found in different young stellar clusters with similar ages. On the one hand, based on Gaia DR2 data, Wright & Parker (2019) found that the massive stars in the Lagoon Nebula Cluster (LNC) exhibit larger velocity dispersion compared to low mass stars, which they interpreted as a consequence of the Spitzer (1969) instability. On the other hand, using Gaia EDR3 for the Orion Nebula Cluster (ONC), Bonilla-Barroso et al. (2022) found that the velocity dispersion is nearly constant as a function of mass. This difference is relevant because, if real, it is evidence

of differences in the formation and/or early dynamical evolution of stellar clusters since there is a possible dynamical mechanism behind each one of those results. On the one hand, stellar collisions¹ promote spatial segregation in mass and velocity, where massive stars concentrate at the center, with a larger velocity dispersion, while lower mass stars are more dispersed in space and with smaller velocity dispersion (e.g., Binney & Tremaine 2008). The Spitzer instability is an extreme case of this process, as we explain in §2. In contrast, if clusters are primarily formed by the collapse of a massive cloud or clump, and then the stellar feedback disperses the parent cloud, temporal fluctuations in the ambient potential scatter stars in energy space. This process, called violent relaxation, results in the same velocity dispersion for all stars independently of their masses (Lynden-Bell 1967).

Determining the dynamical state of a stellar cluster is

¹ Through the text, we call stellar collisions to indicate, as it is usual in the stellar dynamics community, not that two stars physically collide, but that their interaction is strong enough to modify their trajectories substantially.

* E-mail: a.bonilla@irya.unam.mx

Angular bispectrum and trispectrum of scalar-induced gravitational-waves: all contributions from primordial non-Gaussianity f_{NL} and g_{NL}

Jun-Peng Li,^{1,2} Sai Wang,^{1,*} Zhi-Chao Zhao,³ and Kazunori Kohri^{4,5,6}

¹*Theoretical Physics Division, Institute of High Energy Physics,
Chinese Academy of Sciences, 19B Yuquan Road, Shijingshan District, Beijing 100049, China*

²*School of Physics, University of Chinese Academy of Sciences,
19A Yuquan Road, Shijingshan District, Beijing 100049, China*

³*Department of Applied Physics, College of Science, China Agricultural University,
17 Qinghua East Road, Haidian District, Beijing 100083, China*

⁴*Division of Science, National Astronomical Observatory of Japan (NAOJ),
and SOKENDAI, 2-21-1 Osawa, Mitaka, Tokyo 181-8588, Japan*

⁵*Theory Center, IPNS, and QUP (WPI), KEK, 1-1 Oho, Tsukuba, Ibaraki 305-0801, Japan*

⁶*Kavli IPMU (WPI), UTIAS, The University of Tokyo, Kashiwa, Chiba 277-8583, Japan*

Studying the primordial non-Gaussianity of inflationary perturbations is crucial for testing the inflation paradigm of the early universe. In this work, we conduct a comprehensive analysis of the angular bispectrum and trispectrum of scalar-induced gravitational waves (SIGWs) in the presence of local-type primordial non-Gaussianity parameterized by f_{NL} and g_{NL} , deriving their semi-analytical formulae for the first time. Our findings indicate that it is the presence of primordial non-Gaussianity that leads to a non-Gaussian SIGW background, suggesting that the angular bispectrum and trispectrum of SIGWs could serve as probes of the primordial non-Gaussianity. Our numerical results further illustrate that f_{NL} and g_{NL} exert significant impacts on the spectral amplitudes, potentially reaching up to 10^{-5} for the former and 10^{-8} for the latter. In particular, we demonstrate that the angular bispectrum and trispectrum exhibit characteristic dependence on the angular multipoles and frequency bands. They hold potentials to be measured by gravitational-wave detectors that may advance our understanding of the origin of the universe.

I. INTRODUCTION


Primordial non-Gaussianity stands for the deviation from Gaussian distribution of the primordial curvature perturbations, thus characterizing the dynamics of the early universe during inflation [1–7]. Though the standard inflation paradigm predicts the nearly Gaussian perturbations [8, 9], many other inflation models hold no brief for this prediction [10]. In particular, the primordial bispectrum is characterized by an amplitude parameter f_{NL} , while the primordial trispectrum by g_{NL} and so on [11]. Constraints on the primordial non-Gaussianity have been obtained through observations of cosmic microwave background (CMB) [12] and large-scale structure (LSS) [13, 14]. However, these observations are only responsive to the cosmological perturbations on large scales that are comparable to the overall observational patch of the universe, leaving the perturbations on smaller scales to be insensitive. Since modes of smaller wavelength reentered the horizon earlier, the universe before the last-scattering surface would have been opaque to the electromagnetic probes [15]. Therefore, to conquer the above challenge, it is necessary to develop alternative probes that can effec-

tively convey information from the early universe to our detectors. Given that Einstein’s general relativity predicts that gravitational waves (GWs) propagate without dissipation [16, 17], we expect them to be a valuable new messenger of the early universe on small scales, in contrast to the traditional observations such as CMB and LSS on large scales.

The scalar-induced gravitational waves (SIGWs) are sensitive to the local-type primordial non-Gaussianity on small scales, making them potential indicators of this non-Gaussianity. Theoretically, they were produced through non-linear processes by the linear inflationary perturbations that reentered the Hubble horizon in the early universe [18–24]. Taking into account f_{NL} and g_{NL} can lead to significant alterations by several orders of magnitude in both the energy-density fraction spectrum and the angular power spectrum [25], especially within the projected sensitivity regimes of future or futuristic gravitational-wave detection programs [26–50]. This suggests the potential for measuring primordial non-Gaussianity through the search for an anisotropic SIGW background. Other related works can be found in Refs. [51–69] and Refs. [70–72], respectively. Additionally, in conjunction with the production of scalar-induced gravitational waves, these scalar perturbations may gravitationally collapse into primordial black holes

* Correspondence to Email: wangsai@ihep.ac.cn

Convective Mixing: The Formation Channel of Li-rich Giants

Xue-Feng Li^{1,2} *, Jian-Rong Shi^{3,4}, Yan Li^{1,2,5,6}, Hong-Liang Yan^{3,4,7}, Jing-Hua Zhang⁸

¹Yunnan Observatories, Chinese Academy of Sciences, P.O.Box 110, Kunming 650216, China

²University of Chinese Academy of Sciences, Beijing 100049, China

³CAS Key Laboratory of Optical Astronomy, National Astronomical Observatories, Beijing 100101, China

⁴School of Astronomy and Space Science, University of Chinese Academy of Sciences, Beijing 100049, China

⁵Key Laboratory for Structure and Evolution of Celestial Objects, Chinese Academy of Sciences, P.O.Box 110, Kunming 650216, China

⁶Center for Astronomical Mega-Science, Chinese Academy of Sciences, Beijing 100012, China

⁷Institute for Frontiers in Astronomy and Astrophysics, Beijing Normal University, Beijing 102206, China

⁸South-Western Institute for Astronomy Research, Yunnan University, Chengong District, Kunming 650500, China

Accepted XXX. Received YYY; in original form ZZZ

ABSTRACT

Increasing observed data indicate that part of giants has abnormally high lithium (Li) inside their surface, and their proportion is around 1%. Instead of pursuing the feasible mechanisms for extra Li enrichment, we focus on how to inhibit Li depletion from the main sequence (MS) phase of giants. With this in mind, we find that convective mixing is capable of achieving this goal and forming Li-rich giants, which is mainly attributed to the convection model with the convective boundary defined by the Ledoux criterion. Another factor in the formation of Li-rich giants in our convection models is related to the Li abundances of their progenitors. If the Li abundances of the progenitors exceed the meteoritic value (3.3 dex), then the majority of giants will be rich in Li. This is the general pattern of stellar Li abundance evolution without factoring in extra Li depletion. We propose that other Li depletion processes should also be adopted in the future, as they may be the key to the 1% puzzle.

Key words: stars: abundances – stars: evolution – convection

1 INTRODUCTION

For the past few years, the GALAH (Buder et al. 2018, 2021) and the LAMOST surveys (Cui et al. 2012) have provided a large amount of observed samples on the Li abundances ($A(\text{Li})^1$) of giants. The samples show the same problem that the Li abundances of the giants emerge a large-scale, more than four orders of magnitude, distribution (Deepak & Reddy 2019; Kumar et al. 2020; Gao et al. 2021; Martell et al. 2021). For the normal giants with the Li abundance within the range of -1.0 to 1.5 dex, they have been already many extra mixing models to try to explain (Schwab 2020; Mori et al. 2021; Li et al. 2023). However, there are also some abnormal giants with the Li abundance larger than 1.5 dex, i.e., so-called Li-rich giants (e.g., Wallerstein & Sneden 1982; Brown et al. 1989; da Silva et al. 1995; Reddy & Lambert 2005; Kumar et al. 2011; Casey et al. 2016; Yan et al. 2018; Singh et al. 2019; Holanda et al. 2020; Zhou et al. 2021; Kowkabany et al. 2022). This definition originates from the upper limit value obtained by the Li abundance of a star with $1.5 M_{\odot}$ and solar metallicity, after assuming its convective envelope dilute the Li abundance by about 60 times from 3.3 dex (e.g., Charbonnel & Balachandran 2000; Tsantaki et al. 2023). Among them, Kowkabany et al. (2022) had discovered the most Li-rich red giant branch (RGB) star at present, 2MASS J05241392-0336543, its $A(\text{Li})$ is as high as 5.6 dex. In addition, Singh et al. (2019) also reported two red clump

(RC) stars with a $A(\text{Li})$ of ~ 4.0 dex. In general, the proportion of the Li-rich giants is very low, only $\sim 1\%$ (Brown et al. 1989; Gao et al. 2019; Martell et al. 2021). Among the Li-rich giants, the RC stars are majority (e.g., Martell et al. 2021; Singh et al. 2021; Yan et al. 2021).














How the Li-rich giants form is unclear, while some attempts have been made in this field, e.g., the element diffusion effects (Gao et al. 2022). It can be considered from two aspects: one is to increase Li content on the stellar surface, such as the external action (e.g., Siess & Livio 1999; Lebzelter et al. 2012; Casey et al. 2019; Zhang et al. 2020) and the internal process (Cameron 1955; Cameron & Fowler 1971), and the other is to inhibit or weaken Li depletion. In this article, we will focus on the weakening on the Li depletion and explore whether it is possible to form the Li-rich giants.

Stars undergo the Li depletion at various stages, such as the pre-main sequence (PMS) (see e.g. Iben 1965), the main sequence (MS) (see e.g. Sestito & Randich 2005), and the first dredge-up (see e.g. Iben 1967a,b). However, the standard convection model almost does not exist the MS Li depletion processes (e.g., Dantona & Mazzitelli 1984; Deliyannis et al. 1990; Li et al. 2023). At the first dredge-up, the stellar convective envelope extends inward, diluting the surface Li by carrying it to hotter regions. Therefore, the calibration of the bottom boundary of the convective envelope will greatly affect the retained Li content. With regard to the two criteria of convective boundary, i.e., the Schwarzschild and the Ledoux criterion, the main difference is whether the mean molecular weight gradient is zero. Nevertheless, the computation of the convective boundary is still an open topic in stellar evolution code (Gabriel et al. 2014; Anders

* E-mail: lixuefeng@ynao.ac.cn

¹ $A(\text{Li}) = \log(N_{\text{Li}}/N_{\text{H}}) + 12$, where N_{X} is the atomic number densities of X.

Gas-dynamical Mass Measurements of the Supermassive Black Holes in the Early-Type Galaxies NGC 4786 and NGC 5193 from ALMA and HST Observations*

KYLE M. KABASARES ^{1,2,3} JONATHAN H. COHN ^{4,5} AARON J. BARTH ³ BENJAMIN D. BOIZELLE ⁶
JARED DAVIDSON ⁶, JANELLE M. SY ^{7,3} JEYSEN FLORES-VELÁZQUEZ ^{8,3} SILVANA C. DELGADO ANDRADE ⁵
DAVID A. BUOTE ³, JONELLE L. WALSH ⁵ ANDREW J. BAKER ^{9,10} JEREMY DARLING ¹¹ AND LUIS C. HO ¹²

¹Ames Research Center, National Aeronautics and Space Administration, Moffett Field, CA 94035, USA

²Bay Area Environmental Research Institute, Ames Research Center, Moffett Field, CA 94035, USA

³Department of Physics and Astronomy, 4129 Frederick Reines Hall, University of California, Irvine, CA, 92697-4575, USA

⁴Department of Physics and Astronomy, Dartmouth College, 6127 Wilder Laboratory, Hanover, NH 03755, USA

⁵George P. and Cynthia Woods Mitchell Institute for Fundamental Physics and Astronomy, 4242 TAMU, Texas A&M University, College Station, TX, 77843-4242,

⁶Department of Physics and Astronomy, 284 ESC, Brigham Young University, Provo, UT, 84602, USA

⁷Department of Physics, New York University, 726 Broadway, New York, NY, 10003, USA

⁸Institute for Gravitation and the Cosmos, The Pennsylvania State University, University Park, PA 16802, USA

⁹Department of Physics and Astronomy, Rutgers, the State University of New Jersey, 136 Frelinghuysen Road, Piscataway, NJ 08854-8019, USA

¹⁰Department of Physics and Astronomy, University of the Western Cape, Robert Sobukwe Road, Bellville 7535, South Africa

¹¹Center for Astrophysics and Space Astronomy, Department of Astrophysical and Planetary Sciences, University of Colorado, 389 UCB, Boulder, CO 80309-0389, USA

¹²Kavli Institute for Astronomy and Astrophysics, Peking University, Beijing 100871, China; Department of Astronomy, School of Physics, Peking University, Beijing 100871, People's Republic of China

ABSTRACT

We present molecular gas-dynamical mass measurements of the central black holes in the giant elliptical galaxies NGC 4786 and NGC 5193, based on CO(2–1) observations from the Atacama Large Millimeter/submillimeter Array (ALMA) and Hubble Space Telescope near-infrared imaging. The central region in each galaxy contains a circumnuclear disk that exhibits orderly rotation with projected line-of-sight velocities of $\sim 270 \text{ km s}^{-1}$. We build gas-dynamical models for the rotating disk in each galaxy and fit them directly to the ALMA data cubes. At $0''.31$ resolution, the ALMA observations do not fully resolve the black hole sphere of influence (SOI), and neither galaxy exhibits a central rise in rotation speed, indicating that emission from deep within the SOI is not detected. As a result, our models do not tightly constrain the central black hole mass in either galaxy, but they prefer the presence of a central massive object in both galaxies. We measure the black hole mass to be $(M_{\text{BH}}/10^8 M_{\odot}) = 5.0 \pm 0.2 [1\sigma \text{ statistical}]_{-1.3}^{+1.4} [\text{systematic}]$ in NGC 4786 and $(M_{\text{BH}}/10^8 M_{\odot}) = 1.4 \pm 0.03 [1\sigma \text{ statistical}]_{-0.1}^{+1.5} [\text{systematic}]$ in NGC 5193. The largest component of each measurement's error budget is from the systematic uncertainty associated with the extinction correction in the host galaxy models. This underscores the importance of assessing the impact of dust attenuation on the inferred M_{BH} .

1. INTRODUCTION

Supermassive black holes (BHs) are thought to reside at the centers of most, if not all, massive galaxies. With masses between a million to over a billion times that of the Sun, supermassive BHs gravitationally dominate the orbits of objects within their sphere of influence (SOI). The radius of the SOI is often defined as either $r_{\text{SOI}} \approx GM_{\text{BH}}/\sigma_{*}^2$, where σ_{*} represents the stellar velocity dispersion of the spheroidal component of the galaxy,

Corresponding author: Kyle M. Kabasares
kabasars@baeri.org

³ This study was jointly led by Dr. Kyle M. Kabasares and Dr. Jonathan H. Cohn.

* Based on observations made with the NASA/ESA Hubble Space Telescope, obtained at the Space Telescope Science Institute, which is operated by the Association of Universities for Research in Astronomy, Inc., under NASA contract NAS5-26555. These observations are associated with programs 15226 and 15909.

A far-ultraviolet-driven photoevaporation flow observed in a protoplanetary disk

Olivier Berné^{1,*}, Emilie Habart², Els Peeters^{3,4,5}, Ilane Schroetter¹, Amélie Canin¹, Ameet Sidhu^{3,4}, Ryan Chown^{3,4}, Emeric Bron⁶, Thomas J. Haworth⁷, Pamela Klaassen⁸, Boris Trahin², Dries Van De Putte⁹, Felipe Alarcón¹⁰, Marion Zannese², Alain Abergel², Edwin A. Bergin¹⁰, Jeronimo Bernard-Salas^{11,12}, Christiaan Boersma¹³, Jan Cami^{3,4,5}, Sara Cuadrado¹⁴, Emmanuel Dartois¹⁵, Daniel Dicken², Meriem Elyajouri², Asunción Fuente¹⁶, Javier R. Goicoechea¹⁴, Karl D. Gordon^{9,17}, Lina Issa¹, Christine Joblin¹, Olga Kannavou², Baria Khan³, Ozan Lacinbala², David Languignon⁶, Romane Le Gal^{1,18,19}, Alexandros Maragkoudakis¹³, Raphael Meshaka², Yoko Okada²⁰, Takashi Onaka^{21,22}, Sofia Pasquini³, Marc W. Pound²³, Massimo Robberto^{9,17}, Markus Röllig²⁰, Bethany Schefter³, Thiébaud Schirmer^{2,24}, Thomas Simmer², Benoit Tabone², Alexander G. G. M. Tielens^{23,25}, Sílvia Vicente²⁶, Mark G. Wolfire²³, & the PDRs4All team[†].

¹Institut de Recherche en Astrophysique et Planétologie, Université de Toulouse, Centre National de la Recherche Scientifique, Centre National d'Etudes Spatiales, 31028, Toulouse, France

²Institut d'Astrophysique Spatiale, Université Paris-Saclay, Centre National de la Recherche Scientifique, 91405 Orsay, France

³Department of Physics & Astronomy, The University of Western Ontario, London ON N6A 3K7, Canada

⁴Institute for Earth and Space Exploration, The University of Western Ontario, London ON N6A 3K7, Canada

⁵Carl Sagan Center, Search for ExtraTerrestrial Intelligence Institute, Mountain View, CA 94043, USA

⁶Laboratoire d'Etudes du Rayonnement et de la Matière, Observatoire de Paris, Université Paris Science et Lettres, Centre National de la Recherche Scientifique, Sorbonne Universités, F-92190 Meudon, France

⁷Astronomy Unit, School of Physics and Astronomy, Queen Mary University of London, London E1 4NS, UK

⁸UK Astronomy Technology Centre, Royal Observatory Edinburgh, Blackford Hill EH9 3HJ, UK

⁹Space Telescope Science Institute, Baltimore, MD 21218, USA

¹⁰Department of Astronomy, University of Michigan, Ann Arbor, MI 48109, USA

¹¹ACRI-ST, Centre d'Etudes et de Recherche de Grasse, F-06130 Grasse, France

¹²Innovative Common Laboratory for Space Spectroscopy, 06130 Grasse, France

¹³NASA Ames Research Center, Moffett Field, CA 94035-1000, USA

¹⁴Instituto de Física Fundamental (Consejo Superior de Investigación Científica), 28006, Madrid, Spain

1

Most low-mass stars form in stellar clusters that also contain massive stars, which are sources of far-ultraviolet (FUV) radiation. Theoretical models predict that this FUV radiation produces photo-dissociation regions (PDRs) on the surfaces of protoplanetary disks around low-mass stars, impacting planet formation within the disks. We report JWST and Atacama Large Millimeter Array observations of a FUV-irradiated protoplanetary disk in the Orion Nebula. Emission lines are detected from the PDR; modelling their kinematics and excitation allows us to constrain the physical conditions within the gas. We quantify the mass-loss rate induced by the FUV irradiation, finding it is sufficient to remove gas from the disk in less than a million years. This is rapid enough to affect giant planet formation in the disk.

Young low-mass stars are surrounded by disks of gas and dust (protoplanetary disks). These disks have lifetimes of a few million years ($1-3$) and are the sites of planet formation (4). Planet formation is limited by processes that remove mass from the disk such as photoevaporation (5). This occurs when the upper layers of protoplanetary disks are heated by X-ray or ultraviolet photons. Radiative heating increases the gas temperature, bringing the local sound speed above the escape velocity of the disk, causing the gas to escape. The photons could be from the central star (6) or from nearby massive stars (7). Because most low mass stars form in clusters that also contain massive stars, the majority of protoplanetary disks are exposed to radiation, so are expected to experience photoevaporation driven by ultraviolet photons during their lifetime ($7-11$). Theoretical models predict that far-ultraviolet (FUV) photons with energies below the Lyman limit ($E < 13.6$ eV) dominate the photoevaporation, which affects the disk mass, radius, and lifetime ($7, 10, 12-18$), its chemical evolution ($19-21$), and the growth and migration of any planet forming within the disk (22).

However, these processes have not been directly observed. Most observational constraints

3

Stellar Surface Magnetic Fields Impact Limb Darkening

Nadiia M. Kostogryz¹, Alexander I. Shapiro¹, Veronika Witzke¹,
Robert H. Cameron¹, Laurent Gizon^{1,2}, Natalie A. Krivova¹, Hans-G. Ludwig³,
Pierre F. L. Maxted⁴, Sara Seager^{5,6,7}, Sami K. Solanki¹, and Jeff Valenti⁸

¹Max-Planck-Institut für Sonnensystemforschung, Justus-von-Liebig-Weg 3,
37077 Göttingen, Germany

²Institut für Astrophysik, Georg-August-Universität Göttingen,
Friedrich-Hund-Platz 1, 37077 Göttingen, Germany

³Zentrum für Astronomie, Landessternwarte, Königstuhl 12, 69117, Heidelberg,
Germany

⁴Astrophysics group, Keele University, Keele, Staffordshire ST5 5BG, UK

⁵Department of Physics and Kavli Institute for Astrophysics and Space Research,
Massachusetts Institute of Technology, Cambridge, MA 02139, USA

⁶Department of Earth, Atmospheric and Planetary Sciences, Massachusetts
Institute of Technology, Cambridge, MA 02139, USA

⁷Department of Aeronautics and Astronautics, Massachusetts Institute of
Technology, 77 Massachusetts Avenue, Cambridge, MA 02139, USA

⁸Space Telescope Science Institute, 3700 San Martin Drive, Baltimore, MD 21218,
USA

March 4, 2024

Stars appear darker at their limbs than at their disk centers because at the limb we are viewing the higher and cooler layers of stellar photospheres. Limb darkening derived from state-of-the-art stellar atmosphere models systematically fails to reproduce recent transiting exoplanet light curves from the Kepler, TESS, and JWST telescopes — stellar brightness obtained from measurements drops less steeply towards the limb

1

transit profiles (see Figure 6 in Methods) and, in particular, the transit depth, which plays a crucial role in determining the radius of transiting planet. The effect is especially strong shortward of 2000 nm, e.g. the magnetic field of 100 G would induce a change of the transit depth larger than about 30–40 ppm for a Jupiter-size planet transiting the Sun (Figure 4). Such changes can be observed with JWST even for a single transit observation and will also interfere with the interpretation of the JWST transit light curves. Indeed, the first JWST results⁴⁰ indicate that the transit curves are not contaminated by systematic effects in most spectral channels, and the noise can be reduced to just a couple of ppm per spectral bin for most of the exoplanet target stars JWST observes (see Fig. 8 from Rustamkulov et al.⁴⁰).

Discussion

Small-scale surface magnetic fields previously ignored in modeling of stellar limb darkening modify the atmospheric structure and therefore stellar limb darkening. We have shown that adding such magnetic fields into 3D radiation MHD simulations of stellar atmospheres solves the limb darkening conundrum, i.e. the inability of 1D and 3D magnetic field-free models of stellar atmospheres to return limb darkening profiles consistent with observations.

The dependence of the limb darkening on surface magnetic field can be seen as a curse or a blessing depending on one’s point of view. On the one hand, it introduces one more free parameter into the light curve fitting. On the other hand, it offers the exciting possibility of measuring the magnetization of stars hosting transiting planets. In particular, the limb darkening method opens the unique opportunity to measure stellar magnetic fields with the upcoming PLATO mission, which will observe tens of thousands of bright stars on the lower main sequence³⁵.

The effect of magnetic field on limb darkening strongly depends on the wavelength (Figs 3–4) and, thus, ignoring it might introduce spurious features in the transmission spectra obtained with JWST and eventually with ARIEL⁴⁷. This underscores the importance of accounting for the magnetic effect on limb darkening in the analysis of transmission spectra. atmospheric retrievals which is offered by our modeling approach.

Methods

Calculations with MURaM and MPS-ATLAS codes. We utilize the 3D radiative magnetohydrodynamic (MHD) code MURaM^{37,49} (which stands for MPS/University of Chicago

Assessing light pollution in vast areas: zenith sky brightness maps of Catalonia

Hector Linares^{1,2,3}, Eduard Masana³, Salvador J Ribas⁴, Manuel
García-Gil^{5,6}, Martin Aubé^{1,2,7}, Alejandro Sánchez de Miguel^{8,9,10},
Alexandre Simoneau^{1,2}

¹ *Département de géomatique appliquée, Université de Sherbrooke*

² *Département de physique, Cégep de Sherbrooke*

³ *Institut de Ciències del Cosmos (ICC-UB-IEEC), Barcelona, Spain*

⁴ *Parc Astronòmic Montsec - Ferrocarrils de la Generalitat de Catalunya, Àger, Spain*

⁵ *Departament d'Acció Climàtica, Alimentació i Agenda Rural, Generalitat de Catalunya*

⁶ *Departament d'Enginyeria de Projectes i de la Construcció, Universitat Politècnica de
Catalunya, BarcelonaTech, Spain*

⁷ *Physics Department, Bishop's University*

⁸ *Depto. Física de la Tierra y Astrofísica. Instituto de Física de Partículas y del Cosmos
(IPARCOS), Universidad Complutense, Madrid, Spain*
















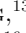







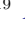



⁹ *Instituto de Astrofísica de Andalucía, Glorieta de la Astronomía, Granada, Spain*

¹⁰ *Environment and Sustainability Institute, University of Exeter, Penryn, Cornwall,
U.K.*

Abstract

Zenith sky brightness maps in the V and B bands of the region of Catalonia are presented in this paper. For creating them we have used the light pollution numerical model *Illumina v2*. The maps have a sampling of 5x5 km for the whole region with an improved resolution of 1x1 km for one of the provinces within Catalonia, Tarragona. Before creating the final maps, the methodology was tested successfully by comparing the computed values to measurements in nineteen different locations spread out throughout the territory. The resulting maps have been compared to the zenith sky brightness world atlas and also to Sky Quality Meter (SQM) dynamic measurements. When comparing to measurements we found small differences mainly due to mismatching in the location of the points studied, and also due to differences in the natural sky brightness and atmospheric content. In the comparison to the world atlas some differences were expected as we are taking into account the blocking effect of topography and obstacles, and also due to a more

Validation of a Third Planet in the LHS 1678 System

MICHELE L. SILVERSTEIN ^{1,2,3,*} THOMAS BARCLAY ² JOSHUA E. SCHLIEDER ² KAREN A. COLLINS ⁴
RICHARD P. SCHWARZ ⁴ BENJAMIN J. HORD ^{2,†} JASON F. ROWE ⁵ ETHAN KRUSE ^{2,6}
NICOLA ASTUDILLO-DEFRU ⁷ XAVIER BONFILS ⁸ DOUGLAS A. CALDWELL ⁹ DAVID CHARBONNEAU ⁴
RYAN CLOUTIER ¹⁰ KEVIN I. COLLINS ¹¹ TANSU DAYLAN ¹² WILLIAM FONG ¹³ JON M. JENKINS ¹⁴
MICHELLE KUNIMOTO ¹³ SCOTT McDERMOTT ¹⁵ FELIPE MURGAS ^{16,17} ENRIC PALLE ^{16,17} GEORGE R. RICKER ¹³
SARA SEAGER ^{13,18,19} AVI SHPORER ¹³ EVAN TEY ¹³ ROLAND VANDERSPEK ¹³ AND JOSHUA N. WINN ²⁰

¹ *University of Maryland, Baltimore County, 1000 Hilltop Circle, Baltimore, MD 21250, USA*

² *NASA Goddard Space Flight Center, Greenbelt, MD 20771, USA*

³ *GSFC Sellers Exoplanet Environments Collaboration, Greenbelt, MD 20771, USA*

⁴ *Center for Astrophysics | Harvard & Smithsonian, 60 Garden Street, Cambridge, MA, 02138, USA*

⁵ *Department of Physics and Astronomy, Bishops University, 2600 Rue College, Sherbrooke, QC J1M 1Z7, Canada*

⁶ *University of Maryland, College Park, MD 20742, USA*

⁷ *Departamento de Matemática y Física Aplicadas, Universidad Católica de la Santísima Concepción, Alonso de Rivera 2850, Concepción, Chile*

⁸ *Univ. Grenoble Alpes, CNRS, IPAG, F-38000 Grenoble, France*

⁹ *SETI Institute, Mountain View, CA 94043 USA/NASA Ames Research Center, Moffett Field, CA 94035 USA*

¹⁰ *Department of Physics & Astronomy, McMaster University, 1280 Main St West, Hamilton, ON, L8S 4L8, Canada*

¹¹ *George Mason University, 4400 University Drive, Fairfax, VA, 22030 USA*

¹² *Department of Physics and McDonnell Center for the Space Sciences, Washington University, St. Louis, MO 63130, USA*

¹³ *Department of Physics and Kavli Institute for Astrophysics and Space Research, Massachusetts Institute of Technology, Cambridge, MA 02139, USA*

¹⁴ *NASA Ames Research Center, Moffett Field, CA 94035, USA*

¹⁵ *Proto-Logic LLC, 1718 Euclid Street NW, Washington, DC 20009, USA*

¹⁶ *Instituto de Astrofísica de Canarias (IAC), E-38205 La Laguna, Tenerife, Spain*

¹⁷ *Departamento de Astrofísica, Universidad de La Laguna (ULL), E-38206 La Laguna, Tenerife, Spain*

¹⁸ *Department of Earth, Atmospheric, and Planetary Sciences, Massachusetts Institute of Technology, Cambridge, MA 02139, USA*

¹⁹ *Department of Aeronautics and Astronautics, MIT, 77 Massachusetts Avenue, Cambridge, MA 02139, USA*

²⁰ *Department of Astrophysical Sciences, Princeton University, 4 Ivy Lane, Princeton, NJ 08544, USA*

ABSTRACT

The nearby LHS 1678 (TOI-696) system contains two confirmed planets and a wide-orbit, likely brown-dwarf companion, which orbit an M2 dwarf with a unique evolutionary history. The host star occupies a narrow “gap” in the HR diagram lower main sequence, associated with the M dwarf fully convective boundary and long-term luminosity fluctuations. This system is one of only about a dozen M dwarf multi-planet systems to date that hosts an ultra-short period planet (USP). Here we validate and characterize a third planet in the LHS 1678 system using TESS Cycle 1 and 3 data and a new ensemble of ground-based light curves. LHS 1678 d is a $0.98 \pm 0.07 R_{\oplus}$ planet in a 4.97-day orbit, with an insolation flux of $9.1^{+0.9}_{-0.8} S_{\oplus}$. These properties place it near 4:3 mean motion resonance with LHS 1678 c and in company with LHS 1678 c in the Venus zone. LHS 1678 c and d are also twins in size and predicted mass, making them a powerful duo for comparative exoplanet studies. LHS 1678 d joins its siblings as another compelling candidate for atmospheric measurements with the JWST and mass measurements using high-precision radial velocity techniques. Additionally, USP LHS 1678 b breaks the “peas-in-a-pod” trend in this system, although additional planets could fill in the “pod” beyond its orbit. LHS 1678’s unique combination of system properties and their relative rarity among the ubiquity of compact multi-planet systems around M dwarfs makes the system a valuable benchmark for testing theories of planet formation and evolution.

Fires in the deep: The luminosity distribution of early-time gamma-ray-burst afterglows in light of the *Gamow Explorer* sensitivity requirements^{★ ★★}

D. A. Kann^{★ ★ ★ 1,2}, N. E. White^{★ ★ ★ ★ 3}, G. Ghirlanda⁴, S. R. Oates⁵, A. Melandri⁴, M. Jelínek⁶, A. de Ugarte Postigo⁷, A. J. Levan^{8,9}, A. Martin-Carrillo¹⁰, G. S.-H. Paek¹¹, L. Izzo^{12,13}, M. Blazek¹⁴, C. C. Thöne⁶, J. F. Agüí Fernández¹⁴, R. Salvaterra¹⁵, N. R. Tanvir¹⁶, T.-C. Chang¹⁷, P. O'Brien¹⁶, A. Rossi¹⁸, D. A. Perley¹⁹, M. Im¹¹, D. B. Malesani⁸, A. Antonelli²⁰, S. Covino⁴, C. Choi^{11,21}, P. D'Avanzo⁴, V. D'Elia^{20,22}, S. Dichiaro^{23,24,25}, H.M. Fausey³, D. Fugazza⁴, A. Gomboc²⁶, K. M. Gorski^{17,27}, J. Granot^{28,29,3}, C. Guidorzi^{18,30,31}, L. Hanlon¹⁰, D. H. Hartmann³², R. Hudec^{6,33,34}, H. D. Jun^{11,35}, J. Kim^{11,36}, Y. Kim²¹, S. Klose³⁷, W. Kluźniak³⁸, S. Kobayashi¹⁹, C. Kouveliotou³, A. Lidz³⁹, M. Marongiu⁴⁰, R. Martone^{2,30}, P. Meintjes⁴¹, C. G. Mundell^{42,43}, D. Murphy¹⁰, K. Nalewajko³⁸, W.-K. Park²¹, D. Szécsi⁴⁴, R. J. Smith¹⁹, B. Stecklum³⁷, I. A. Steele¹⁹, J. Štrobl⁶, H.-I. Sung²¹, A. Updike⁴⁵, Y. Urata⁴⁶, and A.J. van der Horst³

(Affiliations can be found after the references)

Received 5 October 2023 / Accepted 15 February 2024

ABSTRACT

Context. Gamma-ray bursts (GRBs) are ideal probes of the Universe at high redshift (z), pinpointing the locations of the earliest star-forming galaxies and providing bright backlights with simple featureless power-law spectra that can be used to spectrally fingerprint the intergalactic medium and host galaxy during the period of reionization. Future missions such as *Gamow Explorer* (hereafter *Gamow*) are being proposed to unlock this potential by increasing the rate of identification of high- z ($z > 5$) GRBs in order to rapidly trigger observations from 6 – 10 m ground telescopes, the James Webb Space Telescope (JWST), and the upcoming Extremely Large Telescopes (ELTs).

Aims. *Gamow* was proposed to the NASA 2021 Medium-Class Explorer (MIDEX) program as a fast-slewing satellite featuring a wide-field lobster-eye X-ray telescope (LEXT) to detect and localize GRBs with arcminute accuracy, and a narrow-field multi-channel photo- z infrared telescope (PIRT) to measure their photometric redshifts for $> 80\%$ of the LEXT detections using the Lyman- α dropout technique. We use a large sample of observed GRB afterglows to derive the PIRT sensitivity requirement.

Methods. We compiled a complete sample of GRB optical–near-infrared (optical–NIR) afterglows from 2008 to 2021, adding a total of 66 new afterglows to our earlier sample, including all known high- z GRB afterglows. This sample is expanded with over 2837 unpublished data points for 40 of these GRBs. We performed full light-curve and spectral-energy-distribution analyses of these afterglows to derive their true luminosity at very early times. We compared the high- z sample to the comparison sample at lower redshifts. For all the light curves, where possible, we determined the brightness at the time of the initial finding chart of *Gamow*, at different high redshifts and in different NIR bands. This was validated using a theoretical approach to predicting the afterglow brightness. We then followed the evolution of the luminosity to predict requirements for ground- and space-based follow-up. Finally, we discuss the potential biases between known GRB afterglow samples and those to be detected by *Gamow*.

Results. We find that the luminosity distribution of high- z GRB afterglows is comparable to those at lower redshift, and we therefore are able to use the afterglows of lower- z GRBs as proxies for those at high z . We find that a PIRT sensitivity of $15 \mu\text{Jy}$ (21 mag AB) in a 500 s exposure simultaneously in five NIR bands within 1000s of the GRB trigger will meet the *Gamow* mission requirements. Depending on the z and NIR band, we find that between 75% and 85% of all afterglows at $z > 5$ will be recovered by *Gamow* at 5σ detection significance, allowing the determination of a robust photo- z . As a check for possible observational biases and selection effects, we compared the results with those obtained through population-synthesis models, and find them to be consistent.

Conclusions. *Gamow* and other high- z GRB missions will be capable of using a relatively modest 0.3m onboard NIR photo- z telescope to rapidly identify and report high- z GRBs for further follow-up by larger facilities, opening a new window onto the era of reionization and the high-redshift Universe.

Key words. Gamma-ray burst: general – Cosmology: dark ages, reionization, first stars – Space vehicles: instruments – Methods: observational – Techniques: photometric

* This study is partially based on data collected under ESO programmes 089.A-0067(B) (PI: Fynbo), 091.A-0703(A) (PI: Krühler), 091.A-0703(B) (PI: Krühler), 091.C-0934(B) (PI: Kaper).

** Table B.1 is only available in electronic form at the CDS via anonymous ftp to cdsarc.u-strasbg.fr (130.79.128.5) or via <http://cdsweb.u-strasbg.fr/cgi-bin/qcat?J/A+A/>.

*** Deceased

**** E-mail: newwhite@gwu.edu

1. Introduction

At their peak, gamma-ray bursts (GRBs) are the most luminous events in the Universe and occur when either massive stars reach their final stage in a supernova explosion or when binary compact objects—one of which is a neutron star (for a review see Zhang 2018)—merge. In both cases, a relativistic jet emerges powered by accretion onto a newly formed black hole, which results in a bright panchromatic afterglow. In the first few hours to

A foreground-marginalized ‘BK-lite’ likelihood for the tensor-to-scalar ratio

Heather Prince,^{1,2} Erminia Calabrese,³ and Jo Dunkley^{4,2}

¹*Department of Physics and Astronomy, Rutgers, the State University of New Jersey,
136 Frelinghuysen Road, Piscataway, NJ 08854, USA*

²*Peyton Hall, Princeton University, Princeton, NJ 08544, USA*

³*School of Physics and Astronomy, Cardiff University, The Parade, Cardiff, CF24 3AA, UK*

⁴*Joseph Henry Laboratories of Physics, Jadwin Hall,
Princeton University, Princeton, NJ 08544, USA*

The current limit on the tensor-to-scalar ratio from the BICEP/Keck Collaboration (with $r < 0.036$ at 95% confidence) puts pressure on early universe models, with less than 10% of the error on r attributed to uncertainty in Galactic foregrounds. We use the BICEP/Keck BK18 public multi-frequency likelihood to test some further assumptions made in the foreground modeling, finding little impact on the estimate for r . We then estimate foreground-marginalized cosmic microwave background (CMB) B -mode polarization bandpowers. We fit them with a multivariate offset-lognormal distribution and construct a marginalized ‘BK-lite’ likelihood for the CMB B -mode spectrum with no nuisance parameters, serving as a method demonstration for future analyses of small sky regions, for example from the South Pole Observatory or CMB-S4.

I. INTRODUCTION

A key goal towards understanding the physics of the early universe is to constrain or detect primordial tensor perturbations. These would have propagated as gravitational waves, imprinting signals in the cosmic microwave background (CMB) intensity and polarization anisotropy. They uniquely produce primordial divergence-free B -mode polarization, with power predicted to peak at degree scales and larger [1, 2]. B -mode polarization is also generated from the gravitational lensing of the primordial curl-free E -mode polarization, and is additionally produced by thermal dust and synchrotron emission in the Galaxy [e.g., 3].

The tightest constraint on primordial tensor perturbations comes from BICEP3 observations from the South Pole, together with data from BICEP2 and the Keck Array, and supplemented by *Planck* and *WMAP* satellite data, resulting in an upper limit on the ratio of tensor to scalar power at 0.05 Mpc^{-1} of $r < 0.036$ at 95% confidence [4, hereafter BK18]. Independent of BK18, an upper limit of $r < 0.056$ was estimated from *Planck*, using the NPIPE maps [5], and the first flight of the SPIDER balloon experiment gave $r < 0.11$ [6].

These constraints on r depend on the treatment of Galactic foregrounds, especially the polarized dust emission. To constrain the foregrounds in the BK18 analysis, polarization maps at seven effective frequencies are fit to simultaneously constrain r and a seven-parameter foreground model. In the original BICEP2 150 GHz data [7, 8], the foreground level at degree scales was significantly larger than the gravitationally lensed CMB signal expected for a universe with $r = 0$. In contrast, the best-measured B -mode signal in BK18 is now at 95 GHz where the power in foreground emission is more than five times lower, of comparable size to the lensed CMB at degree scales. The foregrounds still need to be modeled, however, and a set of different models were tested in the BK18 analysis, demonstrating the stability of the esti-

ated r to the choices made. In this paper we briefly explore some further assumptions, finding little impact on r using the publicly available products. We then use the BICEP/Keck, *WMAP* and *Planck* data to estimate foreground-marginalized bandpowers for the B -mode angular power spectrum, an extension to the BK18 analysis. We use them to construct a ‘BK-lite’ likelihood which reproduces the same tensor-to-scalar ratio constraint as the corresponding multi-frequency likelihood, following a similar approach adopted for data from the Atacama Cosmology Telescope (ACT) and *Planck*, and for simulated Simons Observatory data [9–12]. This likelihood can be used to test models of the early universe and to obtain distributions of the B -mode bandpowers that include uncertainty due to foregrounds.

This paper is laid out as follows. We review the BICEP/Keck data and likelihood in §II. In §III we explore the foreground model. In §IV we estimate foreground-marginalized CMB B -mode bandpower amplitudes and construct a ‘BK-lite’ likelihood. We conclude in §V.

II. THE BICEP/KECK DATA AND LIKELIHOOD

In this section we review the details of the BK18 likelihood analysis, described fully in e.g., Refs. [4, 13, 14].

A. Data

BICEP3: Q and U Stokes vector maps were made from data gathered from 2016–18 with BICEP3, over $\sim 600 \text{ deg}^2$ in a band centered at 95 GHz. They have the lowest polarization noise yet reported, with a depth of $2.8 \mu\text{K-arcmin}$ [4, 15].

BICEP2/Keck: Stokes maps were made in a smaller $\sim 400 \text{ deg}^2$ region using data gathered with BICEP2 from 2010–12 in a band centered at 150 GHz [14], and with the

A spectroscopic investigation of thermal instability for cylindrical equilibria with background flow

J. Hermans¹ and R. Keppens¹

¹ Centre for mathematical Plasma-Astrophysics, Celestijnenlaan 200B, 3001 Leuven, KU Leuven, Belgium

Received date / Accepted date

ABSTRACT

Context. Flows are omnipresent and govern the dynamics of plasma. Solar tornadoes are a class of apparently rotating prominences, that might be formed by thermal instability. In spectroscopic studies on thermal instability background flow is commonly neglected. *Aims.* We here determine the effect of background flow on thermal instability in cylindrical magnetic field configurations. How various parameters affect the distribution of eigenmodes in the MHD spectrum is also explored. We investigate whether discrete thermal modes exist.

Methods. In an analytical study, we extend upon the literature by including a generic background flow in a cylindrical coordinate system. The non-adiabatic MHD equations are linearised, Fourier-analysed, and are examined to understand how a background flow changes the continua. An approximate expression for discrete thermal modes is derived using a WKB analysis. The analytical results are then verified for a benchmark equilibrium using the eigenvalue code *Legolas*. The eigenfunctions of discrete thermal modes are visualised in 2D and 3D.

Results. The thermal continuum is Doppler-shifted due to the background flow, just like the slow and Alfvén continua. Discrete modes are altered because the governing equations contain flow-related terms. An approximate expression to predict the appearance of discrete thermal modes based on the equilibrium parameters is derived. All analytical expressions match the numerical results. The distribution of the density perturbations of the discrete thermal modes is not a uniform or singular condensation, due to the shape of the eigenfunctions and the dependence of the assumed waveform on the coordinates and wavenumbers. 3D visualisation of the total velocity field shows that the helical field is heavily influenced by the radial velocity perturbation.

Conclusions. We derived analytic expressions for non-adiabatic MHD modes of a cylindrical equilibrium with background flow and verified them using a coronal equilibrium. However, the equations are valid for and can be applied in other astrophysical environments.

Key words. Magnetohydrodynamics (MHD) - Instabilities - Methods: analytical - Sun: filaments, prominences

1. Introduction

The solar atmosphere is a very dynamic environment. Reconnection is the cause of energetic phenomena such as solar flares and jets. Jets may be represented as fast, rotating outflows (Shen 2021). This transient flow of plasma has been observed all around the solar corona (Chitta et al. 2021; Long et al. 2023). Waves and quasi-periodic flows are also common (De Moortel et al. 2015; Banerjee et al. 2021). Upflows from the transition layer and corona are considered the driving force behind the slow solar wind (Barczynski et al. 2021a, 2023). Furthermore, prominences are involved in violent eruptions, creating shock waves throughout the corona and launching coronal mass ejections, CMEs, into space (Webb 2015). Prominences are host to a variety of flows (Kucera 2015).

Solar tornadoes are a kind of prominences with plasma that appears to be rotating around a vertical axis (Pettit 1932). The phenomenon has recently been the topic of the review paper by Gunár et al. (2023). Many observations were made last decade, see e.g. Su et al. (2012); Li et al. (2012); Wedemeyer et al. (2013); Su et al. (2014); Yang et al. (2018). Line-of-sight Doppler velocities were measured by Orozco Suárez et al. (2012). The red- and blue-shifted pattern was interpreted as rotation around a vertical axis. Yang et al. (2018) observed two tornadoes with both coherent, stable red and blue Doppler shifts in favour of this interpretation. Models of helical magnetic struc-

tures with cool plasma flowing helically are constructed by Luna et al. (2015) and Onishchenko et al. (2018). For the tornado studied by Li et al. (2012), the rotational axis is believed to be parallel to the axis of a horizontal flux rope. Such rotational flow in a prominence cavity has recently been studied in a multidimensional simulation of a flux rope prominence (Liakh & Keppens 2023). Prominences are dense structures that are assumed to be suspended in the corona by the magnetic field. Luna et al. (2015) showed that prominence mass can be supported by a vertical helical field if the magnetic field is highly twisted and/or significant poloidal upflows are present. As the rotating nature of tornado prominences is highly controversial, counterarguments and interpretations are provided (Gunár et al. 2023). Panasenco et al. (2014) argued that counterstreaming flows (Schmieder et al. 1991) and oscillations on horizontal threads cause the illusion of rotation. The projection of the 3D structure of a horizontal prominence onto the 2D plane of view can make the field lines look elliptical (Gunár et al. 2018).

Local thermal instability is the preferred method to form cool condensations in hot media, such as prominences in the solar corona. Parker (1953) noticed that the increase of radiative losses with decreasing temperature can lead to runaway cooling. The theory of thermal instability was first described by Field (1965). Claes & Keppens (2019), Claes et al. (2020b), and Hermans & Keppens (2021) performed multidimensional simulations of

The Physical Properties of Changing-look Blazars

SHI-JU KANG ¹, BING LYU ², QINGWEN WU ³, YONG-GANG ZHENG ⁴, AND JUNHUI FAN ⁵

¹*School of Physics and Electrical Engineering, Liupanshui Normal University, Liupanshui, Guizhou, 553004, People's Republic of China*

²*Kavli Institute for Astronomy and Astrophysics, Peking University, Beijing, Beijing, 100871, People's Republic of China*

³*Department of Astronomy, School of Physics, Huazhong University of Science and Technology, Wuhan, Hubei, 430074, People's Republic of China*

⁴*Department of Physics, Yunnan Normal University, Kunming, Yunnan, 650092, People's Republic of China*

⁵*Center for Astrophysics, Guangzhou University, Guangzhou 510006, Peoples Republic of China*

(Received July, 12, 2023; Revised October 30, 2023; Accepted October 30, 2023; Published February 13, 2024)

ABSTRACT

Changing-look active galactic nuclei (AGNs) are a special class of AGNs that change their spectral type from type 1 to type 2 or vice versa. In recent years, a number of changing-look blazars (CLBs) were also reported, which transition between flat-spectrum radio quasars and BL Lacs. The physical properties of CLBs are still unclear. Using the *mclust* R package for Gaussian Mixture Modeling, we performed a clustering analysis for a sample of 105 CLBs selected from the literature. Three kinds of analysis found that CLBs lie in between the parameter distributions of FSRQs and BL Lacs: (i) univariate analysis; (ii) bivariate analysis; and (iii) multivariate analysis, carried out with a dimension reduction approach of the physical properties of the three types of blazars. Our results suggest that CLBs belong to a transition type between FSRQs and BL Lacs, which may be regulated by the change of accretion process and may be similar to other changing-look AGNs.

Keywords: Active galactic nuclei (16) – Blazars (164) — BL Lacertae objects (158) — Flat-spectrum radio quasars (2163)

1. INTRODUCTION

Active galactic nuclei (AGNs) are a special class of galaxies with extremely bright nuclei, which are believed to be powered by the accretion of material into super-massive black holes. Based on the strength of emission lines, AGNs are classified as type 1, with broad lines (1000-20,000 km s⁻¹), or type 2, with only narrow lines (e.g., < 1000 km s⁻¹). Blazars are a subclass of radio-loud AGNs, whose relativistic jets point to us directly (Urry & Padovani 1995). Based on the strength of the optical spectral lines (e.g., the equivalent width (EW) of the spectral line is greater or less than 5 Å), blazars are further classified as flat-spectrum radio quasars (FSRQs) with strong emission lines (EW ≥ 5 Å), and BL Lacerate objects (BL Lacs) with fainter or no emission lines (EW < 5 Å) (Stickel et al. 1991; Stocke et al. 1991).

Changing-look AGNs (CLAGNs) are referred to as sources that experience transitions between type 1 and type 2 with significant variations of broad emission lines (see, e.g., Ricci & Trakhtenbrot 2023 for more discussions and references therein). The discovery of CLAGNs challenges the unified model of AGNs. Similar to CLAGNs, changing-look blazars (CLBs) also experience transitions between states of FSRQs and BL Lacs (e.g., Álvarez Crespo et al. 2016; Mishra et al. 2021; Peña-Herazo et al. 2021; Foschini et al. 2021, 2022, and references therein).

Mishra et al. (2021) reported a CLB, B2 1420+32 (also named OQ 334), which experienced transitions between a FSRQ and BL Lac several times within several years. Recently, more and more CLBs have been discovered. Peña-Herazo et al. (2021) reported 26 CLBs; the authors are confident that three of these have a changing-look nature, based on optical spectra from the Large Sky Area Multi-object Fiber Spectroscopic Telescope (LAMOST) Data Release 5 (DR5) archive. In Foschini

Tip of the iceberg: overmassive black holes at $4 < z < 7$ found by JWST are not inconsistent with the local $\mathcal{M}_{\text{BH}} - \mathcal{M}_{\star}$ relation

JUNYAO LI,¹ JOHN D. SILVERMAN,^{2,3,4,5} YUE SHEN,^{1,6} MARTA VOLONTERI,⁷ KNUD JAHNKE,⁸ MING-YANG ZHUANG,¹ MATTHEW T. SCOGGINS,⁹ XUHENG DING,¹⁰ YUICHI HARIKANE,¹¹ MASAFUSA ONOUE,^{2,4,12} AND TAKUMI S. TANAKA^{3,2,4}

¹*Department of Astronomy, University of Illinois at Urbana-Champaign, Urbana, IL 61801, USA*

²*Kavli Institute for the Physics and Mathematics of the Universe, The University of Tokyo, Kashiwa, Japan 277-8583 (Kavli IPMU, WPI)*

³*Department of Astronomy, School of Science, The University of Tokyo, 7-3-1 Hongo, Bunkyo, Tokyo 113-0033, Japan*

⁴*Center for Data-Driven Discovery, Kavli IPMU (WPI), UTIAS, The University of Tokyo, Kashiwa, Chiba 277-8583, Japan*

⁵*Center for Astrophysical Sciences, Department of Physics & Astronomy, Johns Hopkins University, Baltimore, MD 21218, USA*

⁶*National Center for Supercomputing Applications, University of Illinois at Urbana-Champaign, Urbana, IL 61801, USA*

⁷*Institut d'Astrophysique de Paris, Sorbonne Université, CNRS, UMR 7095, 98 bis bd Arago, 75014 Paris, France*

⁸*Max-Planck-Institut für Astronomie, Königstuhl 17, D-69117 Heidelberg, Germany*

⁹*Department of Astronomy, Columbia University, New York, NY, 10027*

¹⁰*School of Physics and Technology, Wuhan University, Wuhan 430072, China*

¹¹*Institute for Cosmic Ray Research, The University of Tokyo, 5-1-5 Kashiwanoha, Kashiwa, Chiba 277-8582, Japan*

¹²*Kavli Institute for Astronomy and Astrophysics, Peking University, Beijing 100871, P.R.China*

ABSTRACT

JWST is revealing a new remarkable population of high-redshift ($z \gtrsim 4$), low-luminosity Active Galactic Nuclei (AGNs) in deep surveys and detecting the host galaxy stellar light in the most luminous and massive quasars at $z \sim 6$ for the first time. Latest results claim supermassive black holes (SMBHs) in these systems to be significantly more massive than expected from the local BH mass – stellar mass ($\mathcal{M}_{\text{BH}} - \mathcal{M}_{\star}$) relation and that this is not due to sample selection effects. Through detailed statistical modeling, we demonstrate that the coupled effects of selection biases (i.e., finite detection limit and requirements on detecting broad lines) and measurement uncertainties in \mathcal{M}_{BH} and \mathcal{M}_{\star} can in fact largely account for the reported offset and flattening in the observed $\mathcal{M}_{\text{BH}} - \mathcal{M}_{\star}$ relation toward the upper envelope of the local relation, even for those at $\mathcal{M}_{\text{BH}} < 10^8 M_{\odot}$. We further investigate the possible evolution of the $\mathcal{M}_{\text{BH}} - \mathcal{M}_{\star}$ relation at $z \gtrsim 4$ with careful treatment of observational biases and consideration of the degeneracy between intrinsic evolution and dispersion in this relation. The bias-corrected intrinsic $\mathcal{M}_{\text{BH}} - \mathcal{M}_{\star}$ relation in the low-mass regime suggests that there might be a large population of low-mass BHs ($\log \mathcal{M}_{\text{BH}} \lesssim 5$), possibly originating from lighter seeds, remaining undetected or unidentified even in the deepest JWST surveys. These results have important consequences for JWST studies of BH seeding and the coevolution between SMBHs and their host galaxies at the earliest cosmic times.

1. INTRODUCTION

The James Webb Space Telescope (JWST) is revolutionizing the study of high redshift AGNs and the early coevolution of SMBHs with their host galaxies. The unprecedented sensitivity and resolution of NIRC*am* imaging have enabled the first detection of stellar light from AGNs during the reionization epoch ($z \sim 6$) and esti-

mates of their stellar masses. With NIRS*pec*, BH mass estimates, based on the broad H α and H β lines, at such high redshifts are routinely measured with ease. Consequently, several recent studies have investigated the $\mathcal{M}_{\text{BH}} - \mathcal{M}_{\star}$ relation at early cosmic times (e.g., Koccevski et al. 2023; Maiolino et al. 2023; Harikane et al. 2023; Ding et al. 2023; Stone et al. 2023; Yue et al. 2023). This relation, with its slope, normalization, and intrinsic scatter being sensitive to the merger history of galaxies and the impact of AGN feedback, has emerged as one of the most important scaling relations in unraveling the nature of SMBH–galaxy coevolution (e.g., Peng 2007;

Probing AGN jet precession with LISA

Nathan Steinle ^{1,2,*} Davide Gerosa ^{3,4,2} and Martin G. H. Krause ⁵

¹*Department of Physics and Astronomy & Winnipeg Institute for*

Theoretical Physics, University of Manitoba, Winnipeg, R3T 2N2, Canada

²*School of Physics and Astronomy & Institute for Gravitational Wave Astronomy,
University of Birmingham, Birmingham, B15 2TT, UK*

³*Dipartimento di Fisica “G. Occhialini”, Università degli Studi di Milano-Bicocca, Piazza della Scienza 3, 20126 Milano, Italy*

⁴*INFN, Sezione di Milano-Bicocca, Piazza della Scienza 3, 20126 Milano, Italy*

⁵*Centre for Astrophysics Research & Department of Physics, Astronomy and
Mathematics, University of Hertfordshire, College Lane, Hatfield AL10 9AB, UK*

(Dated: March 4, 2024)

The precession of astrophysical jets produced by active-galactic nuclei is likely related to the dynamics of the accretion disks surrounding the central supermassive black holes (BHs) from which jets are launched. The two main mechanisms that can drive jet precession arise from Lense-Thirring precession and tidal torquing. These can explain direct and indirect observations of precessing jets; however, such explanations often utilize crude approximations of the disk evolution and observing jet precession can be challenging with electromagnetic facilities. Simultaneously, the Laser Interferometer Space Antenna (LISA) is expected to measure gravitational waves from the mergers of massive binary BHs with high accuracy and probe their progenitor evolution. In this paper, we connect the LISA detectability of binary BH mergers to the possible jet precession during their progenitor evolution. We make use of a semi-analytic model that self-consistently treats disk-driven BH alignment and binary inspiral and includes the possibility of disk breaking. We find that tidal torquing of the accretion disk provides a wide range of jet precession timescales depending on the binary separation and the spin direction of the BH from which the jet is launched. Efficient disk-driven BH alignment results in shorter timescales of ~ 1 yr which are correlated with higher LISA signal-to-noise ratios. Disk breaking results in the longest possible times of $\sim 10^7$ yrs, suggesting a deep interplay between the disk critical obliquity (i.e. where the disk breaks) and jet precession. Studies such as ours will help to reveal the cosmic population of precessing jets that are detectable with gravitational waves.

I. INTRODUCTION

Astrophysical jets are bipolar outflows observed across astronomical scales and often originate from forming stars or accretion processes involving compact objects such as pulsars, stellar-mass black holes (BHs), and active galactic nuclei (AGN) hosting supermassive BHs [1–15]. Multi-wavelength electromagnetic (EM) observations combined with the long history of modeling of jets have led to advancements in understanding the dynamical evolution of the jet components, interactions with their environments, and their connection to the evolution of their hosts [16, 17].

Among the best studied jets are those associated with AGN [3, 16]. These jets can have an observed range of morphologies [18–20], exhibit substantial variability [18, 21, 22], and extend across a wide range of spatial and angular scales [23]. The components of a jet can be ejected with different apparent proper motions and directions on the sky plane, typically interpreted as arising from the precession of the jet about a rotation axis [18, 19, 24–26]. Observing this precession can be challenging and relating it to the kinematically-driven evolution of the jet at ~ 0.1 pc spatial and ~ 1 mas angular scales is uncertain [27].

The precession of a jet is most easily directly observ-

able if its axis of rotation is sufficiently along the line of sight. A classic example is the “Rosetta Stone” blazar OJ287, whose jet has been observed for 100+ years and is precessing over a timescale of ~ 20 yrs [26, 28], possibly driven by the evolution of a BH binary [29]. The high-redshift blazar J0017+8135 has a jet precessing over a timescale ~ 12 yrs [30]. Alternatively, if the AGN is within sufficient proximity from us, the precession of an off-the-line-of-sight jet can also be directly observed; this is the case of the nearby galaxy M81, whose jet precesses over a timescale of ~ 7 –12 yrs [25, 31, 32]. Other systems observed to host dynamically evolving outflows, such as misaligned bubbles and radio lobes, are thought to be tied to the motion of a jet precessing over timescales \gtrsim Myr [19]. A good example is Hydra A, where 3D hydrodynamic modelling of the high-resolution radio observations suggest a precession timescale of 10^6 yrs [33]. Jet precession is also a possible explanation for the locations of the bubbles in the Perseus cluster, NGC 1275 (3C 84) [34, 35], where the jet precession timescale was measured to be $\sim 10^7$ yrs by identifying the formation of four components: inner jets, outer lobes, ghost bubbles, and ancient bubbles [36], though, “cluster weather”, i.e., gas motions due to substructure mergers, probably also plays a role.

Currently, EM observations of AGNs with jets indicate that many can display strong curvature, see e.g.’s [37, 38], some fraction of which may be due to jet precession [39]. The fundamental cause(s) of jet precession are uncertain, but two main possibilities involve the precession of an

* nathan.steinle@umanitoba.ca

IMPRINTS OF INTERACTION PROCESSES IN THE GLOBULAR CLUSTER SYSTEM OF NGC 3640

ANA I. ENNIS^{*1,2}, JUAN P. CASO^{†3,4,5}, AND LILIA P. BASSINO^{‡5}

¹Waterloo Centre for Astrophysics, University of Waterloo, 200 University Ave W, Waterloo, Ontario N2L 3G1, Canada

²Perimeter Institute for Theoretical Physics, Waterloo, Ontario N2L 2Y5, Canada

³Instituto de Astrofísica de La Plata (CCT La Plata – CONICET, UNLP), Paseo del Bosque S/N, B1900FWA La Plata, Argentina

⁴Consejo Nacional de Investigaciones Científicas y Técnicas, Godoy Cruz 2290, C1425FQB, Ciudad Autónoma de Buenos Aires, Argentina and

⁵Facultad de Ciencias Astronómicas y Geofísicas de la Universidad Nacional de La Plata, Paseo del Bosque S/N, B1900FWA La Plata, Argentina

(Dated: March 4, 2024)
submitted XXX; accepted YYY

ABSTRACT

We present a wide-field study of the globular cluster systems (GCS) of the elliptical galaxy NGC 3640 and its companion NGC 3641, based on observations from Gemini Multi-Object Spectrograph/Gemini. NGC 3640 is a shell galaxy which presents a complex morphology, which previous studies have indicated as the sign of a recent ‘dry’ merger, although whether its nearest neighbour could have had an influence in these substructures remains an open question. In this work, we trace the spatial distribution of the globular clusters (GCs) as well as their colour distribution, finding a potential bridge of red GCs that connects NGC 3640 to its less massive companion, and signs that the blue GCs were spatially disturbed by the event that created the shells.

Keywords: Early-type galaxies (429), Galaxies (573), Globular star clusters (656)

1. INTRODUCTION

Mergers are essential parts of the current Λ Cold Dark Matter paradigm, in which dark matter haloes and galaxies are mainly formed through hierarchical assembly (Peebles 1982; Blumenthal et al. 1984; Davis et al. 1985). In particular, the early evolution of early-type galaxies (ETGs) is dominated by major mergers involving large amounts of gas (Naab et al. 2007). Once they become quiescent, they continue to grow their mass and size through minor dry mergers, with little to no star formation (Naab et al. 2009, e.g.). Aside from being the driving forces behind the mass growth of a galaxy, mergers shape the morphology of galaxies (Hopkins et al. 2010; Kannan et al. 2015, e.g.), feed central supermassive black holes, and potentially trigger central starbursts (Ellison et al. 2011; Satyapal et al. 2014). As such, they are important components of any galaxy formation model.

The frequency of major mergers experienced by a galaxy is influenced by the local density where it resides, as evidenced by the dependence of the fraction of passive galaxies and stellar mass functions with it (e.g. McNaught-Roberts et al. 2014; Etherington et al. 2017). Although this relation is nuanced, it is clear that higher-density environments show larger rates of galaxy mergers, with groups being the most active type of environment.

Tidal features are the most direct evidence of recent mergers, and they have been widely used to characterize the impact of these events on the properties of galaxies. Photometric analysis has shown, for example, that blue ETGs are more likely to present morphological disturbances (Tal et al. 2009; Kaviraj et al. 2011, e.g.), hinting

at the presence of younger stellar populations as a consequence of recent mergers. However, most of the signatures of accretion events are found in the form of low surface brightness structures, which require long exposures to be analysed.

Globular clusters (GCs) located in the halo of galaxies are helpful tools when it comes to tracing the occurrence of recent mergers since they are bright and they are connected to the underlying stellar population, acting as fossil records of the evolutionary history of their host galaxy and carrying in their properties valuable information about its accretion events. In regions where the stellar halo is too faint, GCs have been used as tracers of stellar streams and tidal tails (Napolitano et al. 2022), and when structures can be detected, the colours and positions of the GCs connected to them can shed further light on their origin (Lim et al. 2017; D’Abrusco et al. 2022, e.g.). Since GCs are sparse even in massive galaxies and tidal features are hard to detect, studying this connection requires deep, wide-field observations. In nearby ETGs, rich underlying substructure is related with GC systems with unusual colour and luminosity distributions (e.g. Sesto et al. 2016; Bassino & Caso 2017), and the presence of young GCs (e.g. Strader et al. 2004; Woodley et al. 2010).

The elliptical galaxy NGC 3640, located at a distance of 27 Mpc according to the results from the surface brightness fluctuation method (SBF) (Tully et al. 2013), is part of a loose group conformed by approximately eight galaxies (Madore et al. 2004). This group is thought to be dynamically young since no X-ray emission was detected by ROSAT above 3σ of the background level (Osmond & Ponman 2004). NGC 3640 has an absolute mag-

ABUNDANCES OF NEUTRON-CAPTURE ELEMENTS IN 62 STARS IN THE GLOBULAR CLUSTER MESSIER 15

JONATHAN CABRERA GARCIA,^{1,2} CHARLI M. SAKARI,² IAN U. ROEDERER,^{3,4,5} DONAVON W. EVANS,² PEDRO SILVA,²
MARIO MATEO,⁴ YING-YI SONG,^{6,7} ANTHONY KREMIN,⁸ JOHN I. BAILEY, III,⁹ AND MATTHEW G. WALKER¹⁰

- ¹*Department of Physics and Astronomy and JINA Center for the Evolution of the Elements, University of Notre Dame, Notre Dame, IN 46556, USA*
²*Department of Physics & Astronomy, San Francisco State University, San Francisco CA 94132, USA*
³*Department of Physics, North Carolina State University, Raleigh, NC 27695, USA*
⁴*Department of Astronomy, University of Michigan, Ann Arbor, MI 48109, USA*
⁵*Joint Institute for Nuclear Astrophysics – Center for the Evolution of the Elements (JINA-CEE), USA*
⁶*David A. Dunlap Department of Astronomy & Astrophysics, University of Toronto, 50 St. George Street, Toronto, ON M5S 3H4, Canada*
⁷*Dunlap Institute for Astronomy & Astrophysics, University of Toronto, 50 St. George Street, Toronto, ON M5S 3H4, Canada*
⁸*Physics Division, Lawrence Berkeley National Laboratory, Berkeley, CA 94720, USA*
⁹*Department of Physics, University of California, Santa Barbara, CA 93106, USA*
¹⁰*Department of Physics, Carnegie Mellon University, Pittsburgh, PA 15213, USA*

ABSTRACT

M15 is a globular cluster with a known spread in neutron-capture elements. This paper presents abundances of neutron-capture elements for 62 stars in M15. Spectra were obtained with the Michigan/Magellan Fiber System (M2FS) spectrograph, covering a wavelength range from ~ 4430 - 4630 Å. Spectral lines from Fe I, Fe II, Sr I, Zr II, Ba II, La II, Ce II, Nd II, Sm II, Eu II, and Dy II, were measured, enabling classifications and neutron-capture abundance patterns for the stars. Of the 62 targets, 44 are found to be highly Eu-enhanced *r*-II stars, another 17 are moderately Eu-enhanced *r*-I stars, and one star is found to have an *s*-process signature. The neutron-capture patterns indicate that the majority of the stars are consistent with enrichment by the *r*-process. The 62 target stars are found to show significant star-to-star spreads in Sr, Zr, Ba, La, Ce, Nd, Sm, Eu, and Dy, but no significant spread in Fe. The neutron-capture abundances are further found to have slight correlations with sodium abundances from the literature, unlike what has been previously found; follow-up studies are needed to verify this result. The findings in this paper suggest that the Eu-enhanced stars in M15 were enhanced by the same process, that the nucleosynthetic source of this Eu pollution was the *r*-process, and that the *r*-process source occurred as the first generation of cluster stars was forming.

Keywords: globular clusters: individual (M15) — stars: abundances — stars: atmospheres — stars: fundamental parameters — Galaxy: formation

The Multi-layer Nature of Molecular Gas toward the Cygnus Region

SHIYU ZHANG,^{1,2} YANG SU^{†,1,2} XUEPENG CHEN,^{1,2} MIN FANG,^{1,2} QINGZENG YAN,¹ SHAOBO ZHANG,¹ YAN SUN,^{1,2}
XIAOLONG WANG,^{3,*} HAORAN FENG,^{1,2} YUEHUI MA,¹ MIAOMIAO ZHANG,¹ ZI ZHUANG,^{1,2} XIN ZHOU,¹ ZHIWEI CHEN,¹ AND
JI YANG¹

¹*Purple Mountain Observatory and Key Laboratory of
Radio Astronomy, Chinese Academy of Sciences, Nanjing 210034,
People's Republic of China*

²*School of Astronomy and Space Science, University of
Science and Technology of China, 96 Jinzhai Road, Hefei 230026,
People's Republic of China*

³*Department of Physics, Hebei Normal University,
Shijiazhuang 050024, People's Republic of China*

ABSTRACT

We study the physical properties and 3D distribution of molecular clouds (MCs) toward the Cygnus region using the MWISP CO survey and Gaia DR3 data. Based on Gaussian decomposition and clustering for ¹³CO lines, over 70% of the fluxes are recovered. With the identification result of ¹³CO structures, two models are designed to measure the distances of the molecular gas in velocity crowding regions. The distances of more than 200 large ¹³CO structures are obtained toward the 150 square degree region. Additionally, tens of the identified MC structures coincide well with masers and/or intense mid-IR emission. We find multiple gas layers toward the region: (1) the extensive gas structures composing the Cygnus Rift from 700 pc to 1 kpc across the whole region; (2) the ~ 1.3 kpc gas layer mainly in the Cygnus X South region; and (3) the 1.5 kpc dense filament at the Cygnus X North region and many cometary clouds shaped by Cygnus OB2. We also note that the spatial distribution of YSO candidates is generally consistent with the molecular gas structures. The total molecular mass of the Cygnus region is estimated to be $\sim 2.7 \times 10^6 M_{\odot}$ assuming an X-factor ratio $X_{\text{CO}} = 2 \times 10^{20} \text{cm}^{-2} (\text{K} \cdot \text{km} \cdot \text{s}^{-1})^{-1}$. The foreground Cygnus Rift contributes $\sim 25\%$ of the molecular mass in the whole region. Our work presents a new 3D view of the MCs distribution toward the Cygnus X region, as well as the exact molecular gas mass distribution in the foreground Cygnus Rift.

Keywords: Distance measure (395) — Interstellar medium (847) — Molecular clouds (1072)

1. INTRODUCTION


CO surveys are of great importance and helpful for studying MCs directly and coordinating Galactic emission at multiple wavelength bands (Heyer & Dame 2015). Particularly, stars are born in the densest parts of MCs, therefore studies of MCs can accelerate our understanding of the link between star formation and the surrounding molecular gas environment, as well as the large scale structures of the Milky Way (Dame et al. 2001; Umamoto et al. 2017; Schuller et al. 2017).

As one of the most massive nearby star formation region (SFR) (Reipurth & Schneider 2008), the Cygnus region harbors giant MC complexes (e.g., DR21, Schneider et al. 2010; Cao et al. 2022) and several OB associations (e.g., the well-known Cygnus OB2, Massey & Thompson 1991; Knödseder 2000; Comerón et al. 2002; Hanson 2003; Wright et al. 2010b, 2015). With Cygnus OB2 in the center, Cygnus X region is divided into the northern and southern parts by Schneider et al. (2006). Hundreds of OB stars toward this region indicate intense star formation activity therein,

Corresponding author: Yang Su
yangsu@pmo.ac.cn

* Physics Postdoctoral Research Station at Hebei Normal University

pAGN: the one-stop solution for AGN disc modeling

Daria Gangardt ¹, Alessandro Alberto Trani ^{2,3,4}, Clément Bonnerot ¹,
Davide Gerosa ^{5,6,1}

¹*School of Physics and Astronomy & Institute for Gravitational Wave Astronomy, University of Birmingham, Birmingham, B15 2TT, UK*

²*Niels Bohr International Academy, Niels Bohr Institute, Blegdamsvej 17, Copenhagen, 2100, Denmark*

³*Research Center for the Early Universe, The University of Tokyo, 7 Chome-3 Hongo, Bunkyo-ku, 113-0033, Tokyo, Japan*

⁴*Okinawa Institute of Science and Technology, 1919-1 Tancha, Onna-son, 904-0495, Okinawa, Japan*

⁵*Dipartimento di Fisica “G. Occhialini”, Università degli Studi di Milano-Bicocca, Piazza della Scienza 3, 20126 Milano, Italy*

⁶*INFN, Sezione di Milano-Bicocca, Piazza della Scienza 3, 20126 Milano, Italy*

4 March 2024

ABSTRACT

Models of accretion discs surrounding active galactic nuclei (AGNs) find vast applications in high-energy astrophysics. The broad strategy is to parametrize some of the key disc properties such as gas density and temperature as a function of the radial coordinate from a given set of assumptions on the underlying physics. Two of the most popular approaches in this context were presented by [Sirko & Goodman \(2003\)](#) and [Thompson et al. \(2005\)](#). We present a critical reanalysis of these widely used models, detailing their assumptions and clarifying some steps in their derivation that were previously left unsaid. Our findings are implemented in the pAGN module for the Python programming language, which is the first public implementation of these accretion-disc models. We further apply pAGN to the evolution of stellar-mass black holes embedded in AGN discs, addressing the potential occurrence of migration traps.

Key words: accretion discs — galaxies: active — black-hole physics

1 INTRODUCTION

Active galactic nuclei (AGNs) are compact regions at the center of galaxies powered by gas accretion onto supermassive black holes (BHs) as opposed to solely the radiation from stars. The underlying theory describing the accretion disc of AGNs was first introduced by [Zel’dovich \(1964\)](#) and [Salpeter \(1964\)](#). AGNs have been studied at low and high redshifts across several electromagnetic wavelengths, capturing a wide range of astrophysical phenomena (see [Netzer 2015](#); [Padovani et al. 2017](#); [Hickox & Alexander 2018](#); [Bianchi et al. 2022](#) for broad reviews on the topic). Due to the deep gravitational well surrounding the central BH, the gas in the accretion disc is expected to reach temperatures of $\sim 10^5$ K and surface densities of $\sim 10^5$ g cm⁻². The accretion disc of the central BH extends to sub-pc scales and is surrounded by optically thick material which is coupled to the disc itself. These components are collectively referred to as the AGN disc, which is expected to extend to separations of 1-10 pc ([Netzer 2015](#)). Because of high obscurations and uncertainty in observations, the actual size of AGN discs is somewhat unclear but tends to be larger than what is expected from theoretical models ([Jha et al. 2022](#); [Guo et al. 2022a,b](#)).

AGN discs are unique astrophysical environments with

a rich phenomenology, including high-energy jets, dusty torii, and accreting BHs ([Padovani et al. 2017](#)). In the context of gravitational-wave observations, AGN discs are studied as host environments for compact-binary formation and mergers ([McKernan et al. 2012, 2011](#); [Yang et al. 2019](#); [Secunda et al. 2019](#); [Fabj et al. 2020](#); [Tagawa et al. 2020](#); [Trani et al. 2023](#)). The large escape velocity around a supermassive BH implies that objects are likely to be retained in the disc vicinities, potentially forming a large population of stellar-mass BHs that have a higher likelihood of interacting. The dense gas in the disc can facilitate binary formation, accelerate the inspiral, and induce chains of hierarchical BH mergers ([Gerosa & Fishbach 2021](#); [Santini et al. 2023](#); [Whitehead et al. 2023](#); [Vaccaro et al. 2023](#)). The occurrence of hierarchical mergers in AGN discs crucially depends on the presence of the so-called migration traps, namely locations in the disc where the migration torque changes sign, which is still an open issue in AGN-disc modeling ([Bellovary et al. 2016](#); [Tagawa et al. 2020](#); [Grishin et al. 2023](#)).

Early models of AGNs discs consists of one-dimensional, steady-state, semi-analytic solutions utilizing parametric prescriptions. Subsequent computational advancements allowed for models capturing more complex physics, such as radiative transfer, gas phase transitions, magnetic fields, and general

Late-Time constraints on Interacting Dark Energy: Analysis independent of H_0 , r_d and M_B

David Benisty,^{1,2,*} Supriya Pan,^{3,4,†} Denitsa Staicova,^{5,‡} Eleonora Di Valentino,^{6,§} and Rafael C. Nunes^{7,8,¶}

¹Frankfurt Institute for Advanced Studies (FIAS), Ruth-Moufang-Strasse 1, 60438 Frankfurt am Main, Germany

²Helsinki Institute of Physics, P.O. Box 64, FI-00014 University of Helsinki, Finland

³Department of Mathematics, Presidency University, 86/1 College Street, Kolkata 700073, India

⁴Institute of Systems Science, Durban University of Technology,
PO Box 1334, Durban 4000, Republic of South Africa

⁵Institute for Nuclear Research and Nuclear Energy, Bulgarian Academy of Sciences, Sofia, Bulgaria

⁶School of Mathematics and Statistics, University of Sheffield,
Hounsfield Road, Sheffield S3 7RH, United Kingdom

⁷Instituto de Física, Universidade Federal do Rio Grande do Sul, 91501-970 Porto Alegre RS, Brazil

⁸Divisão de Astrofísica, Instituto Nacional de Pesquisas Espaciais,
Avenida dos Astronautas 1758, São José dos Campos, 12227-010, São Paulo, Brazil

A possible interaction between cold dark matter and dark energy, corresponding to a well-known interacting dark energy model discussed in the literature within the context of resolving the Hubble tension, has been investigated. We put constraints on it in a novel way, by creating new likelihoods with an analytical marginalization over the Hubble parameter H_0 , the sound horizon r_d , and the supernova absolute magnitude M_B . Our aim is to investigate the impacts on the coupling parameter of the interacting model, ξ , and the equation of state of dark energy w and the matter density parameter $\Omega_{m,0}$. The late-time cosmological probes used in our analysis include the PantheonPlus (calibrated and uncalibrated), Cosmic Chronometers, and Baryon Acoustic Oscillations samples and the Pantheon for comparison. Through various combinations of these datasets, we demonstrate hints of up to 2σ deviation from the standard Λ cold dark matter model.

Keywords: Dark Energy; Dark Matter; Interaction; Cosmological parameters.

I. INTRODUCTION

Over the last few decades, cosmological measurements indicating an expanding universe with an acceleration have suggested that Einstein's General Theory of Relativity (GR) alone is probably not the ultimate theory of gravity capable of explaining all the available observational evidences. Observational data from Type Ia Supernovae (SNeIa) [1–3], Baryon Acoustic Oscillations (BAO) [4–7], and the Cosmic Microwave Background (CMB) [8] provided compelling evidence for the modifications either in the matter sector of the universe or in the gravitational sector. The simplest modification is the introduction of a positive cosmological constant, Λ , into the gravitational equations described by Einstein's GR [1, 2, 9–12] and the resulting picture – the so-called Λ -Cold Dark Matter (Λ CDM) cosmological model – has been found to be consistent with a wide range of observational datasets. Nevertheless, the Λ CDM model is now facing both theoretical and observational challenges [13–18]. Consequently, there has been growing momentum for a revision of Λ CDM cosmology in recent times [19–26]. Thus, the question arises: Is GR + Λ the fundamental theory of gravity, or merely an approximation of a

more complete gravitational theory yet to be discovered? One natural avenue of exploration is to consider modified gravity theories, which show theoretical and observational promise in addressing the observed discrepancies. With the ever-increasing sensitivity and precision of present and upcoming astronomical surveys, modified gravity theories emerge as viable contenders alongside GR + Λ . The search for the ultimate answer in this direction is ongoing. According to the existing literature, we currently have a cluster of cosmological scenarios broadly classified into two categories: i) cosmological scenarios within GR, commonly known as dark energy models, and ii) cosmological scenarios beyond GR, commonly known as modified gravity models.

In this article, we focus on the first approach, which means that the gravitational sector of the universe is well described by GR, but the modifications in the matter fields are needed to explain the current accelerating phase and recent observational tensions and anomalies that persist in the structure of the standard cosmological model. The list of cosmological models in this particular domain is extensive, and here we are interested in investigating one of the generalized and appealing cosmological theories in which dark matter (DM) and dark energy (DE) interact with each other via an energy exchange mechanism between them. The theory of interacting DM-DE, widely known as IDE, has garnered massive attention in the community and has been extensively studied with many appealing results [27–63] (also see [63–65]). The IDE models gained prominence in modern cosmology for alleviating tensions in some key cosmological parameters

* benidav@post.bgu.ac.il

† supriya.maths@presiuniv.ac.in

‡ dstaicova@inrne.bas.bg

§ e.divalentino@sheffield.ac.uk

¶ rafadcnunes@gmail.com

On the Significance of Rare Objects at High Redshift: The Impact of Cosmic Variance

CHRISTIAN KRAGH JESPERSEN,¹ CHARLES L. STEINHARDT,^{2,3} RACHEL S. SOMERVILLE,⁴ CHRISTOPHER C. LOVELL,^{5,6}

¹*Department of Astrophysical Sciences, Princeton University, Princeton, NJ 08544, USA*

²*Cosmic Dawn Center (DAWN)*

³*Niels Bohr Institute, University of Copenhagen, Lyngbyvej 2, DK-2100 Copenhagen Ø*

⁴*Center for Computational Astrophysics, Flatiron Institute, 162 5th Avenue, New York, NY 10010, USA*

⁵*Institute of Cosmology and Gravitation, University of Portsmouth, Burnaby Road, Portsmouth, PO1 3FX, UK*

⁶*Astronomy Centre, University of Sussex, Falmer, Brighton BN1 9QH, UK*

ABSTRACT

The discovery of extremely luminous galaxies at ultra-high redshifts ($z \gtrsim 8$) has posed a challenge for galaxy formation models. Most statistical analyses of this tension to date have not properly accounted for the variance due to field-to-field clustering, which causes the number counts of galaxies to vary from field to field, greatly in excess of Poisson noise. This super-Poissonian variance is often referred to as cosmic variance. Since cosmic variance increases rapidly as a function of mass, redshift, and for small observing areas, the most massive objects in deep *JWST* surveys are severely impacted by cosmic variance. In this paper, we introduce a simple model to predict the distribution of the mass of the most massive galaxy found for different survey designs, which includes cosmic variance. The distributions differ significantly from previous predictions using the Extreme Value Statistics formalism, changing both the position and shape of the distribution of most massive galaxies in a counter-intuitive way. We test our model using the `UniverseMachine` simulations, where the predicted effects of including cosmic variance are clearly identifiable. Moreover, we find that the highly significant skew in the distributions of galaxy number counts for typical deep *JWST* surveys lead to a high “variance on the variance”, which greatly impacts the calculation of the cosmic variance itself. We conclude that it is crucial to accurately account for the impact of cosmic variance in any future analysis of tension between extreme galaxies in the early universe and galaxy formation models.

1. INTRODUCTION

In the Λ CDM paradigm, structure forms hierarchically, with perturbations in the matter distribution collapsing and merging to form progressively larger and more massive structures. Current galaxy formation models build on top of this, modelling baryons as falling into the potential wells formed by the collapsed dark matter halos, cooling and turning into stars over time (Somerville & Davé 2015). Recent observations from the James Webb Space Telescope (*JWST*, Gardner et al. 2006) have detected a population of luminous galaxies at extremely high redshifts $z \gtrsim 10$, with both number densities and masses significantly higher than those predicted by pre-launch theoretical models (e.g. Harikane et al. 2023; Leung et al. 2023; Finkelstein et al. 2023). Although there were early claims that these galaxies

were in fundamental tension with the Λ CDM paradigm (Labbé et al. 2023; Boylan-Kolchin 2023), it is now generally accepted that the observed galaxies can be accounted for within the standard Λ CDM paradigm if the effective conversion of baryons into stars is higher than that in the nearby Universe (Dekel et al. 2023). Other possible difficulties in interpreting such observations are the very large uncertainties on stellar mass estimates, as well as additional uncertainties on the contribution from accreting black holes to the observed rest-UV luminosity, and possible evolution in the stellar initial mass function (Steinhardt et al. 2023). However, the unexpectedly high masses of the most massive galaxies are still a potential challenge for galaxy formation models.

The analyses of the most massive galaxies to date have mostly focused either on the *expected* (average) number of galaxies of a certain mass at a given redshift (Boylan-Kolchin 2023), or on the Extreme Value Statistics (EVS) technique (Lovell et al. 2023). However, both approaches neglect field-to-field clustering due to large-scale structure. Field-to-field differences due to clus-

CCD PHOTOMETRY OF TRAPEZIA STARS I¹

A. Ruelas-Mayorga², L. J. Sánchez², A. Páez-Amador², O. Segura-Montero², A. Nigoche-Netro³

Draft version: March 4, 2024

RESUMEN

Presentamos fotometría CCD de las estrellas en cuatro trapecios estelares ADS 15184, ADS 728, ADS 2843, y ADS 16795. El estudio se hace a partir de imágenes tomadas en el Observatorio Astronómico Nacional de San Pedro Mártir (OAN), Baja California, México. El presente trabajo utiliza la técnica de fotometría de apertura para medir las magnitudes U , B , V , R e I de algunas estrellas en estos cúmulos abiertos dinámicamente inestables (trapecios).

Usando el parámetro $Q = (U - B) - 0.72(B - V)$ se obtuvo el tipo espectral de las estrellas estudiadas, también se derivaron su distancia al Sol y su enrojecimiento. Ligeras diferencias en los tipos espectrales derivados a partir del parámetro Q con los listados en SIMBAD, podrían deberse a un valor diferente de 0.72 de la pendiente de la línea de enrojecimiento en el diagrama de dos colores.

ABSTRACT

We present photometric CCD observations of stars in four stellar trapezia ADS 15184, ADS 4728, ADS 2843, and ADS 16795. This study is performed on images obtained at the Observatorio Astronómico Nacional at San Pedro Mártir (OAN), Baja California, México. In this work we utilise aperture photometry to measure the U , B , V , R and I magnitudes of some of the stars in these dynamically unstable stellar clusters (trapezia).

Using the $Q = (U - B) - 0.72(B - V)$ parameter we obtained the spectral type of the studied stars as well as their distance to the Sun and their reddening. Slight differences between the Q -derived Spectral types and those listed in SIMBAD might be due to a different value, from 0.72, for the slope of the reddening line on the two-colour diagram.

Key Words: Galaxy: stellar content, open clusters and associations: individual (ADS15184, ADS728, ADS2843, ADS16795), techniques: photometry

1. INTRODUCTION

The stellar trapezia are formed in the interior of emission nebulae, such as the Orion Nebula. They are physical systems formed by three or more

¹Based upon observations acquired at the Observatorio Astronómico Nacional on the Sierra San Pedro Mártir (OAN-SPM), Baja California, México.

²Instituto de Astronomía, Universidad Nacional Autónoma de México, México D.F., México.

³Instituto de Astronomía y Meteorología, Universidad de Guadalajara, Guadalajara, Jal. 44130, México.

Towards Prebiotic Chemistry on Titan: Impact experiments on organic haze particles

BEN K. D. PEARCE*,¹ SARAH M. HÖRST,¹ CHRISTOPHER J. CLINE,² MARK J. CINTALA,² CHAO HE*,^{3,1}
JOSHUA A. SEBREE,⁴ SHANNON M. MACKENZIE,⁵ R. TERIK DALY,⁵ ALEXANDRA J. PONTEFRACT,⁵ AND CARA PESCIOTTA¹

¹*Department of Earth and Planetary Science, Johns Hopkins University, Baltimore, MD, 21218, USA**

²*NASA Johnson Space Center, Astromaterials Research and Exploration Science, Mail Code X13, 2101 NASA Parkway, Houston, Texas 77058, USA*

³*School of Earth and Space Sciences, University of Science and Technology of China, Hefei, China*

⁴*Department of Chemistry and Biochemistry, University of Northern Iowa, Cedar Falls, IA, USA*

⁵*Applied Physics Laboratory, Johns Hopkins University, Space Exploration Sector, Laurel, MD 20723, USA*

(Accepted to PSJ Feb 11, 2024)

ABSTRACT

Impacts are critical to producing the aqueous environments necessary to stimulate prebiotic chemistry on Titan’s surface. Furthermore, organic hazes resting on the surface are a likely feedstock of biomolecules. In this work, we conduct impact experiments on laboratory-produced organic haze particles and haze/sand mixtures and analyze these samples for life’s building blocks. Samples of unshocked haze and sand particles are also analyzed to determine the change in biomolecule concentrations and distributions from shocking. Across all samples, we detect seven nucleobases, nine proteinogenic amino acids, and five other biomolecules (e.g., urea) using a blank subtraction procedure to eliminate signals due to contamination. We find that shock pressures of 13 GPa variably degrade nucleobases, amino acids, and a few other organics in haze particles and haze/sand mixtures; however, certain individual biomolecules become enriched or are even produced from these events. Xanthine, threonine, and aspartic acid are enriched or produced in impact experiments containing sand, suggesting these minerals may catalyze the production of these biomolecules. On the other hand, thymine and isoleucine/norleucine are enriched or produced in haze samples containing no sand, suggesting catalytic grains are not necessary for all impact shock syntheses. Uracil, glycine, proline, cysteine, and tyrosine are the most unstable to impact-related processing. These experiments suggest that impacts alter biomolecule distributions on Titan’s surface, and that organic hazes co-occurring with fine-grained material on the surface may provide an initial source for further prebiotic chemistry on Titan.

Keywords: Titan — impacts — organic hazes — nucleobases — amino acids — astrobiology

INTRODUCTION

The atmosphere of Saturn’s moon Titan contains multiple layers of organic haze (Atreya 2007; Hörst 2017). These solid particles are naturally produced in N₂/CH₄-rich atmospheres via chemical reactions initiated by collisions, ultraviolet (UV) radiation, or thermal ionization and dissociation (Trainer et al. 2006; Hörst 2017). Laboratory analogs of these haze particles contain a myriad of biomolecules including the nucleobases of RNA and DNA, as well as amino acids and their intermediates (Pearce et al. 2023; Sebree et al. 2018).

Titan’s crust is predominantly water ice, but the surface is also covered in a variety of organic sediments believed to be sourced from the atmospheric hazes (Hörst 2017). Impacts from comets and planetesimals on the icy surface produce melt pools that can survive up to tens of thousands of years (Neish et al. 2018). These post-impact environments are key sites for potential complex prebiotic chemistry. Crater counts on Saturnian moons suggest hundreds to thousands of impacts producing craters >10 km in diameter have occurred on Titan (Zahnle et al. 2003). However, weathering processes such as aeolian infilling and fluvial erosion actively modify Titanian craters, leaving behind only a few dozen craters that have been observed by Cassini RADAR

* bpearce6@jhu.edu; chaohe23@ustc.edu.cn